Small Light Weight LiDAR Systems with Remotely Piloted Aircraft for Powerline Detection

by

Samuel J Moses

A Thesis submitted to the Faculty of Graduate and Postdoctoral Affairs in partial fulfillment of the requirements for the degree of

Master of Applied Science

in

Aerospace Engineering
Department of Mechanical and Aerospace Engineering

Carleton University
Ottawa, Ontario

Abstract

This thesis examines small low-cost light weight LiDAR systems for remotely piloted aircraft (RPA) for power transmission line (PTL) detection. Different PTL samples were used to understand how the low-cost light-weight LiDAR systems perform against them. A performance evaluation was done which included a specification comparison, data comparison, root-mean squared deviation comparison (RMSD) for both de-energized and energized PTLs and a sectional analysis.

For the data comparison, the results showed LiDAR A performed better but not within the advertised precision for 5/6 of the test. The RMSD test resulted in the understanding in the accuracy of the data collected, lower deviations were found in the data collected by LiDAR B, but more consistent deviations were found in LiDAR A data.

A conclusion was made that low-cost light-weight LiDAR systems would not be effective as a stand-alone system for PTL detection so it should be paired with an additional sensor.

Acknowledgments

I would like to take this opportunity to thank the almighty God for his guidance and the everyone who supported me through the completion my master's degree at Carleton University as it has been a difficult journey for me over the Covid-19 pandemic.

Firstly, I want to thank Professor Jeremy Laliberte, as he was an amazing mentor to me over the course of this research. Providing me the opportunity to study/ research at Carleton University. His experience and wealth of knowledge in the field of aerospace engineering has made me be a better researcher and person. The numerous opportunities he has provided me for networking and projects, I am grateful for that. Again, Professor Jeremy Laliberte I want to thank you.

Thank you to all my family members who supported me during my master's degree studies at Carleton university, I know it has been tough with me being stuck in Canada. Being away from family no matter how long is never easy. Sonia M Moses, Samuel C Moses, and Sonja J Moses I want to especially thank you for supporting me throughout this journey it means a lot to me that everyone was there for me. In addition, I want to thank Acacia Frempong-Manso as she has been there to support me emotionally and motivate me when I was feeling down.

Next, I want to give special thanks to Brendan Ooi, and Mr. Salman Shafi for their helpful comments and guidance during this research thesis. Their experience has been a major factor in how my research was conducted with the limited resources at my disposal. I would like to also thank the company Kinectrics, Inc more specifically Andrew Rizzetto and Dan for allowing me to briefly use their lab facility to conduct part of my research and learn more about power transmission lines as this was a major part of my research thesis.

Table of Contents

Acknowledgments iii

Table of Contents iv

List of Tables viii

List of Illustrations ix

List of Appendices xiii

List of Symbols xiv

List of Acronyms xv

Chapter 1: Introduction 1

1.1 Thesis Motivation 1

1.2 Objectives 3

1.3 Thesis Overview 5

Chapter 2: Literature Review 6

2.1 Background 6

2.2 Past Research Papers. 10

2.2.1 Types of Power Transmission Line Detection Systems 10

2.2.2 History of LiDAR 13

2.2.3 How LiDAR works 13

2.2.4 LiDAR, Object Detection and Powerline Inspection 15

2.2.5 LiDAR Performance around Different Surfaces. 19

2.3 Regulations 19

2.4 Examples of Remotely Piloted Aircraft Systems 23

2.5 Proposed Solution 24

Chapter 3: Methodology 25

3.1 Overview 25

3.2 Testing Set up and Mission Profile 25

3.3 Power Transmission Line Samples 29

3.4 LiDAR Systems and Specifications 32

3.5 Remotely Piloted Aircraft Systems (RPAS), specifications and control systems 39

3.6 Ground Stations 41

Chapter 4: Performance Evaluation of Systems 44

4.1 Verification of Selected LiDAR Systems 45

4.1.1 LiDAR A 46

4.1.2 LiDAR B 48

4.1.3 Verification Results Summary 49

4.2 LiDAR Performance Comparison 50

4.2.1 Specifications Comparison 50

4.2.2 Specifications Comparison Summary 50

4.3 LiDAR Data Comparison 51

4.3.1 De-Energized at Room Temperature 52

4.3.2 Energized between 60°C to 120°C 55

4.3.3 Summary of Results 56

4.4 Root-Mean-Square Deviation Comparison 58

4.4.1 De-Energized at Room Temperature 59

4.4.2 Interference Comparison 64

4.4.3 Energized between 60°C to 120°C 68

4.4.4 Discussion of Results 71

4.5 Performance Evaluation Summary 71

4.6 PTL Sample Section Analysis 74

4.7 Miniature Case Study 79

4.7.1 Discussion of results 81

Chapter 5: NRC Case Study 82

5.1: Introduction/ Overview 82

5.2 OPAL-CONICAL 3D LiDAR Specifications 83

5.3 LiDAR Data 84

5.4 Contribution to the Research 88

5.5 General Conclusion 88

Chapter 6: Conclusions, Recommendations and Future Research 90

6.1 Conclusions 90

6.2 Recommendations 92

6.3 Future Research 93

Bibliography 94

Appendices 105

List of Tables

Table 1: Examples of RPAS used in Overhead Line Inspections 23

Table 2: Power Transmission Line Sample Specifications Summary 32

Table 3: HPS-3D160/3D Solid State LiDAR Specifications 34

Table 4:LiDAR A Timing Modes 35

Table 5: LiDAR B Specifications 37

Table 6: 3DR Iris+ Specifications 40

Table 7: Raspberry Pi 3 Model B Specifications 41

Table 8: HP ENVY X360 I7 Specifications 41

Table 9: Microsoft Surface Pro 7 I-3 Specifications 42

Table 10: HD Digital Camera Specifications 43

Table 11: Verification of LiDAR System Results 49

Table 12: Specifications Comparison 50

Table 13:ACSR Drake LiDAR A, B Results at 0.5m 52

Table 14:ACSR Condor aged LiDAR A, B Results at 0.5 m 53

Table 15:ACCC Rome LiDAR A, B Results 54

Table 16:ACSR Cardinal LiDAR A, B Results 55

Table 17:Energized ACCC Rome LiDAR A, B Results 55

Table 18:Energized ACSR Condor aged LiDAR A, B Results 56

Table 19: Summary of LiDAR Data Comparison 57

Table 20:ACSR Drake LiDAR A, B mounted on 3D Iris+ multirotor RPAS results at 0.5 m 80

Table 21: OPAL-CONICAL 3D LiDAR Specifications 84

List of Illustrations

Figure 1:Overhead Line Inspection by Helicopter[2] 1

Figure 2: Different Types of Power Transmission Lines and Structures[5] 3

Figure 3: Power Transmission Line Structure Breakdown[6] 4

Figure 4: The Transmission Line Inspection Robot[10] 8

Figure 5:Multi-Sensor Power Transmission Line Inspection[8] 8

Figure 6: The Seeker aircraft for Pipeline Power Line Patrol[13] 11

Figure 7: LiDAR Basics [20] 14

Figure 8: 3D LiDAR Emitting Direction[21] 15

Figure 9: Sample result data [16] 17

Figure 10: LiDAR sample data from research paper[17] 18

Figure 11: FAA Airspace Classification[29] 21

Figure 12: Transport Canada Airspace Classification[31] 21

Figure 13: Single Circuit, Horizontal Configuration, Self-Supported Lattice Tower[32] 26

Figure 14:Initial LiDAR Testing Stand 27

Figure 15:PTL Sample Codename: ACSR Drake 29

Figure 16:ACSR Drake cross-section 30

Figure 17:PTL Sample Codename: ACSR Condor 30

Figure 18: ACSR Condor cross-section 30

Figure 19:Sample PTL Codename: ACCC Rome 31

Figure 20: ACCC Rome cross-section 31

Figure 21: PTL Sample Codename: ACSR Cardinal 31

Figure 22: ACSR Cardinal cross-section 32

Figure 23:HPS-3D160/3D Solid State LiDAR (LiDAR A)[34] 33

Figure 24: LiDAR A Field of View[35] 35

Figure 25:LiDAR A Advance Settings 36

Figure 26: LiDAR B- Cygbot CygLiDAR D1 2D/3D Dual Solid State TOF LiDAR[36] 37

Figure 27:Cygbot's CygLiDAR Viewer for LiDAR B 38

Figure 28: 3DR Iris+ multirotor RPAS 39

Figure 29:Raspberry Pi 3 Model B 40

Figure 30: HD Digital Camera by ELP 42

Figure 31: Microsoft Excel-Conditional Formatting Rule 44

Figure 32:Aluminum water bottle from LiDAR stand view 46

Figure 33:LiDAR A screenshot of aluminum water bottle at 0.5m 46

Figure 34:LiDAR A point data conditional formatted 47

Figure 35:LiDAR B screenshot of aluminum water bottle at 0.5m 48

Figure 36:LiDAR B data 2D conditional formatted 48

Figure 37:Conditional Formatted LiDAR A ACSR Drake at 0.5 m 52

Figure 38:Conditional Formatted LiDAR B ACSR Drake at 0.5 m 52

Figure 39:Conditional Formatted LiDAR A ACSR Condor aged at 0.5 m 53

Figure 40:Conditional Formatted LiDAR B ACSR Condor at 0.5m 53

Figure 41:Conditional Formatted LiDAR A ACCC Rome at 0.5m 54

Figure 42:Conditional Formatted LiDAR B ACCC Rome at 0.5m 54

Figure 43:Conditional Formatted LiDAR A ACSR Cardinal at 0.5m 54

Figure 44:Conditional Formatted LiDAR B ACSR Cardinal at 0.5m 55

Figure 45:Conditional Formatted LiDAR A Energized ACCC Rome at 0.5m 55

Figure 46:Conditional Formatted LiDAR B Energized ACCC Rome at 0.5m 55

Figure 47:Conditional Formatted LiDAR A Energized ACSR Condor aged at 0.5m 56

Figure 48:Conditional Formatted LiDAR B Energized ACSR Condor aged at 0.5m 56

Figure 49:LiDAR A RMSD for ACSR Drake at 0.5 m 59

Figure 50:LiDAR B RMSD for ACSR Drake at 0.5 m 59

Figure 51:LiDAR A RMSD for ACSR Condor aged at 0.5 m 60

Figure 52:LiDAR B RMSD for ACSR Condor aged at 0.5 m 61

Figure 53:LiDAR A RMSD for ACCC Rome at 0.5 m 62

Figure 54:LiDAR B RMSD for ACCC Rome at 0.5 m 62

Figure 55:LiDAR A RMSD for ACSR Cardinal at 0.5 m 63

Figure 56:LiDAR B RMSD for ACSR Cardinal at 0.5 m 63

Figure 57:Sample 2 Interference Comparison LiDAR A at 0.5 m 65

Figure 58:Sample 2 Interference Comparison LiDAR B at 0.5 m 65

Figure 59:Sample 4 Interference Comparison LiDAR A at 0.5 m 66

Figure 60:Sample 4 Interference Comparison LiDAR B at 0.5 m 67

Figure 61:LiDAR A RMSD for ACCC Rome-Energized at 0.5 m 68

Figure 62:LiDAR B RMSD for ACCC Rome-Energized at 0.5m 69

Figure 63:LiDAR A RMSD for ACSR Condor aged-Energized 70

Figure 64:LiDAR B RMSD for ACSR Condor aged -Energized 70

Figure 65:Electromagnetic spectrum[37] 73

Figure 66: LiDAR A Conditional Formatted ACCC Rome at 0.5 m 75

Figure 67: ACCC Rome at 0.5 Sectional One for LiDAR A 75

Figure 68:ACCC Rome at 0.5 Sectional Two for LiDAR A 76

Figure 69:ACCC Rome at 0.5 Sectional Three for LiDAR A 76

Figure 70:LiDAR B Conditional Formatted ACCC Rome at 0.5 m 77

Figure 71:ACCC Rome at 0.5 Sectional One for LiDAR B 77

Figure 72:ACCC Rome at 0.5 Sectional Two for LiDAR B 78

Figure 73:ACCC Rome at 0.5 Sectional Three for LiDAR B 78

Figure 74: LiDAR A mounted on 3D Iris+ multirotor RPAS 79

Figure 75:LiDAR B mounted on 3D Iris+ multirotor RPAS 80

Figure 76: RMSD per Observation of LiDAR A mounted on a RPAS at 0.5 m 80

Figure 77:RMSD per Observation of LiDAR B mounted on a RPAS at 0.5 m 81

Figure 78:OPAL™ PERFORMANCE SERIES –CONICAL 3D LiDAR[39] 82

Figure 79:Google Earth screenshot of LiDAR Data Collection Area 85

Figure 80:OPAL-Conical 3D LiDAR Data 86

Figure 81: Zoomed in screenshot of OPAL-Conical 3D LiDAR Data 87

List of Appendices

Appendix A- validation and verification set……105

Appendix B- Sample MATLAB code……...107

Appendix C- Power Transmission Line Specifications Sheets…….…….108

List of Symbols

f	Frequency [Hz]
R	Radius [m or mm]
K	Kilo
V	Voltage
℃	Degrees-Celsius
°	Degrees (angle)
i	variable i
N	Number of non-missing data points
x_i	Actual observations time series
$\hat{x}_i$	Estimated time series
W	Watts
Q	Heat transferred
σ	Stefan Boltzmann Constant

List of Acronyms

Acronyms	Definition
UAV	Unmanned Aerial Vehicle
RPA	Remotely Piloted Aircraft
FPV	First-Person View
RPAS	Remotely Piloted Aircraft System(s)
PTL	Power Transmission Line(s)
BLOS	Beyond Line of Sight
LiDAR	Light Detection and Ranging
RADAR	Radio Detection and Ranging
DAA	Detect and Avoid
GCS	Ground Control Station
SAA	Sense and Avoid
PIC	Pilot in Command
FOV	Field of View
VTOL	Vertical Take off and Landing
ROS	Robot Operating System
AI	Artificial intelligence
IR	Infrared
SDK	Software Development Kit
RMSD	Root-Mean-Squared Deviation
RMSE	Root-Mean-Squared Error
ACSR	Aluminium-conductor steel-reinforced

ACCC	Aluminum Conductor Composite Core
NTOF	National Traumatic Occupational Fatalities
LASER	Light Amplification by Stimulated Emission of Radiation
OD	Outer-Diameter
USB	Universal Serial Bus
FPS	Frames per Second
1D	One-Dimensional
3D	Three-Dimensional
2D	Two-Dimensional
4D	Four-Dimensional
LCD	Liquid Crystal Display
AGL	Above Ground Level
MSL	Mean Sea Level
BPS	Beats Per Second
GB	Gigabit
VDC	Volts of direct current
UDP	User Datagram Protocol

Chapter 1: Introduction

1.1 Thesis Motivation

Power transmission lines (PTLs) are currently being inspected using a combination of utility workers and/or-crewed aircraft such as conventional helicopters outfitted with a sensor type payload as seen in Figure 1. These methods are not only expensive but also dangerous, “According to National Traumatic Occupational Fatalities (NTOF) data, the average annual fatality rate for power line workers is 56.3 deaths per 100,000 employees”. The Bureau of Labor Statistics' (BLS) Census of Fatal Occupational Injuries (CFOI) identified forty-two fatalities among electric power installers and repairers in 1993 (38 deaths per 100,000 workers).” and “helicopter of Heli-west hit a crossing power line 10 km NW of Grimstad, Norway while laser scanning a powerline” [1].

Figure 1:Overhead Line Inspection by Helicopter[2]

Using remotely piloted aircraft systems (RPAS) for power transmission lines (PTL) inspections helps mitigate the risk factor, this is done by removing the utility worker from

being in direct contact with or in close proximity to the PTL. In addition, RPAS will remove the risk of having a helicopter encountering the PTL as the inspection is being performed. A news article published by the Sun (UK) shows the unfortunate scenario were a helicopter collided with a PTL, the name of the news article is “Horrifying moment helicopter burns after crashing as it inspected power lines killing pilot and passenger” [3] [4]. The article goes into detail using images and video of how the incident occurred. Although RPAS have potential to improve/ mitigate safety issues and concerns they have their own safety issues such as proximity awareness due to the lack of onboard pilot.

One of the major challenges RPAS have faced while performing a PTL inspection is maneuvering at close distance around the lines and towers. It is exceedingly difficult for the pilot- in- command (PIC) to judge the distance between RPAS and the PTL since most of these inspections are performed with a limited or reduced visibility. With the development RPAS systems over the years there has been many different developments in detect and avoid systems such as DJI uses on their DJI RPAS and Skydio with new RPA capable of object detection and scanning, however this is not designed specifically for PTLs but for general object detection. Currently, there are a few commercial drones with alike systems implemented. These systems usually depend visual spectrum sensing and deep learning software. This leaves space for opportunities such as developing/ improving a detection/ sense and avoid system using sensors such as light detection and ranging (LiDAR) which would fall outside the visual spectrum to allow for safer PTL inspections by RPAS while reducing the risk of a RPAS colliding with a PTL. For this reason, a detect and avoid system can be improved, to be more efficient and decrease the risk of an accident occurring.

1.2 Objectives

Recently, there has been several papers written on the use of RPAS on or around PTLs and their structures. Regarding PTL components that will be inspected but not limited to overhead ground wires, insulators, crossarms, conductor bundle. The majority of PTL inspections are conducted from a stand-off distance (this distance varies depending on the sensor), type of RPA being used and the configuration of the PTLs; this can be due some RPA not being able to accurately detecting the power transmission lines and alerting the pilot in command (PIC). The general aim of this research is to investigate the performance of different low-cost light-weight LiDAR systems for PTL detection and provide documentation on their accuracy along, including if they can be used exclusively for PTL detection. Figures 2 and 3 show the several types of PTL and their main components.

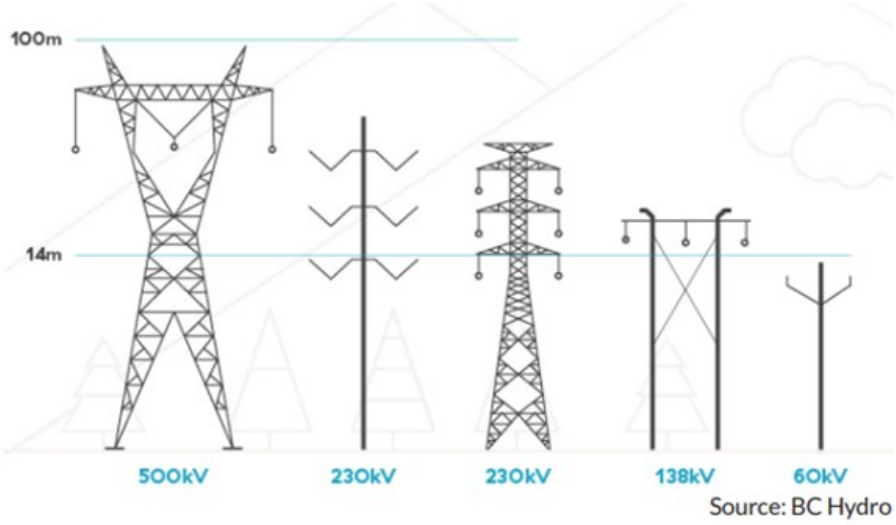

Figure 2: Different Types of Power Transmission Lines and Structures[5]

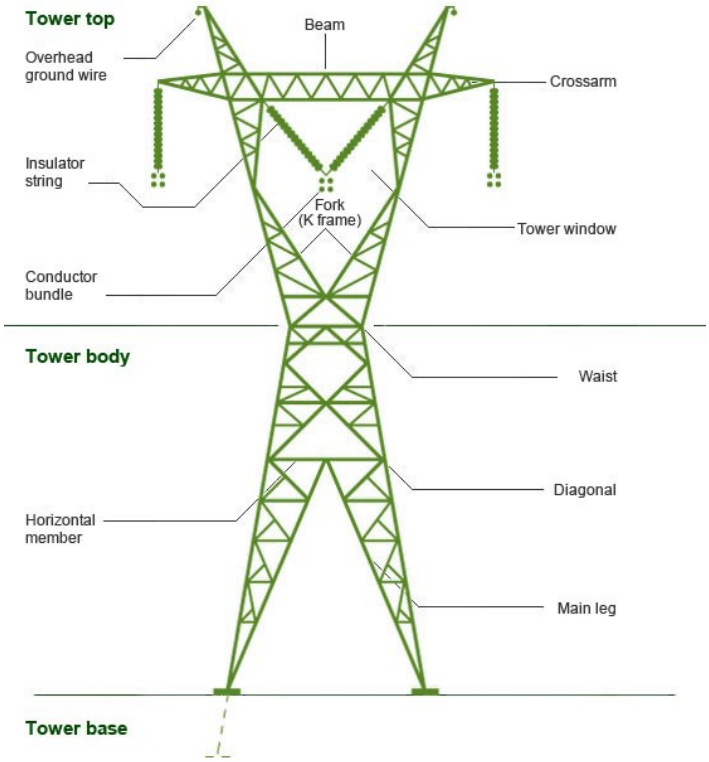

Figure 3: Power Transmission Line Structure Breakdown[6]

The main objectives of this research are:

1. Demonstrate the detection of power transmission lines using light-weight LiDAR systems.
2. Determine the accuracy of the chosen light-weight LiDAR systems in different operating conditions
3. Be able to install the LiDAR onto a small RPAS without significantly decreasing its performance
4. Demonstrate that the light-weight LiDAR system can withstand electromagnetic interference.

1.3 Thesis Overview

This thesis presents the results of the investigation and evaluation of low-cost light-weight LiDAR systems, as they were compared based on their specifications and performance in the detection of the acquired PTLs. The need for developing a detect and avoid system came from research into powerline transmission line and how remotely piloted aircraft (RPA) are being utilized. One common issue found was LiDAR systems used in PTL inspections were more focused on the support structures, such as the tower of the PTL and not on detection of the actual PTL itself, in addition legacy LiDAR systems tend to be expensive, heavy and are not easy of use in terms of interface.

This thesis is organized (starting after Chapter 1: Introduction) in the following chapters:

Chapter 2: this chapter presents the literature review, it contains the background information, past research papers, and a look into the different regulations that govern RPAS during power transmission line operations.

Chapter 3: this chapter discusses the methodology, proposed solution including different sensors/- LiDARs to be used and looking at more a theoretical solution.

Chapter 4: this chapter discusses the evaluation of the data and performance from the different sensor systems when is comes to detecting, measuring distance from the test objects, a section of the conditional formatted PTL analysis, and a miniature case study.

Chapter 5: Case Study

Chapter 6: This chapter will cover the conclusion, recommendations, and future work.

Chapter 2: Literature Review

Chapter Overview

This chapter discussed systems that relate to RPAS, power transmission line inspections, DAA systems, and low-cost light-weight LiDAR systems background information on the thesis topic. The DAA systems were discussed as a technical background that is relevant to this thesis. This chapter also reviewed a combination of analyses of different low-cost detection LiDAR systems that are available, RPAS, and reviews of past research papers on the topic. Regulations for RPAS operations will also be examined.

2.1 Background

Canada has well over ten million consumers of electricity, with an estimate of over 150,000 kilometres of power transmission lines that needs to be inspected and maintained [7]. For this research, the proposed assets for detection would be PTLs ranging 60 kV to 500 kV, making up an estimate of over 35 percent of the PTLs. The focus will be the >500 kV PTL as there are more factors to consider while performing inspections. Some factors include but are not limited to high wind turbulence, higher electro-magnetic interference and beyond visual light of sight (BVLOS) regulations. These factors are related to the placement of the PTLs and with higher kV PTLs comes higher electromagnetic fields causing interference. At the time of conducting this research, several different methods have been/ are being developed for mitigating the risk to utility workers. The most common are RPA outfitted with cameras and sensors to help inspectors have a better understanding of the PTLs. As the cameras would allow the inspectors to assess any physical damage to the PTL, sensors/ LiDAR's will go a step further and allow the inspector to detect any

anomalies in either the energy outputs or irregular heat signatures. "Today, powerline inspection is done mostly by aerial systems, capturing data with LiDAR, RGB cameras as well as specific thermal infrared and UV sensitive sensors. During flights, results are reported by visual observation and later analyzed and verified using the captured data"[8] as shown in Figure 4.

Some challenges associated with working on energized PTLs can range from electromagnetic interference (for RPA) which can affect the RPA components giving inaccuracy information to the PIC, electrocution (traditional method), burns and falls from high elevations (traditional methods), and "According to the research of the World Health Organization, we can suffer from insomnia, anxiety, headache, skin burns, fatigue, and muscle pain because of radiations from HV power lines."[9] however, this would not be the focus of this research as it will be on detection of PTLs.

Some companies have opted with using an automated device that can be attached to PTLs and perform the inspection as needed as shown in Figure 4 below. This method has been used to mitigate the human risk factor, however set up and takedown times have been major draw backs. Typically for this type of inspection it will involve appropriately three to five crew members and a boom-lift vehicles to be able to attach and detach the device, an RPA has the potential of decreasing the need for so many crew members and the boom-lift vehicles.

Figure 4: The Transmission Line Inspection Robot[10]

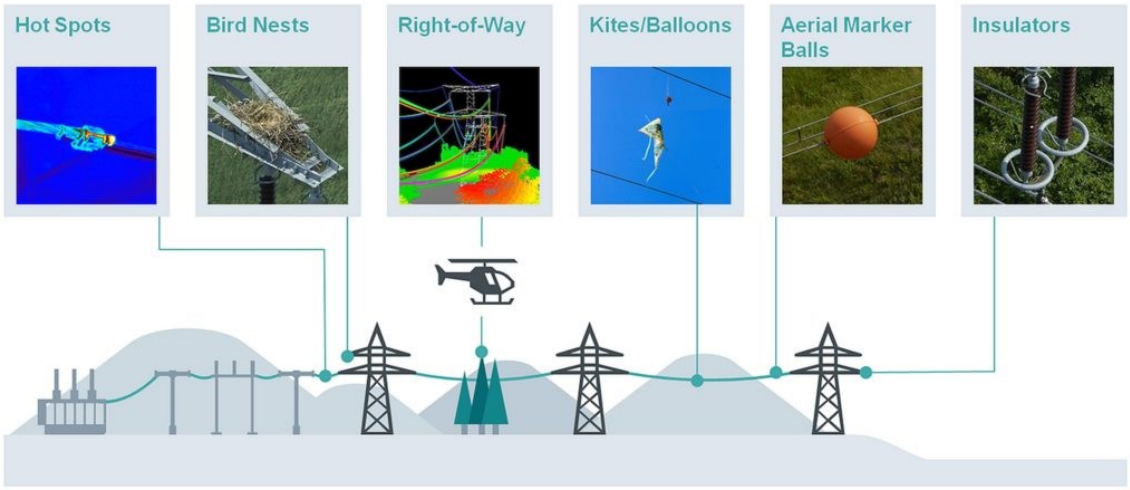

Figure 5:Multi-Sensor Power Transmission Line Inspection[8]

Every year PTLs become damaged by falling debris or through the failure of faulty components. This leads to it being important, not only inspect the PTLs but also the surrounding environments to ensure that there are no potential dangers nearby. PTLs tend not to be inspected as often as they should, which results in greater risk for the public with the growing demand being placed on them. One of the major drawbacks to performing inspections on the components/assets mentioned above is they may be energized. These

energized components produce what is known as a electromagnetic field which has the potential to interfere with components on board the RPAS, potentially leading to incorrect readings or damage to a component like the flight controller. RPAS pilots are aware of this risk and tend to keep their RPAS at a safe distance but deploy high-performance imaging solutions capable of zooming with little distortion to the image. Other ways RPAS can perform is by using various instruments to measure the output of the energized components to detect any defects. These defects unless visible to the naked eye would go undetected and exposing personnel using traditional methods (helicopter with inspector physically inspecting) to the danger of being electrocuted.

With using RPAS for PTL inspection applications, the question becomes can a RPAS successfully perform the inspection autonomously or with little input from the pilot. This scenario was looked at in a publication by Nguyen, et al which examined inspection of PTL components by RPAS and deep learning [11]. This research has proposed it is possible to detect PTLs with low-cost light-weight LiDAR systems on RPAS, whether it be a fixed wing RPAS (for the long distance/ duration inspections) and a multirotor RPAS (for short distance). It appears that using a fully autonomous system the writers/ researchers opted for a visual approach to the inspection as this goes hand in hand with deep learning software, the question then become what happens what sensors such as LiDAR are introduce. Since there are already being used in the inspection itself. Can LiDAR systems serve a dual purpose as a detection system and an inspection tool? From research it was found that some common problems with using RPAS for PTL inspections was that they are not able to get as close to the PTL without the risk of obtaining inaccurate readings or potentially interfering with the onboard systems, this would be my area of focus.

To understand these limitations research would be on different testing methods on how to safely operate a RPAS near PTLs. The research would involve looking at the tolerance level of each component near the magnetic fields that PTLs generates and identifying which one gives the best result, however focusing on the accuracy of light weight LiDAR systems, and then using it as a base to compare to the larger more commercial systems. Different RPAS configurations will be looked at based on the application (long distance with high endurance or short distance). This data will then be used to determine the best sensor or combination of sensors and instruments within my research to create an efficient detect and avoidance system that will be able to allow a RPAS to successful manoeuvre around PTLs within a close proximity.

2.2 Past Research Papers.

In this section, a few of the research papers were reviewed and discussed about the types of power transmission line detection systems, the history of LiDAR, how LiDAR works, the use of LiDAR for power transmission line inspections, and LiDAR performance around different surfaces.

2.2.1 Types of Power Transmission Line Detection Systems

A PTL line inspection crew would be dispatched to inspect the PTL manually, this meant that they had to climb the poles, inspect the towers (as shown in Figure 1) and work around vegetation in the surrounding area. For small scale operations/ grids less than 2000 kilometers this would have been practical [12] but for larger operations covering over tens of thousands of kilometers it would involve having to deploy many inspectors and that tends to be expensive. This led to manned aircraft (such as helicopters) being accompanied by the line inspectors, they were known as the eagle-eyed inspectors. However, this process

still had the same issue were the PTLs must be inspected manually leaving the same hazards/ dangers for the line inspectors. This was a step forward as it as it gives way to the development of manned aircraft being outfitted to different payloads such as high-resolution cameras. This addition allowed for fixed-wing aircraft (see Figure 6) to be involved as fixed-wing manned aircrafts to have better endurance than that of a rotary aircraft. Figure 6 shows the seeker aircraft, "Seeker is a stable and efficient sensor platform, but also offers best in class visibility to enable crew to visually inspect countless lengths of Pipeline and Power Line safely and efficiently." [13]

Figure 6: The Seeker aircraft for Pipeline Power Line Patrol[13]

The hazards of conducting a PTL inspection with a manned aircraft unfortunately does not stop at the dangers to the line inspector but also to the manned aircraft. There have been several cases of manned aircrafts encountering PTL whether than be during a PTL inspection or just a fly by. For Canada, The Civil Aviation Daily Occurrence Reporting Systems (CADORS) which is a section of Transport Canada that deals with reporting an aviation incident that has occurred. At the time of drafting this paper, using this CADORS and having "powerline" as a keyword and showing incidents up until March 29th, 2022, there was a record of over forty incident reports and several of them resulted in fatalities and/ or injuries.

Expanding the search further to cover the North American territories more specifically, the United States which their airspace is govern by a section of Federal Aviation Administration (FAA) called the National Transportation Safety Board (NTSB). By searching the NTSB reports using “powerline” as a keyword, it showed a result of over three hundred reports and briefly reviewing the title a great number of them had to deal with manned aircraft encountering powerline either while performing an inspection or a pass by. These reports identify some of the hazards that PTLs pose to manned aircraft, leading to various research in the field of overhead PTL detection. One of the most recent research publications in the field of PTL detection was by the U.S. Army Research Laboratory, the patent number is US 9,964,658 B2 and the date of patent was May 8th, 2018, “Method of autonomous power line detection, avoidance, navigation, and inspection using aerial crafts”[14]. This paper gives general overview of detection and avoidance an aircraft for powerline inspections. The system is supposed to work with both manned and unmanned aircraft. “Automatic autonomous vision-based power line inspection: A review of current status and the potential role of deep learning”[15] is another research paper that uses a different point of view for the process of PTL inspections, this paper focuses having majority of the phases of inspection to be autonomous, using vision based and deep learning as the main part of the data analysis of the inspection. This paper covers some interesting points and mentions some of the challenges involved with this approach.

One system mentioned in various research articles was the use light detection and ranging (LiDAR) in powerline inspections, as it one of the systems also used over detection systems, as shown in “Design and Validation of a School Bus Passing Detection System Based on Solid-State LiDAR” [16]. The contents of the research paper involve using a

LiDAR to detect vehicles passing by school buses as the stop sign is in place and triggering a camera to take a photo of that vehicle. This research paper in addition to "Application of LiDAR technology in power line inspection" [17] along a few other papers made good, researched points of using LiDAR as the main system for detecting and avoiding PTLs during an inspection, hence LiDAR will be the subject device of this research as viable RPA sensor.

2.2.2 History of LiDAR

LiDAR is a technically term from the phase light detection and ranging, it is closely related to RADAR which is radio detection and ranging. This first usage of light detection/ emitting can be found as early as 1930s where the first attempts were made to investigate the structure of the atmosphere. It was not until the 1960s that LiDAR was used and then in the 1980s were became more publicly available on manned aircraft. This development allowed for more precise measurements when it comes global positioning systems (GPS). LiDAR is a remote sensing technique that using a laser to measure elevations, the laser emits a light that can be ultra-violet, visible or near-infrared.

Some types of LiDAR systems are as follows: Terrestrial, Mobile, Static, Airborne, Topographic, Bathymetric, and Satellite LiDAR. Three of the most well-known types of LiDAR are the airborne, topographic, and mobile as these three types are used in similar applications. These applications are as follows but not limited to urban planning, infrastructure mapping forestry and object detection.[18], [19]

2.2.3 How LiDAR works

LiDAR systems work when light from the laser (transmitter) projected to a surface (pulse) and is reflected from the surface. This reflected light is then detected by the receiver

upon returning to the LiDAR (often referred to as the return). The time taken between the pulse being emitted and collected is referred to as the time of flight (TOF), which is used to develop distance maps of the objects or terrain in the field of view of the LiDAR system. Figure 7[20] shows a layout of how LiDAR systems work.

At the time of this research LiDAR systems are being used in a variety of applications such as autonomous vehicle navigation, forestry, farming, land surveying and power line inspection for maintenance.

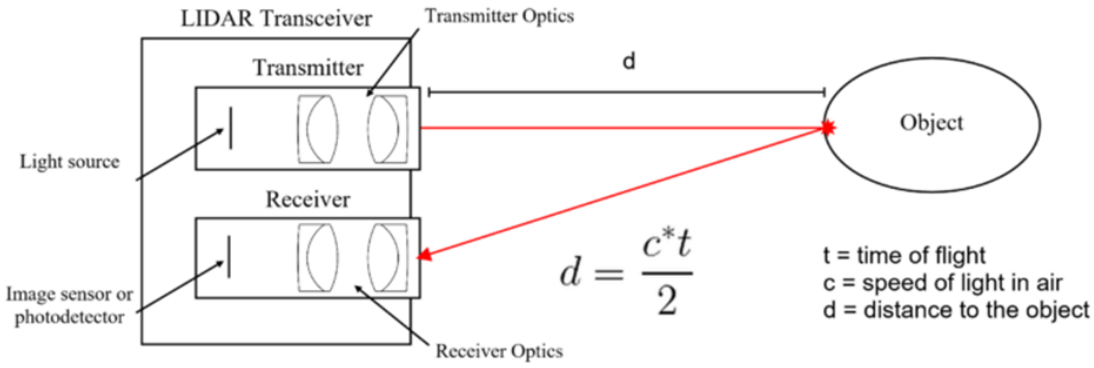

Figure 7: LiDAR Basics [20]

At this time there are 1D, 2D, 3D and 4D LiDAR systems, in the present research 3D LiDAR systems will be used. 3D LiDAR systems typically works by having laser beams emitted on the X, Y and Z axes. With 3D LiDAR systems being able to collect data on the X, Y and Z axes, this has allowed it to be the preferred LiDAR systems in 3D mapping and detection applications. For 3D LiDAR systems the main components are a laser, a scanner (transmitter), a specialized receiver, and this will be same for other types of LiDAR systems.

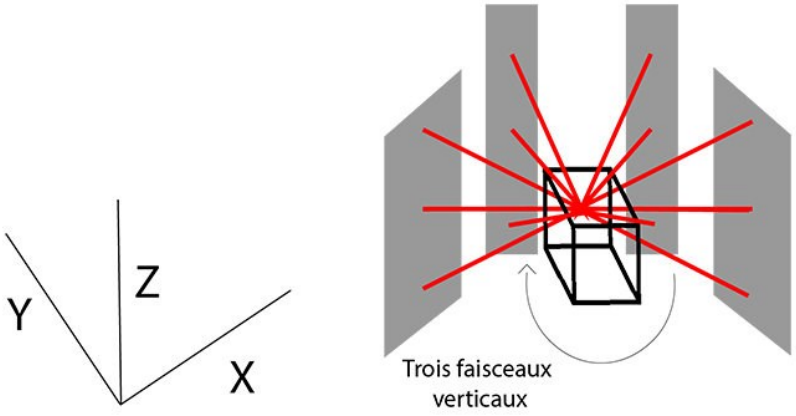

Figure 8: 3D LiDAR Emitting Direction[21]

2.2.4 LiDAR, Object Detection and Powerline Inspection

As previously stated, LiDARs has been used in various applications and from these applications LiDAR can be further categorized. These categorizes are as follows: 2D LiDAR and 3D LiDAR. 2D LiDAR uses a single beam of light towards an object on the horizontal and vertical axis collecting the X and Y distance values of the object. 2D LiDAR are smaller than their 3D LiDAR relatives. 3D LiDAR unlike the 2D LiDAR it emits a beam of light 360 degrees collecting values on the X, Y, Z axis making it suitable for mapping and scanning applications. 3D LiDAR have been widely used in many applications including object detection, making it a great candidate for this research.

H. W. Yoo et al. [20] authored a research article that investigates to use LiDAR object detection capabilities for autonomous driving. The authors mentioned the limitations of using high resolution 3D imaging cameras for high level automated driving, and in summary the level of target values were not met to have a safe and reliable autonomous driving based the to automotive industry. Through to the recent development of MEMS-

based LiDAR and its benefits such as being light weight and having a low power consumption, 1D MEMS scanning mirrors on scanning LiDAR are being used for object detection.

LiDAR systems continue to be used in detecting and avoiding, one research paper which investigates comparing two types of systems in a controlled environment was authored by Daniel Faust [22] .In this paper Daniel Faust focused on examining the interference between the two depth measurement sensors Hypersen HPS-3D160 and Intel RealSense D435. This document looked more at using the LiDAR for detecting space debris objects, whereas this research will be more focused on powerline detection in standard operating conditions. According to the author the LiDAR performed well minus the side effects from the influences.

Another research paper that mentions the Hypersen HPS-3D160 was by J. H. Mott and B. Kotla, [16]. This research paper investigates the issue of the accidents involving vehicles passing school bus when stopped causing injuries of death. The author uses the LiDAR for vehicles as they approach the bus while the stop sign is out and then this triggers the dashcam to take an image of the passing vehicle license plate, in addition they also used an LCD display to illustrate the data for the LiDAR system. Figure 9 shows the results data from the experiment conducted and the experiment was deemed a success as it was less expensive than the other alternatives, the next step would be to make the connection of the LiDAR remote.

Measured Distance (meters)	LiDAR-measured Average Distance (millimeters)	Camera-triggered/Plate Captured (YES/NO)
1 m	996 mm	No
2 m	1995 mm	No
3.5 m	3493 mm	No
4 m	3989 mm	No
4.5 m	4490 mm	No
5 m	4990 mm	Yes
5.5 m	5495 mm	No
6 m	5998 mm	No
6.5 m	6495 mm	No
7 m	6995 mm	No
7.5 m	7496 mm	No
8 m	7999 mm	No
9 m	8990 mm	No
9.5 m	9945 mm	No
10 m	9994 mm	No

Figure 9: Sample result data [16]

Typically, LiDAR technology is associated with being expensive, and sometimes slightly difficult to work with. The research paper by D. Fernandes et al. [23] investigates using a low-cost LiDAR set up to conduct object detection. There was heavy focus on using the point cloud data for the deep learning application and according to the author there were some limitations due to the low-cost stimulation. The research paper addresses some of the steps that would be involved in object detection and simultaneous localization and mapping.

The research paper written by X. Li and Y. Guo "[17] goes into detail on the principle of how LiDAR works during PTL inspection and how the data is processed after the inspection is completed. Figure 10 below shows the data the author collected, indicating there is potential for the LiDAR to provide more information during the inspection. This provides the basis on which future research can be conducted into LiDAR technology for

possible real time processing and PTL detection as LiDAR as been used for similar applications as object detection in vehicles.

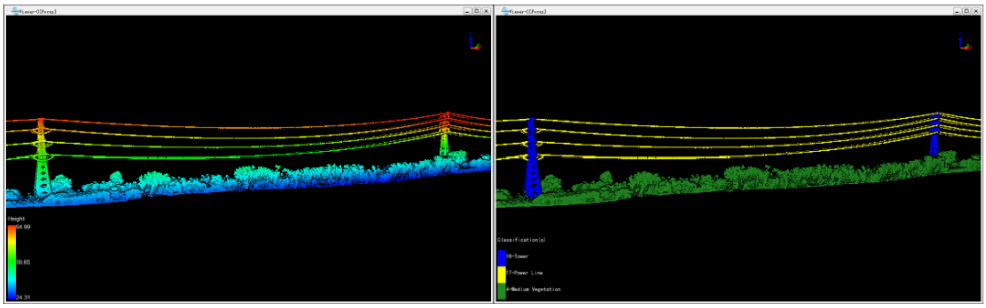

Figure 10: LiDAR sample data from research paper[17]

As the previously mentioned papers looked more in LiDAR and the usage of LiDAR in object detection applications, here are a few research papers based on remotely piloted aircraft (RPA) systems and power transmission lines (PTL) inspections. “Two-Layer Routing for High-Voltage Powerline Inspection by Cooperated Ground Vehicle and Drone”[24], this research paper investigates using both a ground vehicle and RPA to conduct high voltage powerline inspections. “Design, Integration and Implementation of an Intelligent and Self-recharging Drone System for Autonomous Power line Inspection”[25], this research papers investigates the idea of making PTL inspections full autonomous as still having to manually control the RPA in each phase of the inspection according to their research would not be very efficient. “A Drone Based Transmission Line Components Inspection System with Deep Learning Technique”[26] this research paper examines the use of deep learning techniques (convolutional neural networks (CNNs)) to detect PTL components such as cracked insulators, and broken wires rope and analyze them for damage. LiDAR systems are used in any different applications, the accuracy and

performance on different surfaces is a factor to consider as PTL are made up of different components.

2.2.5 LiDAR Performance around Different Surfaces.

As LiDAR systems emit a laser of light to a surface, a concern arises in which difference surfaces can affect the accuracy of a LiDAR system. A research paper that investigates affect of the accuracy of LiDAR is “Effects of temperature environment on ranging accuracy of LiDAR” by Shanghai Radio Equipment Research Institute[27]. What they did was to investigate the different in time between the pulse transmitted and the pulse returned and found that as the temperature increased in the environmental conditions so did the difference in time between the transmitted pulse and the returned pulse. It is scientifically known that darker objects absorb wavelengths better than lighter objects. As lasers are a form of light, it brings up an important question, how are LiDAR system’s accuracy affected by darker objects? PTLs after a period become aged and the color can go from shiny silver to fully black. The emitted light from a laser is also known as “coherent light” since the light emitted is different to that of emitted by the sun or a light bulb. The light emitted from a laser if directional while the light emitted from the sun, or a light bulb goes in many different directions.

2.3 Regulations

RPA operations over the vicinity of Canada are currently governed by Transport Canada and for operations in the United States (US) the airspace is regulated by the Federal Aviation Administration (FAA). Transport Canada, like FAA oversees the establishing, managing, and developing safety and security standards and regulations for civil aviation, which also includes unmanned civil aviation.

As the popularity of RPAS increases, more regulations are being implemented to control how RPA are being used. These regulations ensure that any misuse of RPA will result in fines, jail time or both. For RPAs pilots in Canada should follow the rules in the Canadian Aviation Regulations (CARs) more specifically the rules and regulations in CARs Part IX [28]. For RPA pilots in USA should follow 14 CFR Part 107 Small Unmanned Aircraft Systems [29].

In comparing the rules and regulations from both Transport Canada and FAA there are a number of similarities, there are however some differences in the two. FAA was the first to implement a section of their airspace regulations specifically for RPAS as Canada followed some time after. For both, there is a requirement for the RPA to be registered and the registration number on the RPA to be always visible. RPA pilot certificate is required for both. Transport Canada has their RPA certificate divided in basic operations and advance operations, FAA label theirs recreational and commercial operations. The basic and recreational section are very identical, they are both the lowest level certificate for which an RPA can have. Next level for Transport Canada and FAA is the advance operations and commercial operations respectively, this level allows for RPA pilots to perform services and receive compensation. Operations involving beyond visual line of sight (BVLOS), for Transport Canada they have a special flight operations certificate (SFOC) a copy of this application can be found in the appendix section of this document. For the FAA, their have a BLVOS wavier and it is reviewed on a case-by-case basis. Some of the main RPA rules and regulations both Transport Canada and FAA have are as follows; fly at or below 400 feet above ground level (AGL), keep your drone within sight, do not fly in restricted airspace, do not fly near other aircraft, especially near airports, do not fly

over groups of people, do not fly over stadiums or sporting events, and do not fly while impaired. As of this moment, FAA is starting to implement the use of Remote ID in all RPA registered in the US[30].

Both FAA and Transport Canada classify their airspace differently and this can be seen in Figures 11 and 12 respectively.

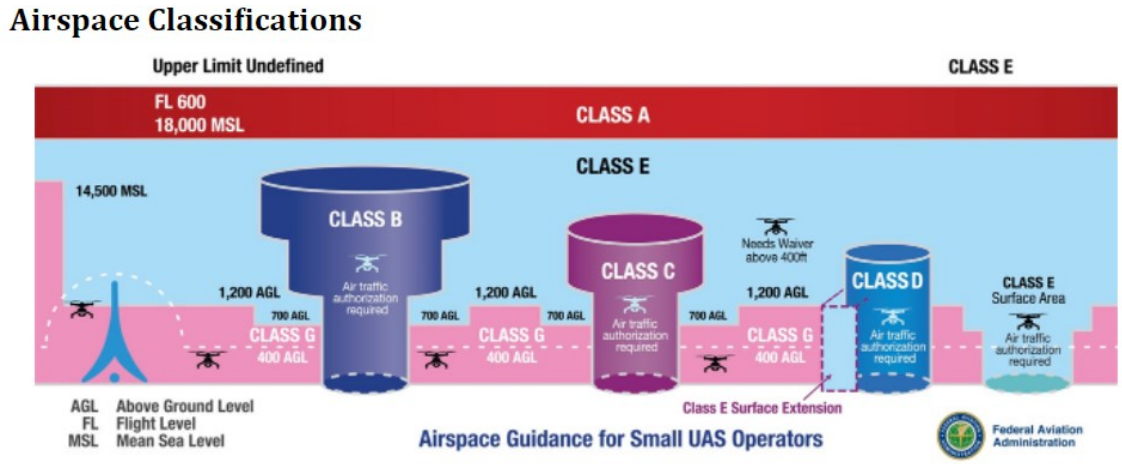

Figure 11: FAA Airspace Classification[29]

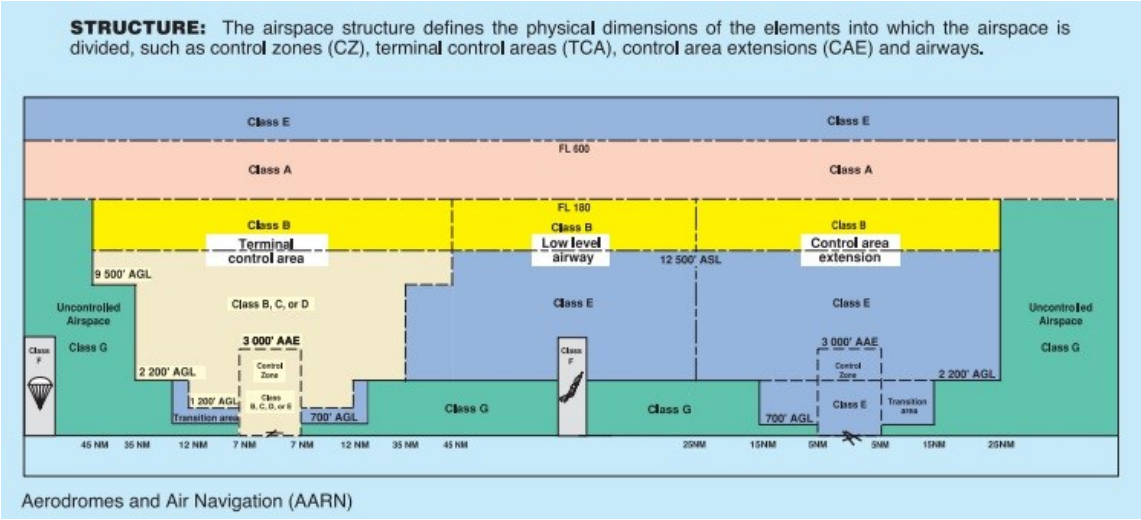

Figure 12: Transport Canada Airspace Classification[31]

For this research, the focus will be on the Transport Canada rules and regulations. Part IX of CARs contains most of the rules and regulations that apply to drones up to twenty-five kilograms, (above 25 kilograms a special flight operation certificate is

required) operations over civilians, and beyond visual light of sight operations. Transport Canada divided up their obtainable certifications for RPAS operators from Basic Operations, which are for recreational or negligible risk operators. The next certification is Advanced Operations certificate, this is based around the operators using their RPA for commercial purposes, in controlled airspace (non-Class G) and/or near bystanders. These operations both require a visual observer to be present.

For unusual circumstances where an operation has been done outside of the of Advanced operations certification, the operator/s would have to apply for a special flight operations certicate (SFOC). A scenario of this would be an overhead line inspection, these operations usually involve the RPA being beyond visual line of sight (BVLOS). As of writing this document, SFOCs are only issued if the operator demonstrates to the Minister (Transport Canada) that they will be able to perform the operation without affecting the safety of others in the operations area.

2.4 Examples of Remotely Piloted Aircraft Systems

Table 1: Examples of RPAS used in Overhead Line Inspections

Make/Model of aircraft:	**Payload (s):**	**What it was used for but not limited to:**
DJI M200 and M300 series	DJI Zenmuse L1, H20T, XT2 R, P1	LiDAR mapping, surveying, infrastructure inspections etc.
DJI Mavic 2 Enterprise: Industrial Scout Package	Spotlight, Beacon, loudspeaker	Search and rescue and structural inspections etc.
Autel Evo II Dual	FLIR thermal 640 sensor, 8K Visible Sensor	Infrastructure inspections, search, and rescue etc.
Altura Zenith RTF	Pensar, minirae 3000, RFID scanner	Landfill monitoring, infrastructure inspections etc

Table 1 gives an example of a few RPAS that can be used for conducting PTL inspections, these are the more commercially available RPAS. Custom RPAs are also used to perform these types of operations. Harris Aerial's carrier h6 hybrid is one such custom RPA used in operations like that of overhead powerline inspection. This is just one example of a custom RPAS as there are many other excellent examples. The benefit of having a custom build RPA is the flexibility of customizing of the different components based on the operation to be performed. The PIC of custom RPA should ensure that their aircraft follows the guidelines provided by Transport Canada. As these RPAS can be used for inspection, they would also have the capability for being used in detection of PTLs as well.

2.5 Proposed Solution

By reviewing the previously mentioned research papers, one common limitation for RPA performing PTL inspection was the detection aspect as PIC focus more on their proximity to the PTL rather than collecting the data, directly increasing the margin for error in the collected results. Since LiDAR systems are already being used in the inspection of the PTL structures, the focus of this research will be accuracy of detection of different PTLs of light-weight low-cost LiDAR systems on RPAS. The RPA systems used will be the smaller and more commercially available ones. To complete the objectives mentioned in Chapter 1, the research will have been conducted in a neutral environment (neutral environment refers to an environment with as minimal interference as possible) and different samples at different distance to evaluate the limits of the selected LiDAR systems.

The theoretical solution for this thesis investigated the development of LiDAR systems for RPA. LiDAR systems has proven to be a very resourceful system for detection and avoidance as it is already used for vehicles' detection and avoidance systems. The focus of the research and analysis portion of this paper will investigate and compare available LiDAR systems (2D and 3D LiDAR). The comparison will look at how well the LiDAR are able to detect selected objects and then a de-energized and energized PTL sample. In addition, the LiDAR must be lightweight to prevent any significant lost in the RPA's flight maneuverability. As many RPA already have some version of a camera, and at this moment very few uses LiDAR. For the ones that use a LiDAR system, it is also a matter of looking into retrieving additional information for detection of PTLs.

Chapter 3: Methodology

3.1 Overview

LiDAR systems have been used on RPA to assist in PTL inspection process and in other applications, such as object detection for autonomous vehicles and robots as well as 3D scanning of buildings, terrain, and objects. Currently on the market there are many LiDAR systems including 1D (single point), and 2D, 3D scanning versions. As such it is important to select to correct LiDAR or combination of LiDAR systems that will fulfill the mission. This chapter provided an overview of the methodologies used to complete this thesis, as well as the software systems used to assist with the evaluation of the LiDAR systems.

3.2 Testing Set up and Mission Profile

LiDAR systems used in PTL inspections focus on the structural components as shown in Figure 13. The testing for this research focused entirely on the PTL and how the selected low-cost light-weight LiDAR systems performed around the PTL conductors themselves. The LiDAR data was collected from each of the selected LiDAR systems and was analyzed post collection. Each test was run more than once, this was done to check consistency in the results.

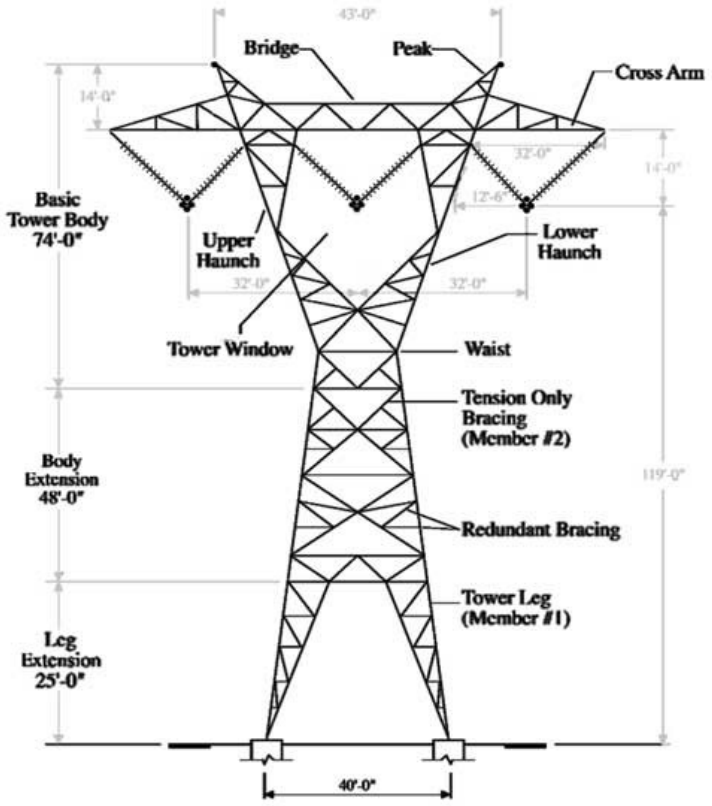

Figure 13: Single Circuit, Horizontal Configuration, Self-Supported Lattice Tower[32]

In evaluating LiDAR systems, the first approach is performing a bench test to understand the strengths and limitations of each selected LiDAR systems. Bench tests simplify the evaluation process by removing the requirement to obtain special flight operations certificates and outdoor laser operation permits from Transport Canada in performing a bench test it achieved the following:

- Understanding limitations of the selected LiDAR systems
- Determining the software compatibilities
- Testing various objects to understand the selected LiDAR systems

After the bench test was done, the selected LiDAR systems will be mounted on an RPA and with the motor running to identify any sources of interference. The data collected from each LiDAR system are post-processed by analyzing using Microsoft Excel and MATLAB

and compared to each other. Microsoft Excel was used for the initial comparison and rapid visualization by means of the function “conditional formatting” and to clean up the data for use in MATLAB. MATLAB was used to perform the root-mean squared deviation (RMSD) which is how the accuracy of each LiDAR system was determined. The LiDAR was then mounted on some of the RPAS (listed in Section 3.4) and similar test to that of the bench test was done. For the LiDAR mounted on a RPAS test was to see the following:

1. LiDAR performance around another RPAS components
2. Any differences in the data collected on the bench versus on an RPAS, and
3. Does there need to be a combination of LiDAR systems better detection

A testing matrix was used for understanding the capabilities of each of the selected light-weight LiDAR systems, mostly from a visual perceptive. To ensure the accuracy of the test being conducted a testing stand was used (as shown in Figure 14), the purpose of this is allowing all test to be consistent testing conditions.

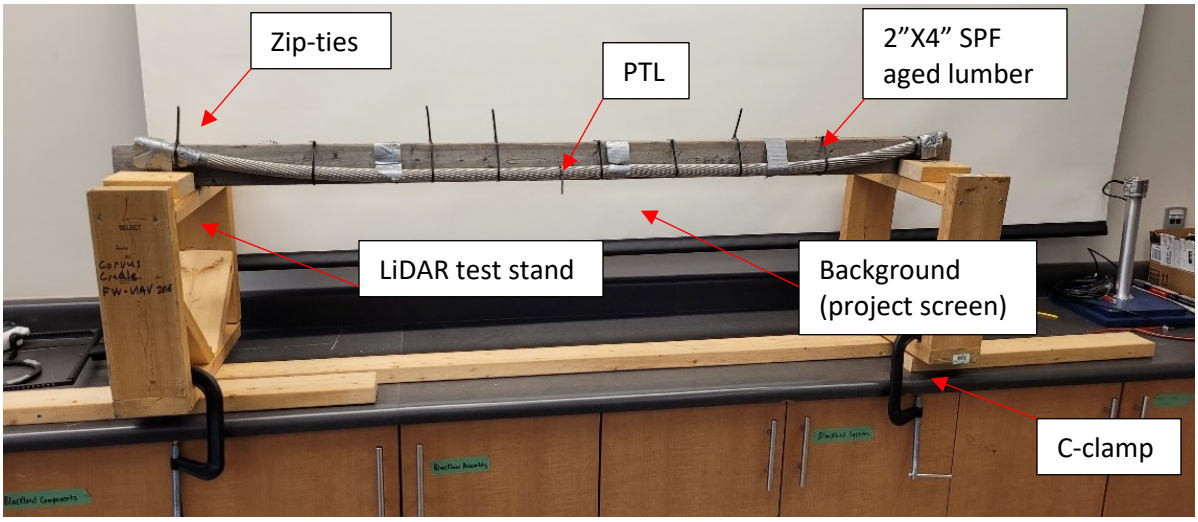

Figure 14:Initial LiDAR Testing Stand

Mission Profile

The mission profile from the research phase (beginning) to the completion (end) phase was as follows: the research and bench test phase involved the gathering equipment

and setting up test. The next phase was the validation and verification phase (validation refers to equipment meeting the users needs and objectives, while verifications determines if the design meets the requirements and specifications as advertised) which involved collecting test data to verify the LiDAR system worked as expected. The verification section of validation and verification phase suited the needs of this research regarding the initial examination of the selected low-cost light-weight LiDAR systems. This was achieved by evaluating the LiDAR system against different objects.

The following phase was the performance comparison, which involved comparing the advertised specifications of the selected LiDAR systems to each other, this allowed better understanding of the specifications such as the advertised FOV and the detection range. A data comparison was done, where the data of selected systems were comparison based on actual measurements versus the measurements taken by the selected LiDAR systems along with the conditional formatting technique being used. The root mean squared (RMSD) deviation for the data used in the pervious phase and a graph of RMSD vs observation was plotted to examine how each of the selected LiDAR system performance and the possible deviation in the data results. The RMSD method was used to better understand difference between the actual vs taken measurements and what were the highest deviation at what observation. Data was collected for PTL samples de-energized and energized; an interference comparison was also done to determine how much the background (and/ or testing area) behind the PTL samples had an influence on the results and analysis. After a mini case study was done, which involved collecting data at 0.5m using the LiDAR systems attached to an RPA to see if when powered on, the components

of the RPA would have an additional impact on the selected LiDAR systems. With this a conclusion was written, and recommendations were provided along with future work.

3.3 Power Transmission Line Samples

There are several types of PTLs used in the field, to ensure the accuracy of the the light-weight low-cost LiDAR systems of this research, various samples of PTLs were obtained and evaluated. These samples are predominantly used in a real-world situation, so it allows for closer to real world simulation. This section will describe the collected PTL samples, their technical names, and a brief description about each sample.

"KCMil – A method of measuring conductor size that stands for thousand circular mils. K represents kilo for 1,000. C represents circular, and mil, M, is 1/1000 of an inch. A wire that is one mil in diameter has an area of one circular mil or 1 KCMil. KCMil replaced MCM for sizing conductors."- Electric Utility Training by Professional Training Systems, Inc

Figure 15:PTL Sample Codename: ACSR Drake

PTL Sample Specifications
Size: 795 KCMil
No. of Strands: 26
Nom. OD: 28.13 mm
Nominal total linear weight: 1627 kg/km
Construction: "Aluminum 1350-H19 wires, concentrically stranded about a steel core. Standard core wire for ACSR is class A galvanized. Class A core stranding is also available in zinc-5% aluminum-mischmetal alloy coating."[33]

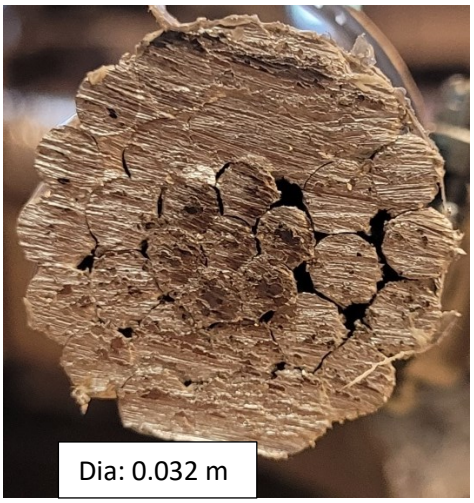

Figure 16:ACSR Drake cross-section

Figure 17:PTL Sample Codename: ACSR Condor

PTL Sample Specifications
Size: 795 KCMil
No. of Strands: 54
Nom. OD: 27.73mm
Nominal total linear weight: 1521 kg/km
Construction: "Aluminum 1350-H19 wires, concentrically stranded about a steel core. Standard core wire for ACSR is class A galvanized. Class A core stranding is also available in zinc-5% aluminum-mischmetal alloy coating."[33]

Figure 18: ACSR Condor cross-section

Figure 19:Sample PTL Codename: ACCC Rome

PTL Sample Specifications
Size: 1169 KCMil
No. Of Strands: 21 est.
Nom.OD: 29.90mm
Nominal total linear weight: 1641.9 kg/km
Construction: ACCC is produced with 1350 O-tempered aluminum. ACCC exhibit lay length (ratios) that conform to ASTM B 857 or EN 50540. Minimum tensile strength of annealed aluminum conforms to ASTM B 609 and EN 50540

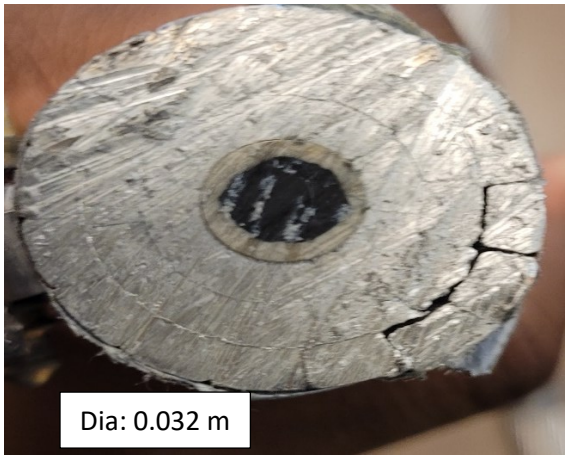

Figure 20: ACCC Rome cross-section

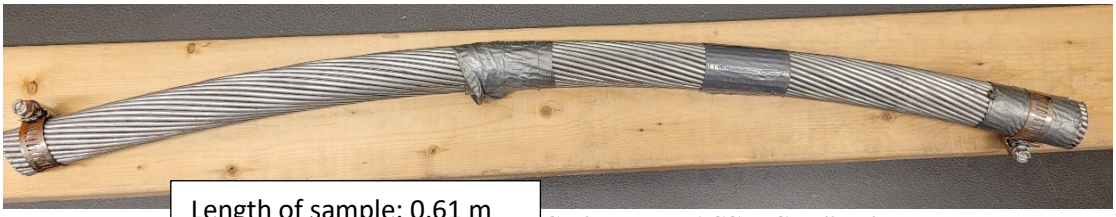

Codename: ACSR Cardinal

PTL Sample Specifications
Size: 954 KCMil
No. Of Strands: 54
Nom.OD: 30.38mm
Nominal total linear weight: 1826 kg/km
Construction: "Aluminum 1350-H19 wires, concentrically stranded about a steel core. Standard core wire for ACSR is class A galvanized. Class A core stranding is also available in zinc-5% aluminum-mischmetal alloy coating."[33]

Figure 22: ACSR Cardinal cross-section

Table 2: Power Transmission Line Sample Specifications Summary

PTL Sample Codename	Size (KCMil)	No. of Strands	Nom.OD (mm)	Nominal total linear weight (kg/km)
ACSR Drake	795	26	28.13	1627
ACSR Condor	795	54	27.73	1521
ACCC Rome	1169	21	29.90	1642
ACSR Cardinal	954	54	30.38	1826

Table 2 summarizes the specifications of each of the PTL samples. From the specifications ACCC Rome as the highest KCMil while ACSR Drake and ACSR Condor have the lowest, ACSR Condor and ACSR Cardinal has the most strands while ACCC Rome have the least. For the total kg per km ACSR Cardinal is the heaviest and ACSR Condor is the lightest. From the table, it would be expected the PTL sample with the largest number of strands to be more visible to the selected LiDAR systems, the same is expected for the PTL with the largest Nom. OD.

3.4 LiDAR Systems and Specifications

This section showcases the selected low-cost light-weight LiDAR systems used in this research. These LiDAR systems were chosen based on availability, weight (as this will

be a key factor in relation to the RPA flight performance) and specifications. For the remainder of this document, the Hypersen HPS-3D160/ 3D Solid-State LiDAR/ 3D TOF Ranging Sensor and the Cygbot CygLiDAR D1 will be labelled as “LiDAR A” and “LiDAR B” respectively. This research focuses on characterization and comparison of the LiDAR’s specifications and features rather than the company and brand.

LiDAR A- Hypersen LiDAR: HPS-3D160/ 3D Solid-State LiDAR/ 3D TOF Ranging Sensor

Figure 23:HPS-3D160/3D Solid State LiDAR (LiDAR A)[34]

Table 3: HPS-3D160/3D Solid State LiDAR Specifications

Measuring range	0.25 – 12 m
Weight	110 *1 g
Power consumption	3 – 5 W
Precision	± 2 cm
Frame rate	35 Hz / Adjustable
Communication interface	USB, RS23, IO, LAN
Power supply	12 – 24 V
Operating temperature	-10 ℃ – 55 ℃
Output data	Depth data, average distance, signal strength, quantity of weak signal pixels, quantity of saturated pixels, maximum distance, minimum distance
Emitting angle	76 °（Horizontal）x 32 °（Vertical）

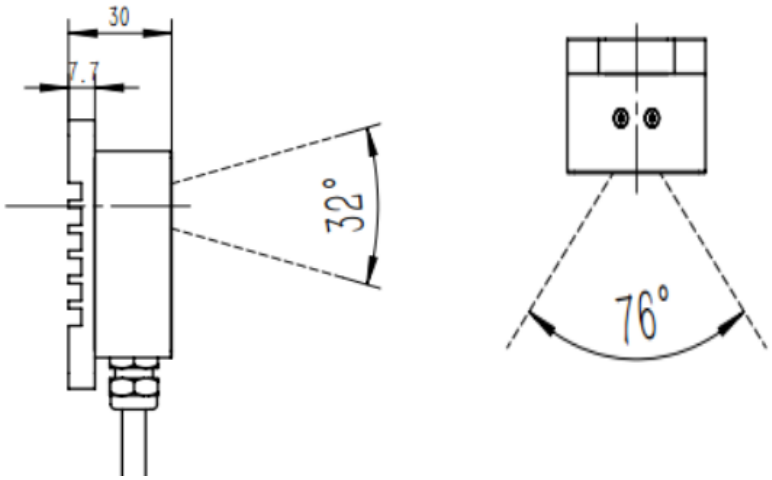

Figure 24: LiDAR A Field of View[35]

Table 4:LiDAR A Timing Modes

Integration time mode			
Mode	Applications	Integration Time Description	Frame Rate
HDR-DISABLE	Static and fixed environment	Manual setting	The longer the integration time, the lower the frame rate
AUTO-HDR	Obstacle avoidance, sensitive to close proximity environment	Auto adjust	High
SUPER-HDR	Most objects in the environment, black objects are also identifiable	Calculate the remaining frames based on the set maximum integration time	Low
SIMPLE-HDR	Measuring environment within a specified distance	Adjust two sets of integration time according to the measurement distance range	Medium, stable

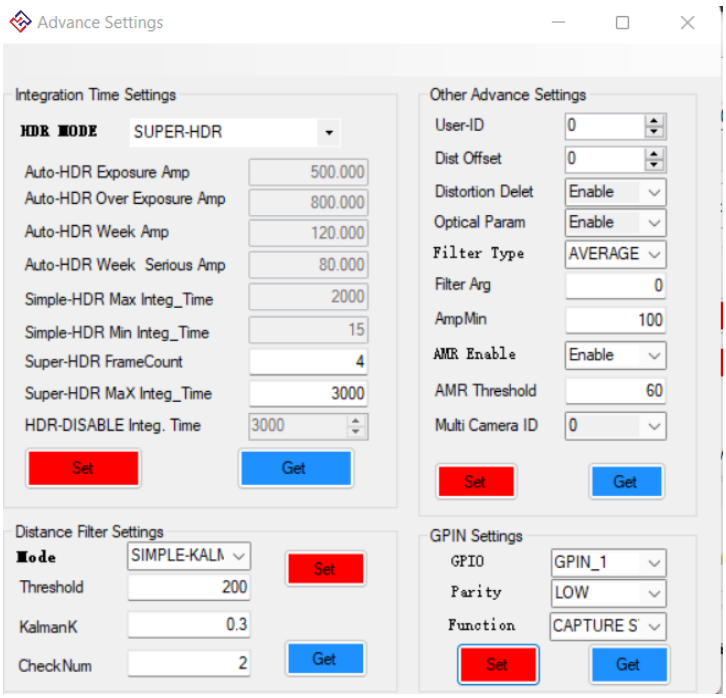

Figure 25:LiDAR A Advance Settings

Figures 23 – 25, and Tables 3-4 display the essential information about LiDAR A available at the time of conducting this research. Figure 23 displays how the LiDAR A looks without the connection wires. Table 3 shows the specifications of LiDAR A such as weight, frame rate and emitting angle. Figure 24 shows what the projected area would be for LiDAR A based on the FOV with mathematical calculation. Table 4 show the timing modes integrated into LiDAR A, for this research SUPER-HDR mode was used. Figure 25 show the advance settings that were used for this research.

LiDAR B-Cygbot CygLiDAR D1

Figure 26: LiDAR B- Cygbot CygLiDAR D1 2D/3D Dual Solid State TOF LiDAR[36]

Table 5: LiDAR B Specifications

Detection Range	Range affected by reflectivity 2D: 200mm ~ 8,000mm 3D: 50mm ~ 2,000mm (*DRM)
Distance Accuracy	±1%
Resolution (mm)	2D: 1° (Angle) 3D: 160 x 60 (Pixel)
Field of View (FOV)	2D/3D Horizontal: 120° 3D Vertical: 65°
Wavelength	*Laser Diode: NIR 808nm LED: NIR 808nm
Measuring speed	2D: 15Hz 3D: 15Hz
Dimensions (W H D)	37.4 * 37.4 * 24.5 (mm^3)
Weight	28g
Interface	UART TTL 3.3V 3,000,000 bps
Input power source	5V, 500mA
Operating temperature	-10°C ~ 50°C

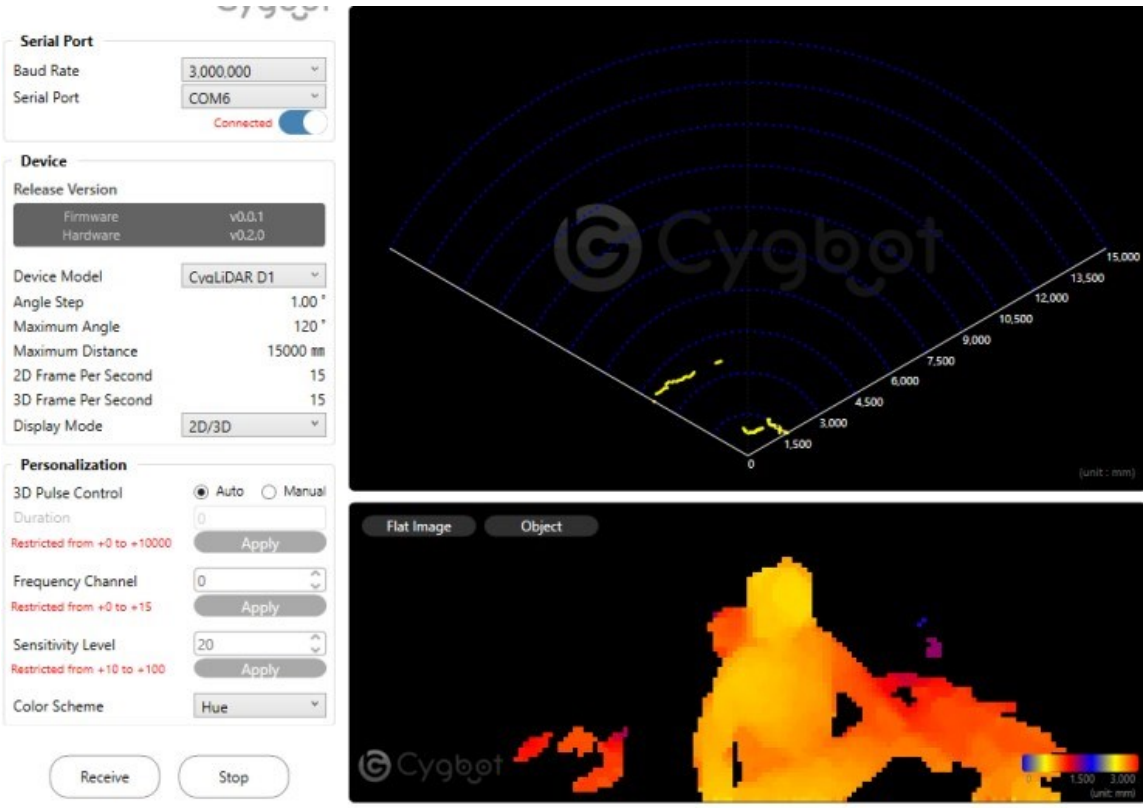

Figure 27:Cygbot's CygLiDAR Viewer for LiDAR B

Figures 26 – 27 and Table 5 display the essential information about LiDAR B available at the time of conducting this research. Figure 26 displays an image of how LiDAR B looks without the connection wires. Table 5 summarizes the specifications of the LiDAR B, with information on the detection range, FOV and weight. Figure 27 show the setting (on the left side of the image) and the real-time data viewer (on the right side of the image).

3.5 Remotely Piloted Aircraft Systems (RPAS), specifications and control systems

Towards the end of this research, different RPAS were used to conduct test/ simulations flights. Even with the focus of this thesis being comparing the different LiDAR system, the type of RPAS being used are commercially available and purchased by the Carleton University's Mechanical and Aerospace engineering department. The reason for using commercially available RPAS is to have reliable test flights and test how the LiDAR system affects the flight characteristics of the commercial RPAS. This section will outline relevant information of each RPAS, and control systems used and/or researched for potential work.

3DR Iris+

Figure 28: 3DR Iris+ multirotor RPAS

The 3DR Iris+ is a quadcopter designed and sold by 3D- Robotics, the intent behind this quadcopter was to allow researchers and developers a DIY (do it yourself) RPA that can be modified to accommodate several types of payloads. This RPA was useful for understanding how to mount and integrate different LiDAR systems into a current RPA. Unfortunately, RPA has been discontinued and is no longer in production. However, the

completed CAD models and drawings were released and made open source by 3DR for continued community development.

Table 6: 3DR Iris+ Specifications

Motor to motor dimensions	550 mm
Weight (with battery)	1282 g
Average flight time	16- 22 minutes
Payload capacity	400 g
Flight controller	Pixhawk

Raspberry Pi 3

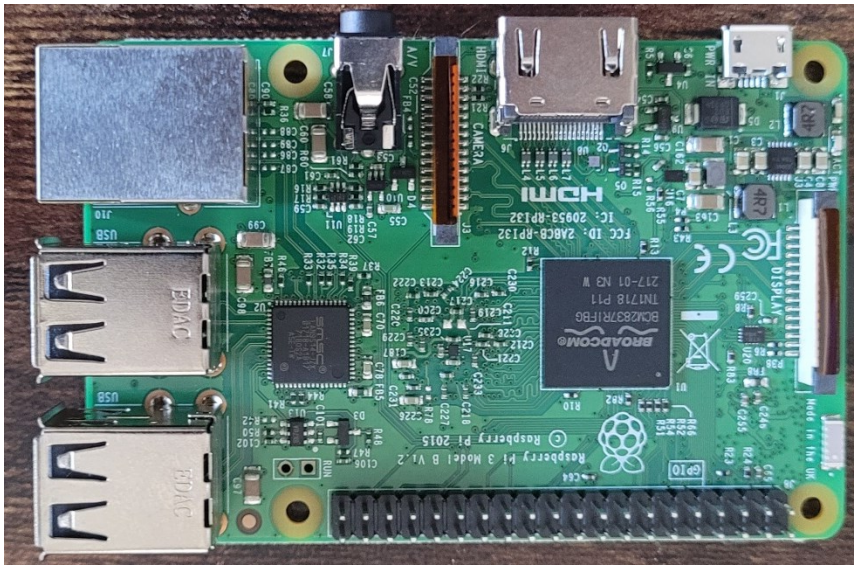

Figure 29:Raspberry Pi 3 Model B

Raspberry Pi3 Model B is the first model of the generation three of the Raspberry Pi models. The Raspberry Pi3 was used with LiDAR A for data collection. The Raspberry Pi was able to successfully collect the average distance of the nearest object to LiDAR A.

The Raspberry Pi3 was to be the replace of a desktop, to allow different programming languages to be used with the selected LiDAR system for this project.

Table 7: Raspberry Pi 3 Model B Specifications

Processor	Broadcom BCM2837 64bit
Clock Speed	1.2GHz
Memory	1GB LPDDR2
Power	Micro USB socket 5V1, 2.5A
GPU	Dual Core Video Core IV® Multimedia Co-Processor. Provides Open GL ES 2.0, hardware accelerated OpenVG, and 1080p30 H.264 high-profile decode.
Dimensions	85 x 56 x 17mm

3.6 Ground Stations

The ground station refers to the hardware platform which was used for data processing as this plays a significant role in how the data was processed for this research. The following mentioned computers are what were to process the several types of data produced by the LiDAR systems.

HP ENVY x360 I-3- Laptop

Table 8: HP ENVY X360 I7 Specifications

Operating Systems	Windows
Processor	Intel® Core™ i7-1165G7 2.8GHz, 4 cores + Intel® Iris® Xe Graphics and 8 Logical Processors
Installed Physical Memory (RAM)	12.0 GB
Resolution	1920 x 1080 x 60 hertz

Microsoft Surface Pro 7 I-3

Table 9: Microsoft Surface Pro 7 I-3 Specifications

Operating Systems	Windows
Processor	11th Gen Intel® Core™ i3- 1005G1 1.20 GHz, 2 cores, 4 Logical Processors
Installed Physical Memory (RAM)	4.0 GB
Resolution	2736 X 1824 X 59 hertz

Figure 30: HD Digital Camera by ELP

Figure 30 shows the camera used to take the photos, the camera was chosen based on availability and image quality. The model of the camera is ELP-USBFHD05MT-KL36IR. It was determined the camera has a smaller FOV than both selected LiDAR systems. The FOV was determine by visibly comparing the objects in captured by the camera and the objects captured by the selected LiDAR systems, and it was determined that the LiDAR systems had a larger FOV. This information is important for the verification section of this research.

Table 10: HD Digital Camera Specifications

Resolution	2.0 Megapixel 1080p
Sensor	1/2.7" CMOS OV2710
Connectivity Technology	USB
Operating temperature	-20°C – +70°C
Dimensions	42mm *42mm*42mm
Capture Speed	30 FPS
Weight	199.58 g
Image Stabilization	Optical

Chapter 4: Performance Evaluation of Systems

This chapter discusses the performance evaluation of the selected LiDAR systems. The evaluation was a validation and verification test done with the selected objects (aluminum water bottle, baseball, and football). The next evaluation was the comparison of the selected LiDAR specifications to each other. After the root-mean squared deviation was performed to evaluate the accuracy of the LiDAR systems, an interference test was done after to validate the there was not much interference product by the background.

Conditional formatting is a function in Microsoft excel that helps make patterns and trends in the data visible to the user. The data value formatting and presentation are changed based on a set of rules defined by the user. For this research project the conditional formatting rules were set as shown in Figure 31.

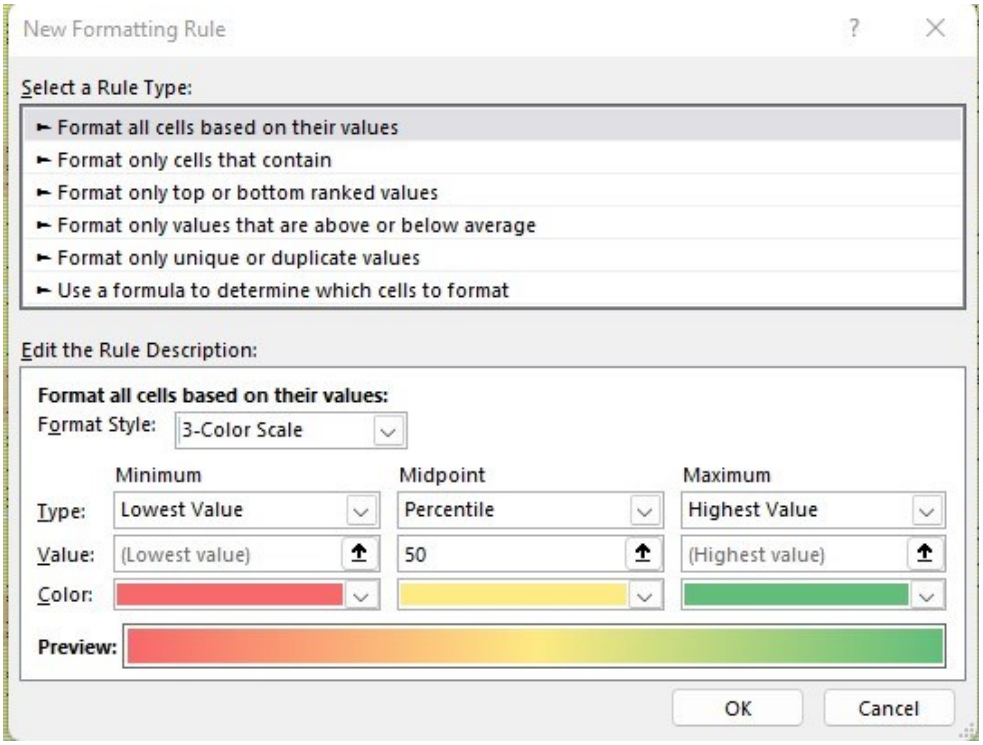

Figure 31: Microsoft Excel-Conditional Formatting Rule

4.1 Verification of Selected LiDAR Systems

In this section the selected LiDAR systems were evaluated against different objects to verify that the light-weight LiDAR system worked as advertised based on their specifications. A testing matrix was used assist with the verification process, as the limitations of the selected light-weight LiDAR systems were examined. These limitations included distance from the object in question, if material and surface texture had any affects on the LiDAR systems ability. The selected objects used were an aluminum water bottle, CFL (Canadian Football League) official size football and an official league baseball. These objects were chosen based on their dimensions, texture, material, and availability of information on the objects. The aluminum water bottle was chosen due to its similarities to that of a PTL. For the verification of the selected LiDAR systems the other objects in the FOV of the LiDAR system were not considered as the distance from the LiDAR systems were known as well as the shape of the objects.

Images of the objects and their dimensions can be found in the Appendix section of this document. For this section, the data displayed/discussed will be from for the metal water bottle at 0.5m as it would be the closest selected object in material to that of the PTLs.

General Tasks of the Verification of Selected LiDAR Systems:

- Determine the software needed for each of the selected light-weight LiDAR systems interface.
- Examine data output and finalize a common data output between the two selected light-weight LiDAR systems.

Figure 32:Aluminum water bottle from LiDAR stand view

4.1.1 LiDAR A

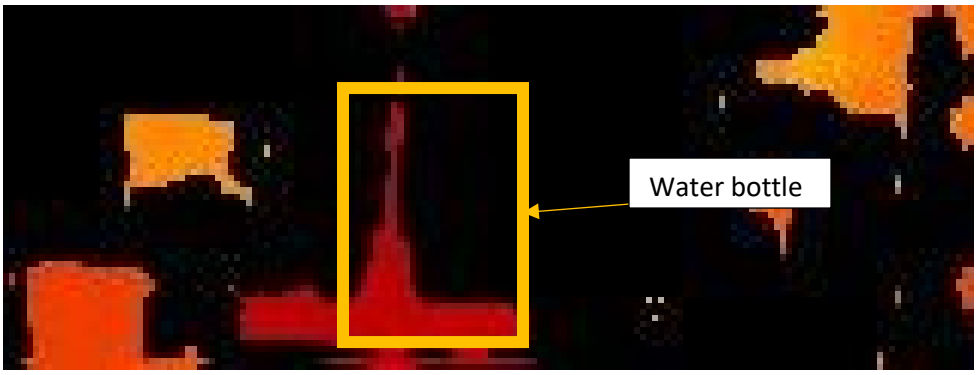

Figure 33:LiDAR A screenshot of aluminum water bottle at 0.5m

Figure 33 shows a screenshot of the LiDAR A as it was collecting the point cloud data at 0.5 m, Figure 32 shows a picture of the original object. In Figure 33 the highlighted yellow box shows the location of the aluminum water bottle, and the color scale was red (object closest to LiDAR system), orange has the mid point and black as the LiDAR system

is not detecting any objects in that area. The data output came as CSV files, then conditional formatting function was used to be able to view the point cloud data in a 2D format for verification purposes. Along with what was shown in Figure 33, LiDAR A interface also as a graph mapping the average distance, a visual representation of the 3D point cloud data. For this research, the software used was HPS-3D160 client master which was developed by the Hypersen company for use of their HPS-3D160 devices.

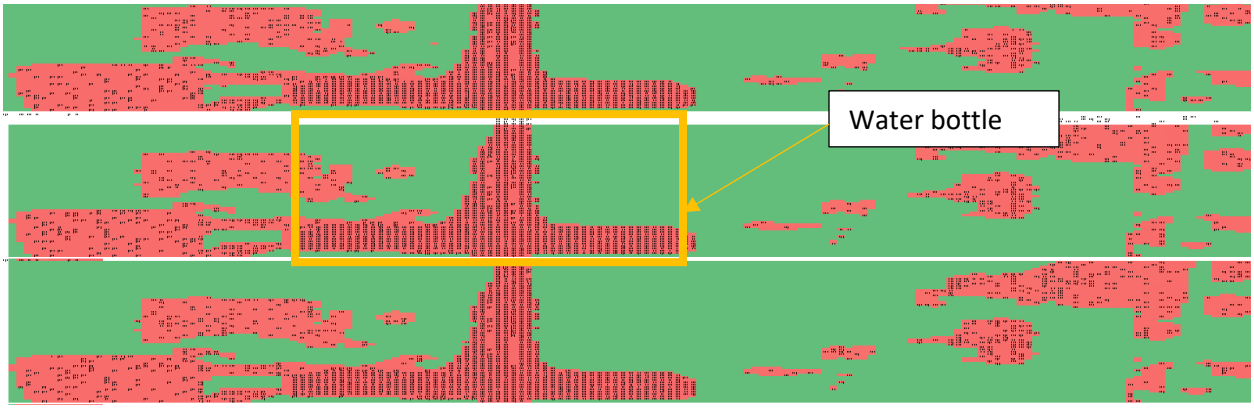

Figure 34:LiDAR A point data conditional formatted

Figure 34 shows the conditionally formatted data from LiDAR A at 0.5 m, The color scale helped understand data distribution and variation of the object in question. The color scale was selected based on the point thresholds, minimum point (red), midpoint (yellow), and maximum point (green). Visually comparing Figures 34 and 33, the FOV of Figure 29 is larger than that of Figure 28. Comparing the Figure 33 to Figure 32, the aluminum water bottle image is slightly disfigured, this can imply that LiDAR A does not work well with curve surfaces.

4.1.2 LiDAR B

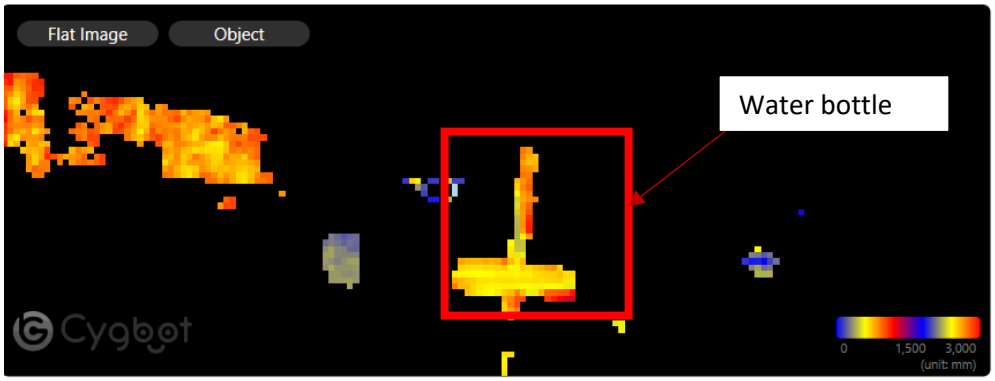

Figure 35:LiDAR B screenshot of aluminum water bottle at 0.5m

Figure 35 shows a screenshot of the LiDAR B (the original object can be found in Figure 32) as it was collecting the point cloud data at 0.5m. The data output came as text files, these files then had to be converted to CSV file by importing them into Microsoft Excel. For LiDAR B interface it shows the color scale and the relative distance in milliammeters as the data is being collected. The aluminum water is highlighted in the red box of Figure 35, the FOV of LiDAR B is notably larger than that of LiDAR A which is corrected based on the specifications of both LiDAR systems. The interface of LiDAR B is simple to use, for this research the software downloaded was CygLiDAR Viewer, developed. Developed by the Cygbot company for use with their devices.

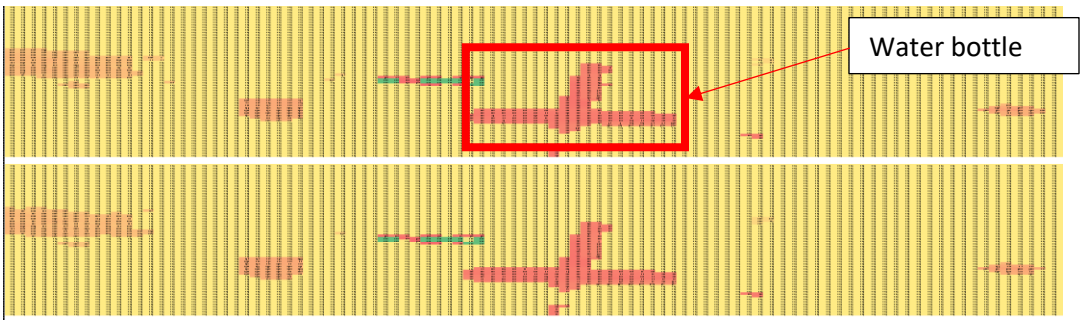

Figure 36:LiDAR B data 2D conditional formatted

Figure 36 shows the conditionally formatted data for LiDAR B at 0.5 m. After the data was collected, it was then imported into Microsoft Excel and use its conditional

formatting function to be able to view the point cloud data in a 2D format for verification purposes. The color scale was selected based on the point thresholds, minimum point (red), midpoint (orange), and maximum point (yellow/ green) as shown in Figure 31. In comparing the Figures 35 and 36, it is clear to see the difference in FOV and detail in the items detected. As LiDAR A the aluminum water bottle along with objects in the background as they were visible with some detail. However, LiDAR B the PTL was visible but not many of the objects in the background were visible.

Table 11: Verification of LiDAR System Results

Objects	LiDAR System		Distance measured (meters)		
			0.5	1	1.5
Aluminum water bottle	LiDAR B	LiDAR A	X	X	X
Baseball			X	X	X
Football			X	X	X

*X- denotes that the test was successful

4.1.3 Verification Results Summary

The results from Table 11 show that both LiDAR systems passed the verification test for this research. The test was considered if the LiDAR system was able to detect the objects in the raw data point cloud and post process data. The point cloud data provided by both systems was able to identify the selected objects. This test does not cover the accuracy at which they were able to see the object, and for a test to be denoted as successful, the LiDAR system had to detect both in the interface and in the post data analysis as shown in Figures 33 to 36.

4.2 LiDAR Performance Comparison

In this section, a direct comparison of the selected LiDAR systems mentioned in Chapter 3.4, their specifications. As both of this LiDAR systems are considered light weight low-cost systems, a comparison between the manufacturer specifications. The specifications used were taken directly from each manufacturer's user manual and these can be found in chapter 3.4

4.2.1 Specifications Comparison

Table 12: Specifications Comparison

Specifications	LiDAR A	LiDAR B
Weight	110g	28g
Measuring Range	250mm to 12000mm	2D:200mm to 8,000mm 3D:50mm to 2,000mm
Field of View	Horizontal: 76 ° Vertical: 32 °	2D/3D Horizontal: 120° 3D Vertical: 65°
Operating Temperature	-10°C ~ 55 °C	-10°C ~ 50°C
Precision	± 20 mm	± 10 mm (based on the data from this research)
Power Supply	12 – 24 V	5V
Dimensions	78 x 40x 30 mm	37.4 x 37.4 x 24.5 mm

4.2.2 Specifications Comparison Summary

The LiDAR B is 82 g (grams) lighter than LiDAR A. This weight comparison is just on the actual system itself and not the cable components as that can changed depending on the application. With a lighter weight system, LiDAR B would have less of an impact on an RPA performance. The measuring range starts 50 mm more on the LiDAR A,

however, LiDAR A as a measuring 4000 mm more than that of LiDAR B. Theoretically that would make the LiDAR A better for longer range detecting. The FOV is wider both vertically and horizontally on LiDAR B, and both have similar operating temperatures. Since the LiDAR B can only do USB (as of writing this document) that limits it to 5V for power supply while LiDAR A requires 12-24 V for operating. Base on the specifications provided by each manufacture both LiDAR systems have particularly useful features and depending on the application use one may have an advantage over the other. For usage on lightweight RPAS, (just based on specifications) LiDAR B would be the light-weight LiDAR system of choice.

4.3 LiDAR Data Comparison

This section compares the data values taken from each LiDAR system, this will be the first comparison done as it consisted of evaluating the LiDAR systems de-energized and at room temperature (20° C and 25 °C), the second comparison evaluated at the PTL being energized with temperature between 60° C and 120° C, these tests were done in the safety of the lab at Kinectrics, Inc. The data shown in this section are all for the distance at 0.5 m. *Note: all LiDAR distance values are in millimetres (mm). The actual measurement is the measurement from the LiDAR system to the PTL sample, the farthest measurement is the measurement from the LiDAR system to the background behind the LiDAR stands and the nearest measurement is the closest measurement taken by the LiDAR systems to the PTL. These measurements are taken from the center of the PTL.*

4.3.1 De-Energized at Room Temperature

Sample 1: ACSR Drake

Figure 37:Conditional Formatted LiDAR A ACSR Drake at 0.5 m

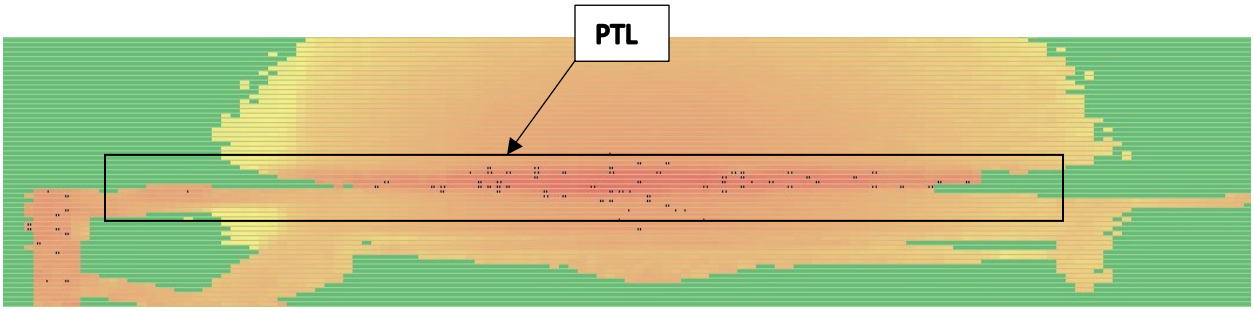

Figure 38:Conditional Formatted LiDAR B ACSR Drake at 0.5 m

Table 13:ACSR Drake LiDAR A, B Results at 0.5m

	Actual Measurements (mm)	Farthest Measurement (mm)	Nearest Measurement (mm)	Difference (Actual vs Nearest) (mm)
LiDAR A	500	1348	406	94
LiDAR B	500	4081	605	105

Figures 37 and 38 show sample 1: ACSR Drake conditional formatted at 0.5 m (500 mm), notably LiDAR B has the larger field of view as it was able to detect the LiDAR test stand. Using the same conditional formatting rules from Figure 31, LiDAR A shows the background as majority a midpoint while LiDAR B identifies it as the furthest point. Table 13 compares the real-world measurement (actual measurement) to the closest data value of each LiDAR system and LiDAR A has the lowest difference of 94 mm.

Sample 2: ACSR Condor aged

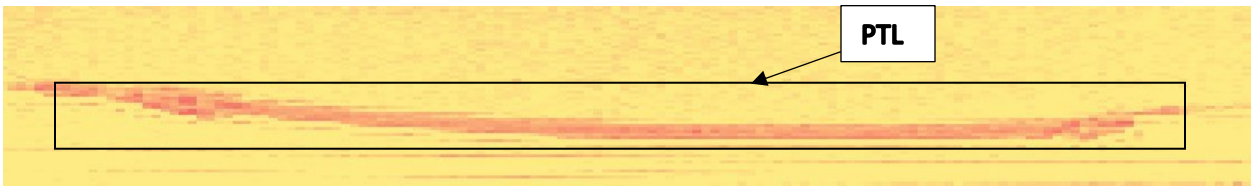

Figure 39:Conditional Formatted LiDAR A ACSR Condor aged at 0.5 m

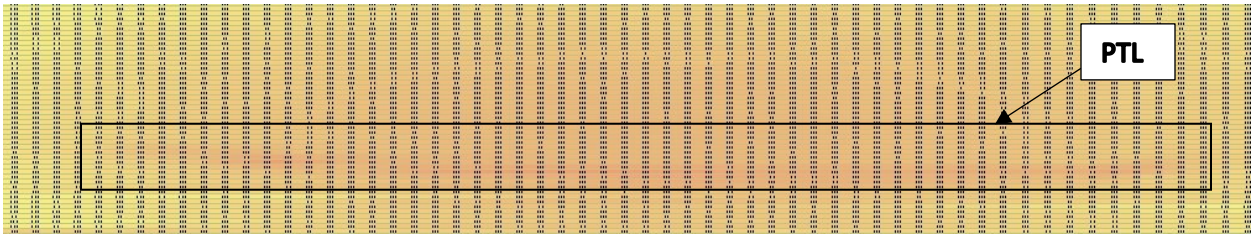

Figure 40:Conditional Formatted LiDAR B ACSR Condor at 0.5m

Table 14:ACSR Condor aged LiDAR A, B Results at 0.5 m

	Actual Measurements (mm)	Farthest Measurement (mm)	Nearest Measurement (mm)	Difference (Actual vs Nearest) (mm)
LiDAR A	500	1100	412	88
LiDAR B	500	4081	358	142

Figures 39 and 40 show the conditional formatting for sample 2: ACSR Condor at 0.5 m by LiDAR A and B, respectively. Both LiDAR system have the background as the midpoint, comparing the real-world measurement (actual measurement) to the measurement taken by the LiDAR systems, LiDAR A had the lowest distance difference of 88 mm. It should be noted, for this sample that it is an aged sample, which means the sample has served its operational life span.

Sample 3: ACCC Rome

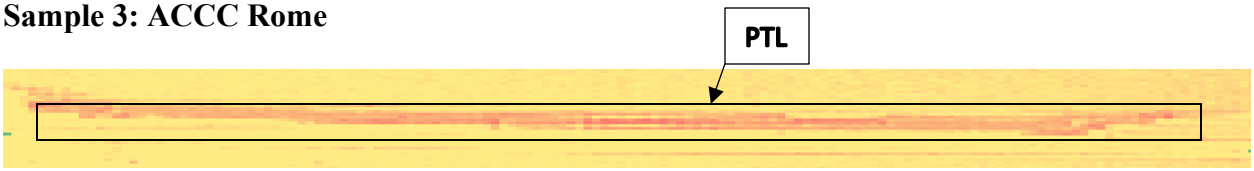

Figure 41:Conditional Formatted LiDAR A ACCC Rome at 0.5m

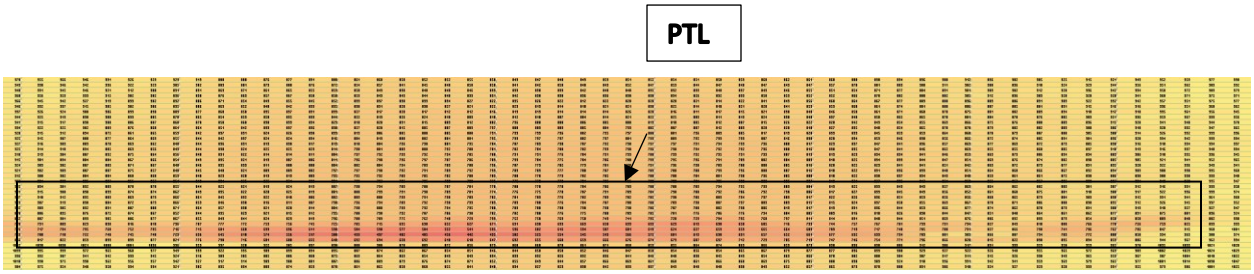

Figure 42:Conditional Formatted LiDAR B ACCC Rome at 0.5m

Table 15:ACCC Rome LiDAR A, B Results

	Actual Measurements (mm)	Farthest Measurement (mm)	Nearest Measurement (mm)	Difference (Actual vs Nearest) (mm)
LiDAR A	500	1259	471	29
LiDAR B	500	4081	442	58

Figures 41 and 42 show sample 3: ACCC Rome conditional formatted at 0.5 m for LiDAR A and B, respectively. This sample is different than the samples 1, 2 which are ACSR samples. LiDAR A has the lowest difference of the actual versus taken value of the LiDAR systems with a value of 29 mm.

Sample 4: ACSR Cardinal

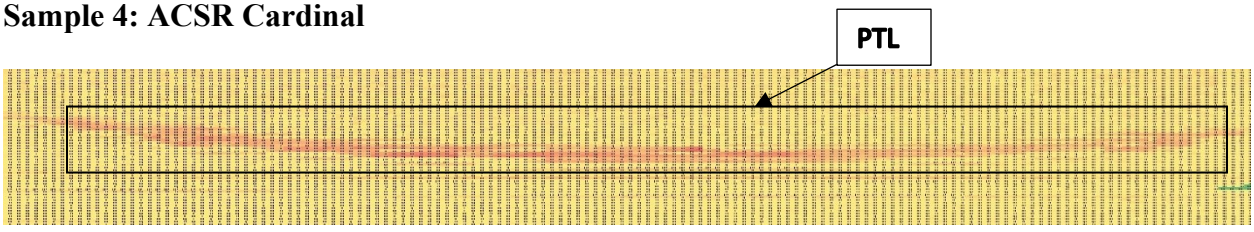

Figure 43:Conditional Formatted LiDAR A ACSR Cardinal at 0.5m

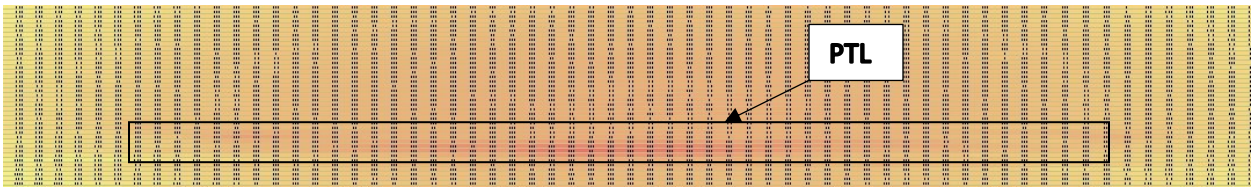

Figure 44:Conditional Formatted LiDAR B ACSR Cardinal at 0.5m

Table 16:ACSR Cardinal LiDAR A, B Results

	Actual Measurements (mm)	Farthest Measurement (mm)	Nearest Measurement (mm)	Difference (Actual vs Nearest) (mm)
LiDAR A	500	1086	506	6
LiDAR B	500	4081	550	50

Figures 43 and 44 show the conditional formatted for sample 4: ACSR Cardinal at 0.5 m by LiDAR A and B, respectively. LiDAR A has the lowest difference between the actual versus the taken value of the LiDAR systems with a value of 6 mm. This is the lowest difference value of all the samples taken.

4.3.2 Energized between 60°C to 120°C

Sample 1: ACCC Rome

Figure 45:Conditional Formatted LiDAR A Energized ACCC Rome at 0.5m

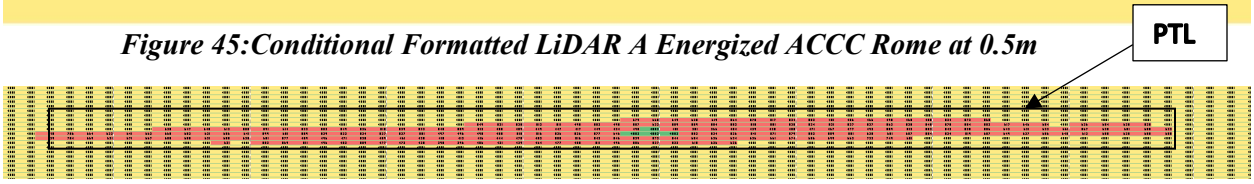

Figure 46:Conditional Formatted LiDAR B Energized ACCC Rome at 0.5m

Table 17:Energized ACCC Rome LiDAR A, B Results

	Actual Measurements (mm)	Farthest Measurement (mm)	Nearest Measurement (mm)	Difference (Actual vs Nearest) (mm)
LiDAR A	500	1050	528	28
LiDAR B	500	4081	401	99

Figures 45 and 46 show the conditional formatted for the sample ACCC Rome-energized at 0.5 m by LiDAR A and B, respectively. LiDAR A has the lowest difference between the actual vs nearest measurement of 28 mm.

Sample 2: ACSR Condor aged

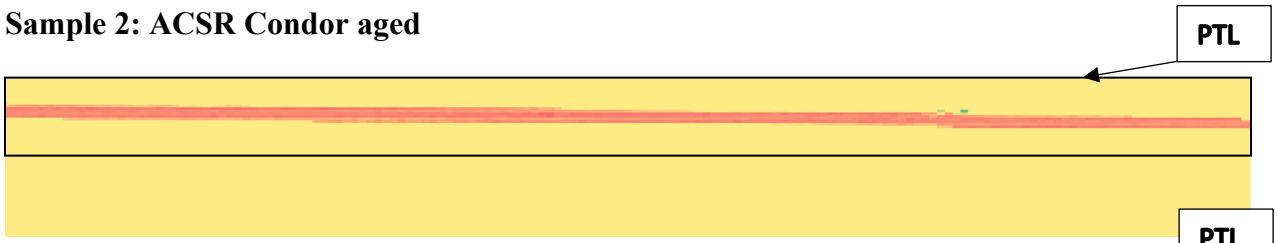

Figure 47:Conditional Formatted LiDAR A Energized ACSR Condor aged at 0.5m

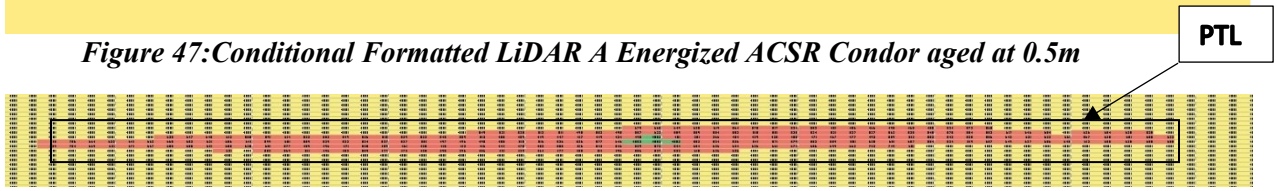

Figure 48:Conditional Formatted LiDAR B Energized ACSR Condor aged at 0.5m

Table 18:Energized ACSR Condor aged LiDAR A, B Results

	Actual Measurements (mm)	Farthest Measurement (mm)	Nearest Measurement (mm)	Difference (Actual vs Nearest) (mm)
LiDAR A	500	1050	384	116
LiDAR B	500	4083	327	173

Figures 47 and 48 show the conditional formatted for ACSR Condor aged-energized at 0.5 m for LiDAR A and B, respectively. LiDAR A had the lowest value for the difference between actual versus nearest measurement of 116 mm.

4.3.3 Summary of Results

This section summarizes the data displayed in Sections 4.3.1 and 4.3.2. These sections focus on the measurements taken by the LiDAR systems vs the actual measurement from the LiDAR to the PTL sample. Note: the main assumption for this section is that since the LiDAR systems were placed directly 0.5 m away from the PTL

sample that the nearest point calculated by the systems should be approximately 0.5 m or 500 mm.

Table 19: Summary of LiDAR Data Comparison

	LiDAR A: Difference between actual and nearest measurement (mm)	**LiDAR B**: Difference between actual and nearest measurement. (mm)
De-Energized		
Sample 1: ACSR Drake	94	105
Sample 2: ACSR Condor aged	88	142
Sample 3: ACCC Rome	28	54
Sample 4: ACSR Cardinal	6	50
Energized		
Sample 1: ACCC Rome	28	99
Sample 2: ACSR Condor aged	116	173

Table 19 displays the results from the data comparison test, as shown LiDAR B was less accurate at determining the actual distance to the PTL samples than LiDAR A. The farthest measurement (mm) and nearest measurement (mm) were found using the Microsoft Excel using the =max(), =min() and =avg() functions .One of the main take aways were: these differences in measurements are mostly outside of what the manufacture advertised, which were 2 cm or 20 mm and 1% for LiDAR A and LiDAR B respectively except for sample 4: ACSR cardinal. For sample 4 is which the difference between actual and nearest measurements were 6mm for LiDAR A. With sample 3 and 4 being the lowest measurement difference, this is potential due to the material and surfaces of samples 3 and 4 as these were the shinier of the samples. Comparing the de-energized and energized PTLs there does not seem to be that much of a difference, a raising the question if heat has any impact on the LiDAR system performance. A general conclusion of this analysis can be

made that LiDAR A performed closest to the advertised specifications and overall better than LiDAR B.

4.4 Root-Mean-Square Deviation Comparison

One of the most notable features for a LiDAR system is the accuracy, in this section will examine the accuracy of the selected LiDAR systems. The accuracy in this section was determined by method of root mean squared deviation technique (RMSD). The root mean squared deviation or more commonly known root mean squared error (RSME) is the standard deviation of the prediction errors. The predicted errors look at how far the data points are from the line of best fit. How this method is beneficial for this research, is the RMSD, takes a series of observations (frames) collected by the LiDAR systems by calculating the squared difference between the collected value and the theoretical/ predicted value, adding then dividing them by the number of observations, giving the equation shown below. *Note: all LiDAR values and RMSD values are in millimetres (mm).*

The general equation for the RMSD:

$$RMSD = \sqrt{\frac{\sum_{i=1}^{n}(\mathcal{X}_i - \widehat{\mathcal{X}}_i)^2}{N}} \qquad \text{(Equation 1)}$$

$RMSD$ = root-mean-square deviation

i = variable i

N = number of non-missing data points

$\mathcal{X}_i$ = actual observations time

$\widehat{\mathcal{X}}_i$ = estimated time

4.4.1 De-Energized at Room Temperature

Sample #1- ACSR Drake

RMSD between LiDAR A and LiDAR B = 2359 mm

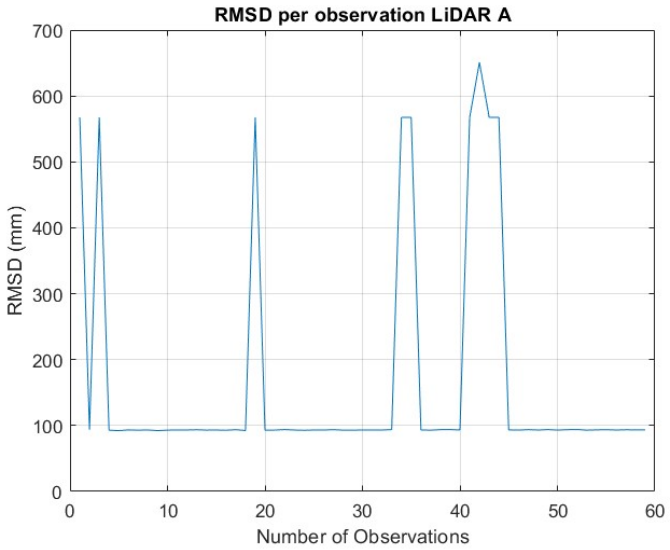

Figure 49:LiDAR A RMSD for ACSR Drake at 0.5 m

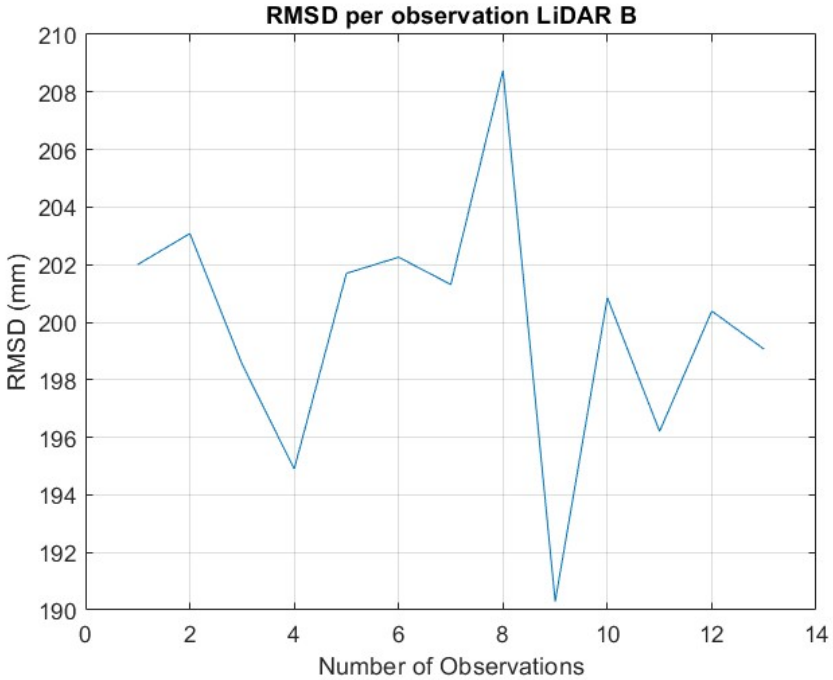

Figure 50:LiDAR B RMSD for ACSR Drake at 0.5 m

Figures 49 and 50 show the RMSD vs the number of observations at 0.5 m for LiDAR A and B respectively for ACSR Drake sample. First notable observation is the difference of the number of observations between LiDAR A and B, LiDAR A with an approximate 58 observations and LiDAR B with 13. The RMSD per observations are higher for LiDAR A than LiDAR B, however, they are more constant during majority of the observations. In both LiDAR systems there are spikes in the RMSD, this indicates higher difference of actual versus the measured value than the other observations.

Sample #2- ACSR Condor aged

RMSD between LiDAR A and LiDAR B = 3667 mm

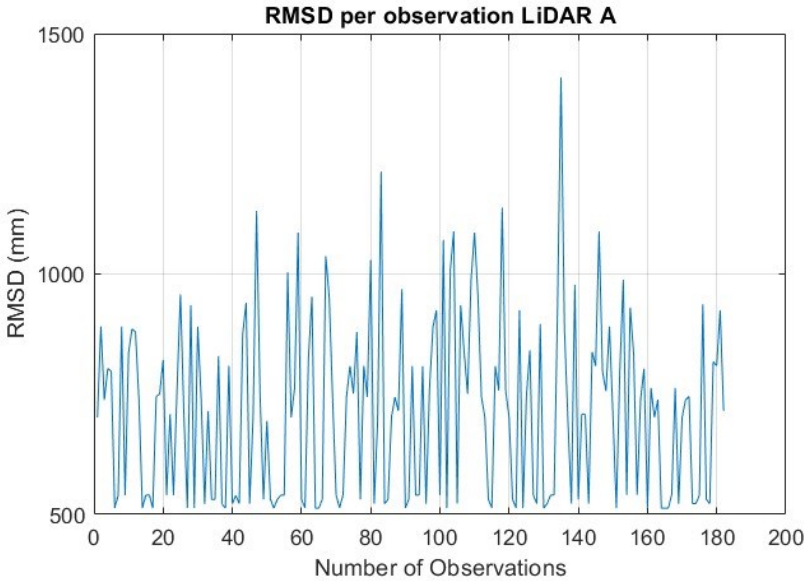

Figure 51:LiDAR A RMSD for ACSR Condor aged at 0.5 m

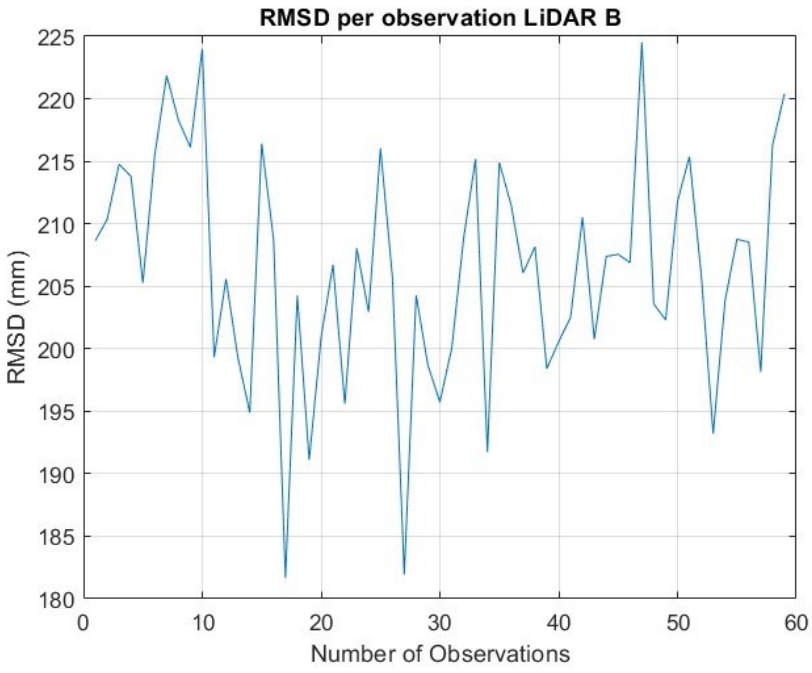

Figure 52:LiDAR B RMSD for ACSR Condor aged at 0.5 m

Figures 51 and 52 show the RMSD vs the number of observations at 0.5 m for LiDAR A and B respectively for ACSR Condor aged sample. Like the previous sample LiDAR A has more observations and higher and more spikes in the RMSD. With LiDAR A having much larger spikes, the data can be unreliable since some of the values are approximately 1400 mm. LiDAR B highest RMSD value was 225 mm compared to LiDAR A 1400 mm. The spikes represent the change in accuracy of the data taken, the larger the spike the less accurate that data is, and the lower the spike (or RMSD) the more accurate the data is.

Sample #3: ACCC Rome

RMSD between LiDAR A and LiDAR B = 2951 mm

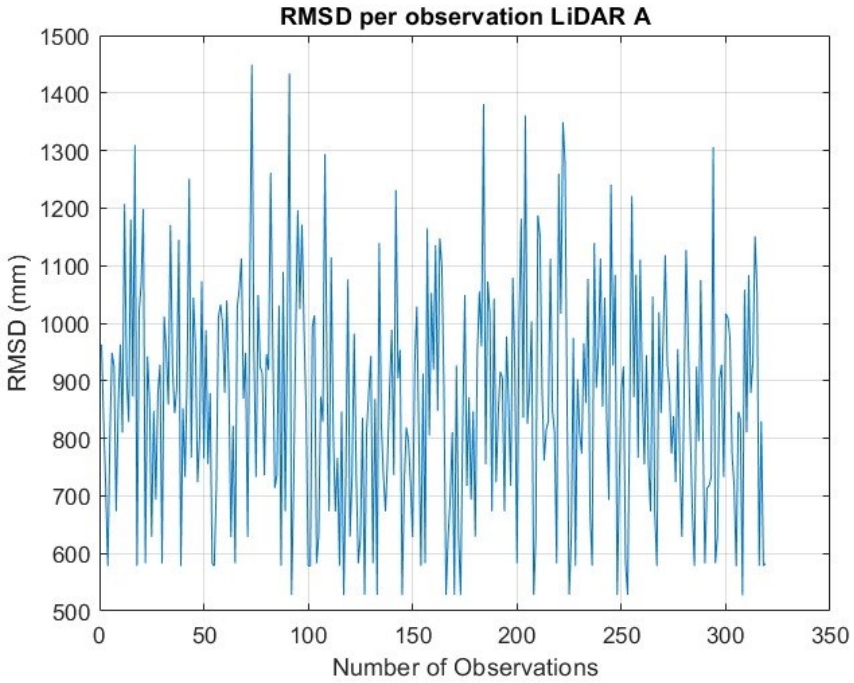

Figure 53:LiDAR A RMSD for ACCC Rome at 0.5 m

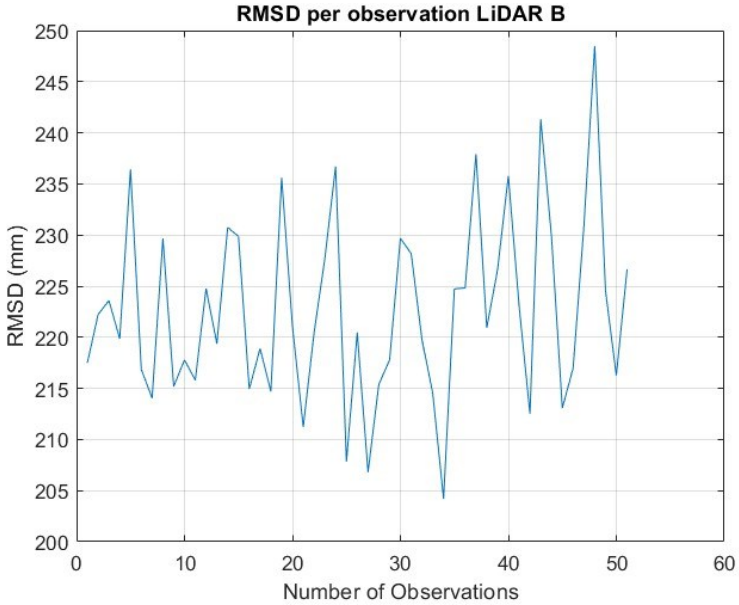

Figure 54:LiDAR B RMSD for ACCC Rome at 0.5 m

Figures 53 and 54 show the RMSD vs the number of observations at 0.5 m for LiDAR A and B respectively for the ACCC Rome sample. LiDAR A shows a lot more spikes in the RMSD while LiDAR B have frequent spikes but at a lower RMSD.

Sample 4: ACSR Cardinal

RMSD between LiDAR A and LiDAR B = 3847 mm

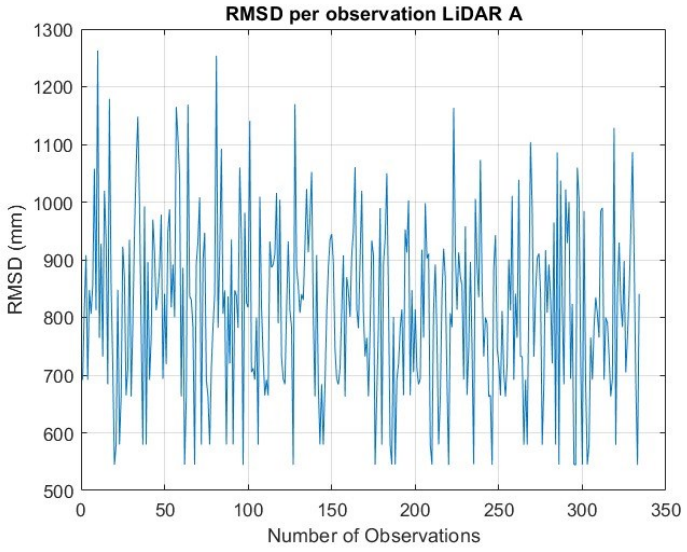

Figure 55:LiDAR A RMSD for ACSR Cardinal at 0.5 m

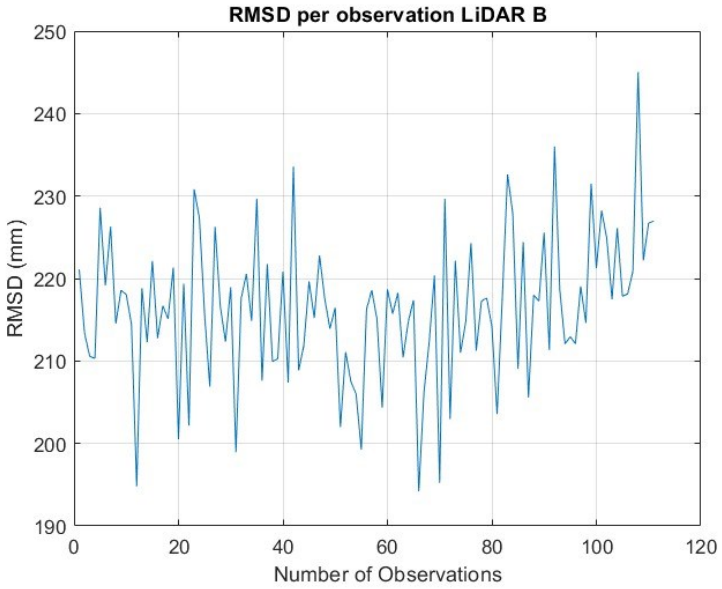

Figure 56:LiDAR B RMSD for ACSR Cardinal at 0.5 m

Figures 55 and 56 show the RMSD vs the number of observations at 0.5 m for LiDAR A and B respectively for the ACSR Cardinal sample. Like the previous samples LiDAR A has the higher value, and more spikes per observations.

4.4.1.1 Discussion of results

Figures 49 to 56 shows the results of the RMSD for the data collected by LiDAR A and B for samples 1-4. Based on the results LiDAR B has the lower RMSD per observation than LiDAR A. For this section, it was not the expected result as LiDAR A was more accurate than LiDAR B in the data comparison section (Section 4.3). It is to know that LiDAR A has more observations than LiDAR B, during the test LiDAR A frame per second (fps) was 13-15 fps while LiDAR B was closer to 5-10 fps. The theory for the larger RMSD spikes for LiDAR A, is since LiDAR A can detect more of the objects around the PTL and the background, it is possible that it also is picking up more local interference causing less accurate results. Another theory about LiDAR A, is that the power supply was fluctuating causing some distortions and leading to higher RMSD values.

4.4.2 Interference Comparison

Based on the results from Section 4.4.1 an interference comparison was performed to understand if the interference level due to the background of the background and from the LiDAR systems. To perform this test the LiDAR systems were pointed at a blank surface (in this case, the background behind the PTL set up). The RMSD was calculated for the interference comparison and compared to that of LiDAR A and B. Samples 2 and 4 were selected for this section.

Sample 2: ACSR Condor aged

LiDAR A RMSD difference = 3229 mm

LiDAR B RMSD difference = 1334 mm

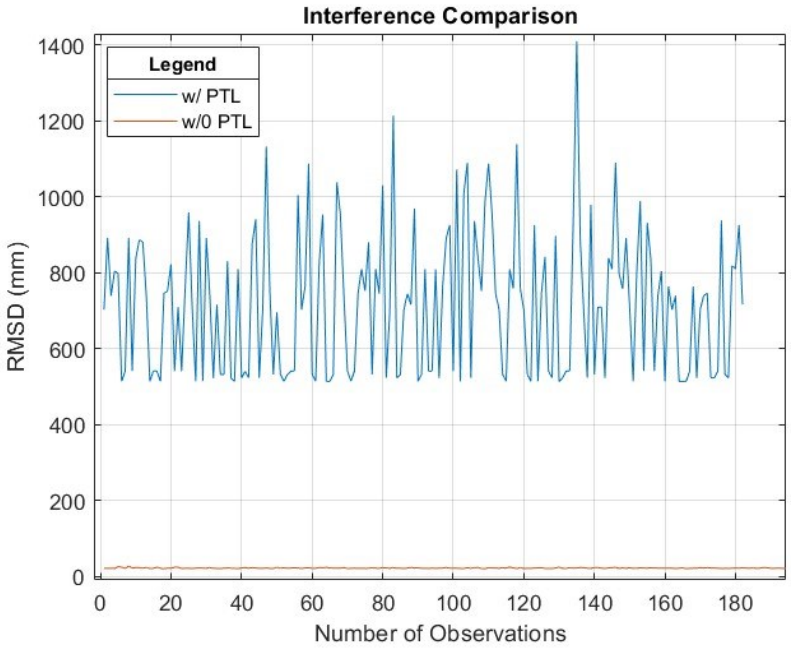

Figure 57:Sample 2 Interference Comparison LiDAR A at 0.5 m

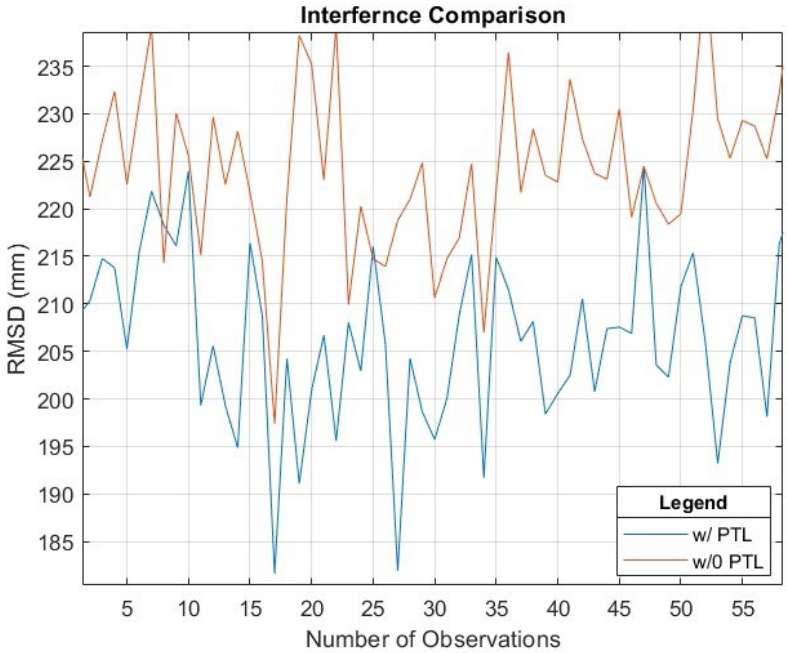

Figure 58:Sample 2 Interference Comparison LiDAR B at 0.5 m

Figures 57 and 58 show the interference comparison for LiDAR A and B respectively at 0.5 m, these graphs show the RMSD per observation for the data with PTL and without the PTL. The orange (or data line) graph shows the RMSD without the PTL sample (just the background and the LiDAR stand) and the blue graph shows the RMSD per observation with the PTL. Figure 57 indicates for LiDAR A, without the PTL the RMSD per observation is exceptionally low, almost zero is some observations. While LiDAR B (Figure 58) the RMSD per observation is higher without the PTL than without and have more spikes in the RMSD.

Sample 4: ACSR Cardinal

LiDAR A RMSD difference = 3536 mm

LiDAR B RMSD difference = 1241 mm

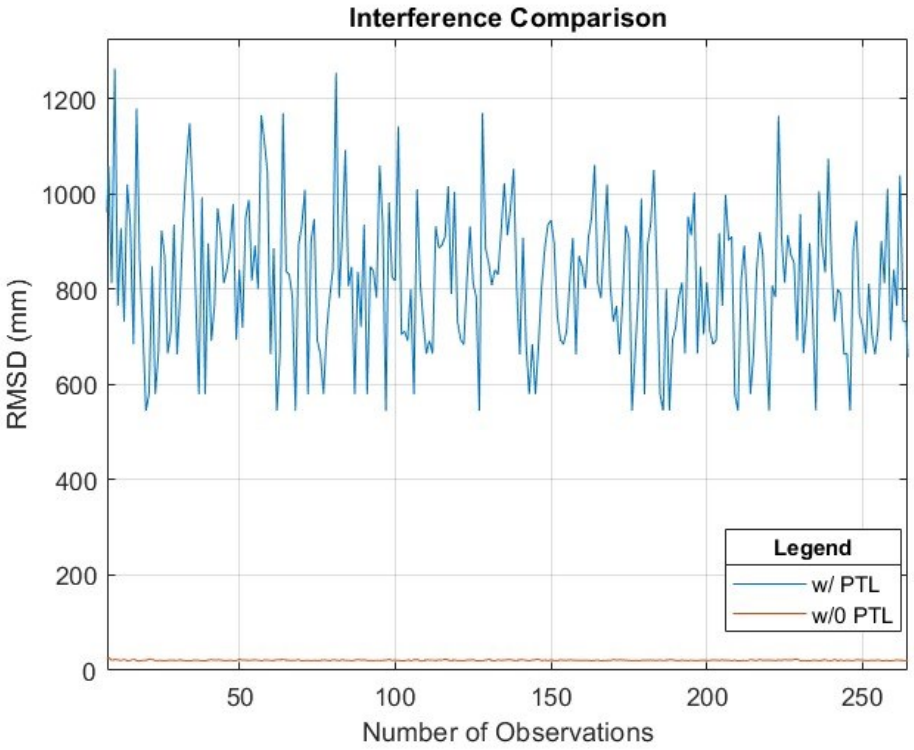

Figure 59:Sample 4 Interference Comparison LiDAR A at 0.5 m

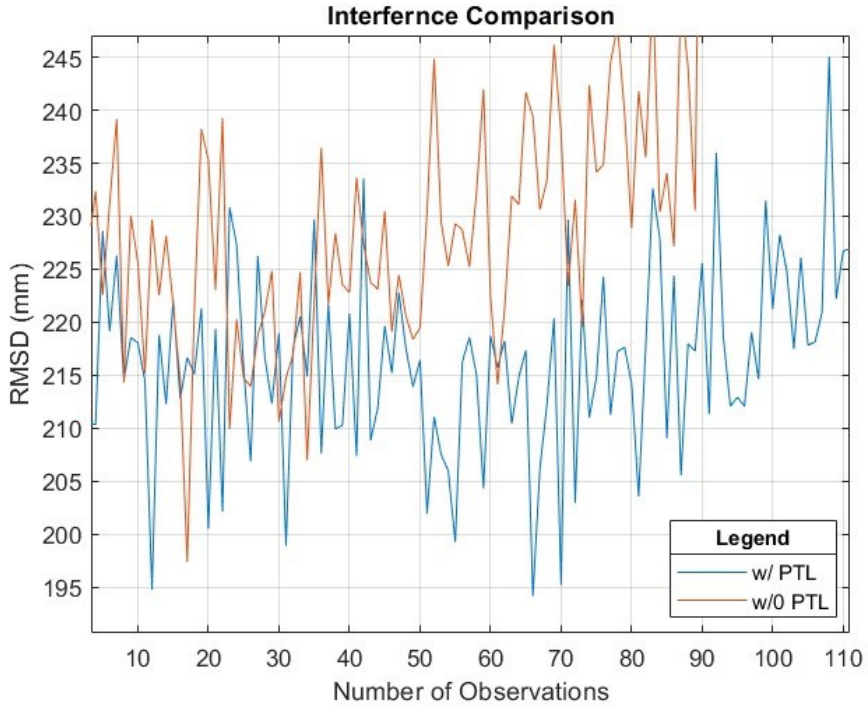

Figure 60:Sample 4 Interference Comparison LiDAR B at 0.5 m

Figures 59 and 60 show the interference comparison for LiDAR A and B respectively at 0.5 m, these graphs show the RMSD per observation for the data with PTL and without the PTL. The results are like that of sample 2.

Discussion of results

Figures 57 to 60 show the results on the interference comparison test and for LiDAR A and B the environment/background. For LiDAR A the background did not have an affect on the actual results, as the RMSD was significantly lower than that of the RMSD taken with the PTL sample. It would appear there are other factors, which would have to be considered or there is interference going on internally with the LiDAR system, with LiDAR B the affect on the background is directly proportional to that of the data with the PTL sample included. The theory going into this test was, the RMSD with the PTL would

be like the RMSD without the PTL. This test does prove the theory incorrect, highlighting LiDAR A and B results were affect by the background/ environment.

4.4.3 Energized between 60°C to 120°C

For this section, the test was performed at Kinectrics Inc. in their high voltage lab. The purpose of this test was to examine how the LiDAR systems data would be affected in more realistic operational conditions. As the PTL span was energized its temperature was between 60°C and 120°C. The frequency was approximately 60 Hz and the voltage was approximately 120 V. The data is shown for the distance of 0.5 m.

Sample 1: ACCC Rome- Energized

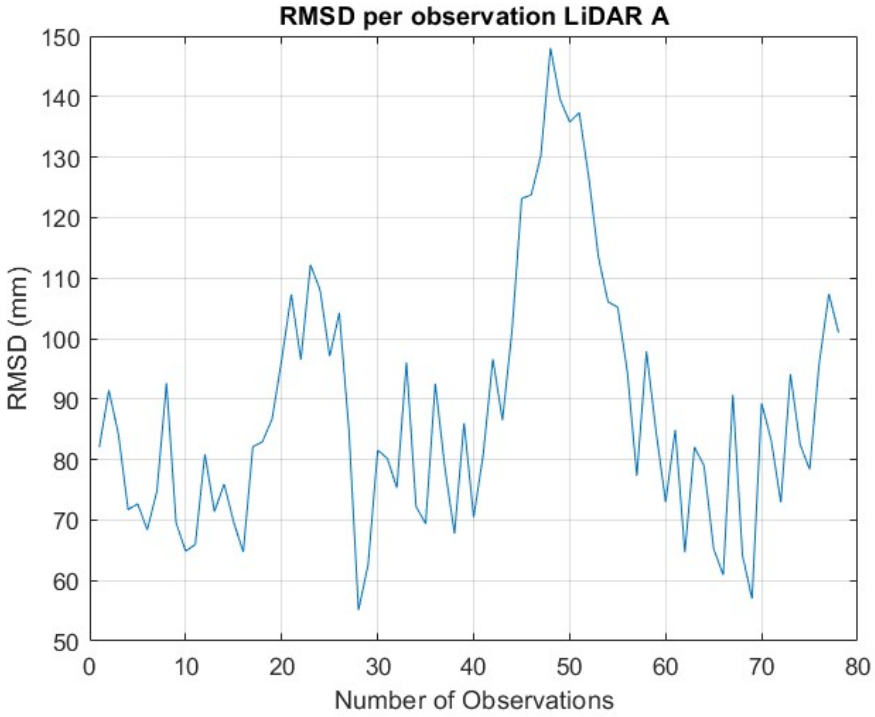

Figure 61:LiDAR A RMSD for ACCC Rome-Energized at 0.5 m

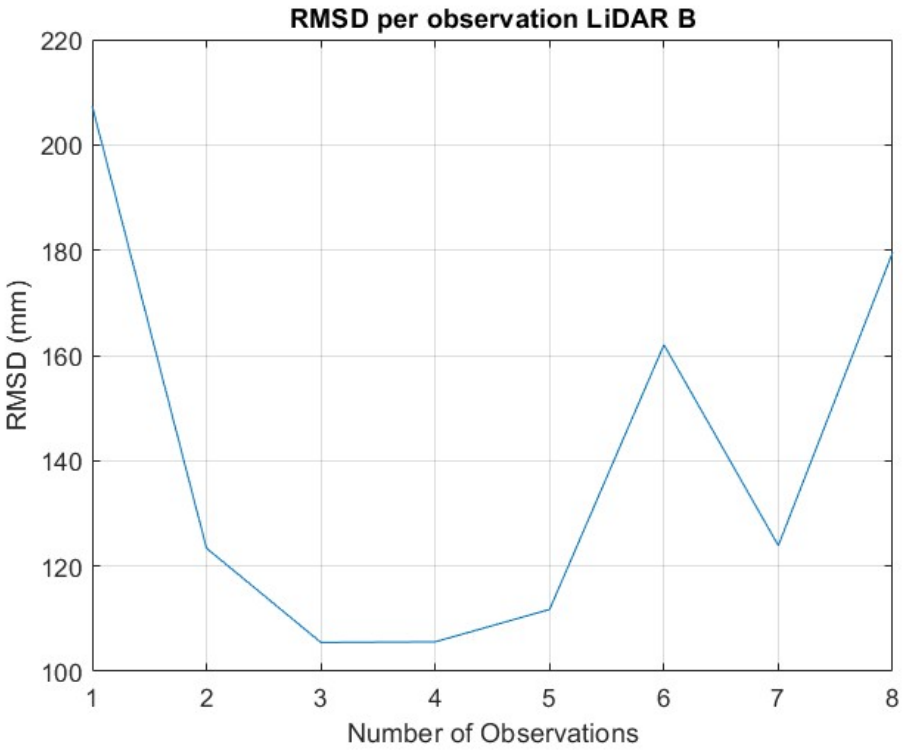

Figure 62:LiDAR B RMSD for ACCC Rome-Energized at 0.5m

Figures 61 and 62 show the RMSD for ACCC Rome-energized at 0.5m for LiDAR A and B, respectively. As expected with this test being performed in a high voltage lab and the ACCC Rome being having a shiny surface, the RMSD values in the results are significantly lower than the de-energized RMSD values.

Sample 2: ACSR Condor Aged-Energized

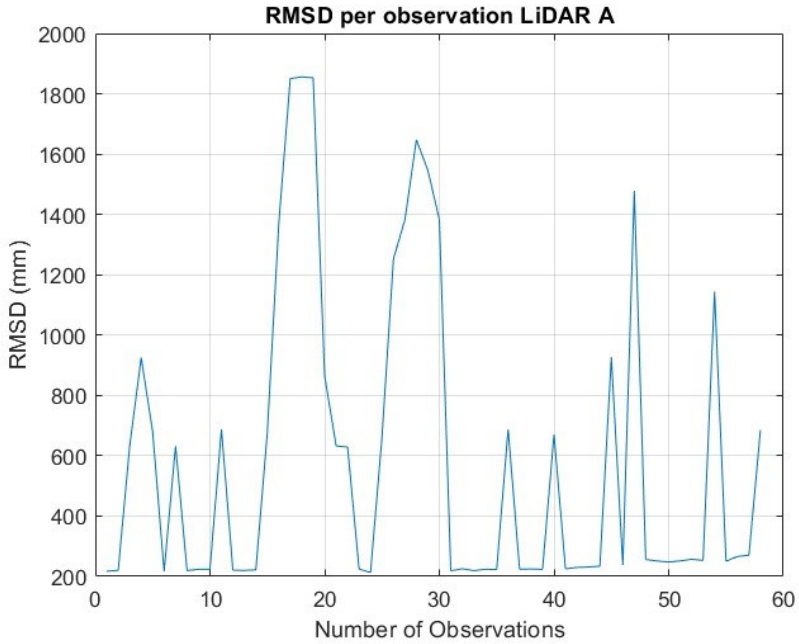

Figure 63:LiDAR A RMSD for ACSR Condor aged-Energized

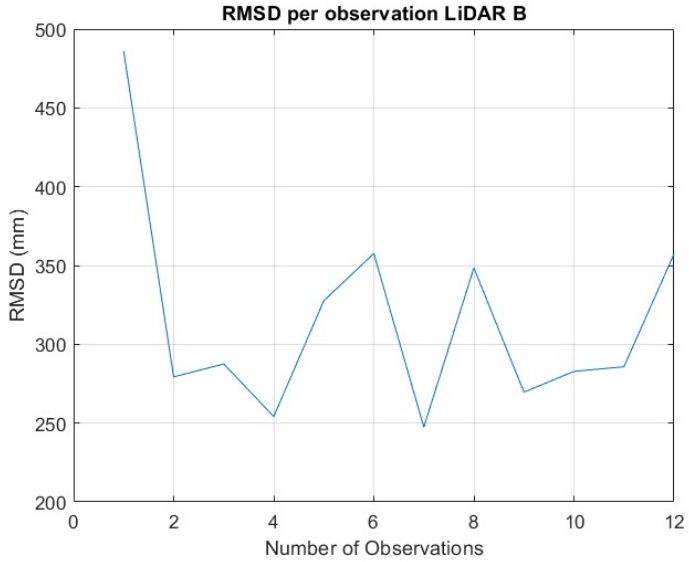

Figure 64:LiDAR B RMSD for ACSR Condor aged -Energized

Figures 63 and 64 show the RMSD for ACSR Condor aged-energized at 0.5m for LiDAR A and B, respectively. LiDAR A the RMSD values have similar spikes to the de-

energized test done, however the low RMSD are approximately 200 mm. LiDAR B the RMSD values are slightly higher than in the ACCC Rome sample.

4.4.4 Discussion of Results

The test described in this section were performed in an actual testing lab for high voltage power transmission lines, under the careful supervision of the lab technicians. This allows for less interference from external sources (such as background or other random objects. The ACCC Rome sample had lower RMSD values for LiDAR while LiDAR B results were the same as the de-energized samples. The results from this section indicate that there is more accuracy from the LiDAR systems when the test is performed in a high voltage lab and energizing the PTL samples there were no significant difference in results than that of the de-energize PTL samples. The RMSD data didn't accounted for false detections as the distance from the LiDAR system to the PTL sample were known and there were no objects between. The RMSD vs Number of Observations graphs represent the RMSD for every observation (frame) taken by the LiDAR systems, in each observation the RMSD is calculated based on predicted values and actual values taken by the LiDAR system. Each observation includes the PTL sample and the background (projector screen), the ACSR Drake PTL sample was the only sample which included the 2' x4' spruce-pine-fir wood and zip ties to stop the PTL sample from coiling and causing potential injury to anyone in the area.

4.5 Performance Evaluation Summary

This section is a general summary of the results of Chapter 4. Both LiDAR systems were able to pass the validation and verification test as both were able to detect the selected objects (shown in section 4.1 based on the point cloud data. This test does not cover the

accuracy at which they were able to see the object, and for a test to be denoted as successful, the LiDAR system had to detect both in the interface and in the post data analyzation as shown in Figures 33 and 35. The next performance evaluation done was comparing the specifications from LiDAR A and B. LiDAR B is 82 g (grams) lighter than that of LiDAR A. This weight comparison is just on the actual system itself and not the cable components as that can changed depending on the application. With a lighter weight system, LiDAR B would have less of an impact on an RPA performance. The measuring range starts 50mm more on the LiDAR A, however, LiDAR A has a maximum range of 4000 mm more than that of LiDAR B. Theoretically that would make the LiDAR A better for longer range detecting.

The FOV is wider both vertically and horizontally on LiDAR B, and both have similar operating temperatures. For communication interface, while LiDAR A can do USB, RS23, IO, and LAN, the LiDAR B can only connect via USB at the time of conducting this research. Since the LiDAR B can only be connected via USB, it limits it to 5V for power supply while LiDAR A requires 12-24V for power supply. Base on the specifications provided by each manufacturer both LiDAR systems have particularly useful features however, depending on the application use one may have an advantage over the other.

The performance evaluation examined the data collected by the LiDAR systems; Table 19 highlights the results from the data comparison test. LiDAR B was less accurate at determining the actual distance to the PTL samples than LiDAR A. The farthest measurement (mm) and nearest measurement (mm) were found using the Microsoft excel using the =max() and =min() functions. One of resulting factors were: the differences in measurements are mostly outside of what the manufacture advertised, which were 2 cm or

20 mm and 1% (for this research 10mm) for LiDAR A and LiDAR B respectively except for sample 4: ACSR cardinal. For sample 4 is which the difference between actual and nearest measurements were 6 mm for LiDAR A

Comparing the de-energized and energized there does not seem to be that much of a difference, this does bring up a question if heat has any impact on the LiDAR systems? LiDAR A uses a wavelength of 850 nm and LiDAR B uses a wavelength of 808 nm.

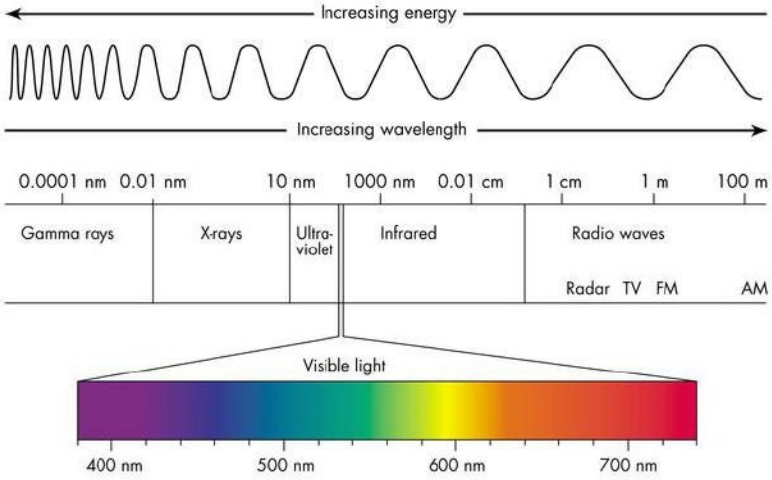

Figure 65:Electromagnetic spectrum[37]

Based on the wavelength of both LiDAR systems, it would place them just above the visible light and in the IR spectrum. “Thermal radiation is electromagnetic radiation emitted from all matter that is at a non-zero temperature in the wavelength range from 0.1 μm to 100 μm.”[38] which places both LiDAR systems in that range, with LiDAR A at 850 nm and LiDAR B at 805 nm, for their operational wavelengths. One micrometre (μm) is equal to one thousand nanometres (nm). Suggesting that IR radiation does have an affect on the data taken from the LiDAR systems.

A general conclusion of this section can be made LiDAR A performed better in this test. The final performance evaluation was the determination of the RMSD and comparison between the LiDAR systems. Figures 49 to 56 shows the results of the RMSD for the data

collected by LiDAR A and B for samples 1-4. Based on the results LiDAR B has the lower RMSD per observation than LiDAR A. For this section, it was not the expected result as LiDAR A was more accuracy than LiDAR B in the data comparison section. It is to know that LiDAR A has more observations than LiDAR B, during the test LiDAR A frame per second (fps) was 13-15 fps while LiDAR B was closer to 5-10 fps. It is LiDAR A could have experienced a lot more interference (noise) than LiDAR B due to the power supply or scatter in the room where the test was conducted. Figures 57 to 60 show the results on the interference comparison and for LiDAR A the environment/background of which the test was performed had little affect on the results, it would appear there are other factors, that would have to be considered or there is interference going on internally with the LiDAR system, with LiDAR B the affect on the background is directly proportional to that of the data with the PTL sample included. This test does prove that with LiDAR A and B there was interference from the background/ environment of which the test was performed. The results of this section were performed in an actual testing lab for high voltage power transmission lines, under the careful supervision of the lab technicians. This allows for less interference from external sources, which is visible in the lower RMSD values to that of the de-energized values.

4.6 PTL Sample Section Analysis

In this section, Figures 66 and 70 was divided into three sections and each section analysed by graphical method. The purpose of this analysis is to understand the change in LiDAR data measurements from the PTL sample relative the background. The first frame of each data set was used. For each graph, the X-axis numbering starts from the section to the bottom and the Y axis denotes the distance measurement at the corresponding point.

The numbering on the X-axis starts at 1 and end at 59 with 30 being the midpoint (as the mid-point of the sectional cut).

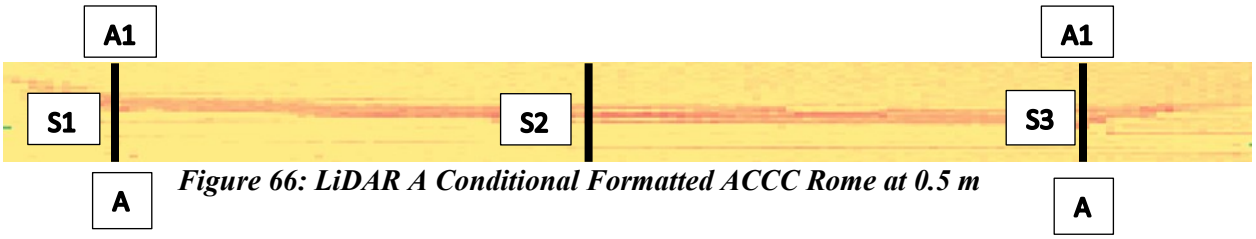

Figure 66: LiDAR A Conditional Formatted ACCC Rome at 0.5 m

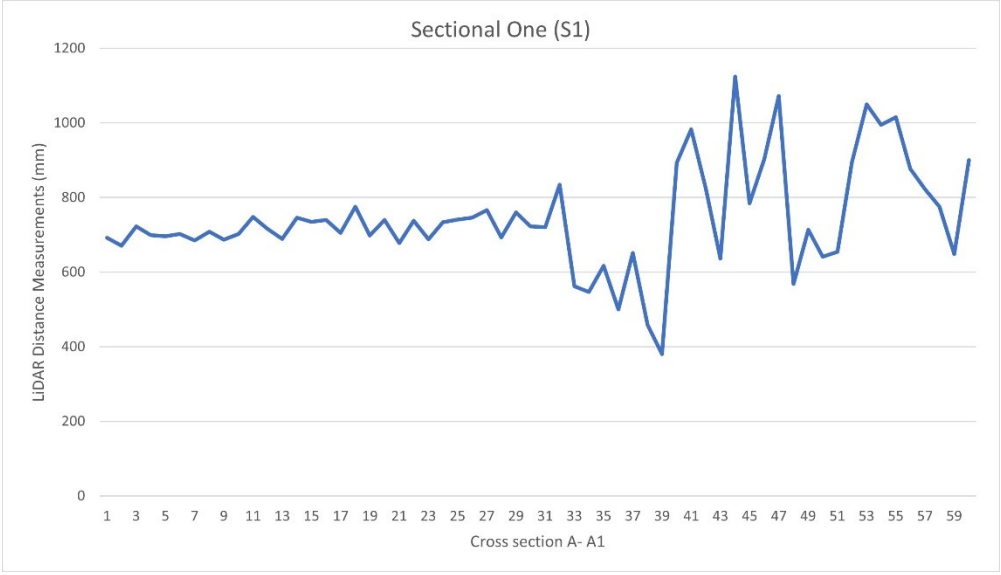

Figure 67: ACCC Rome at 0.5 Sectional One for LiDAR A

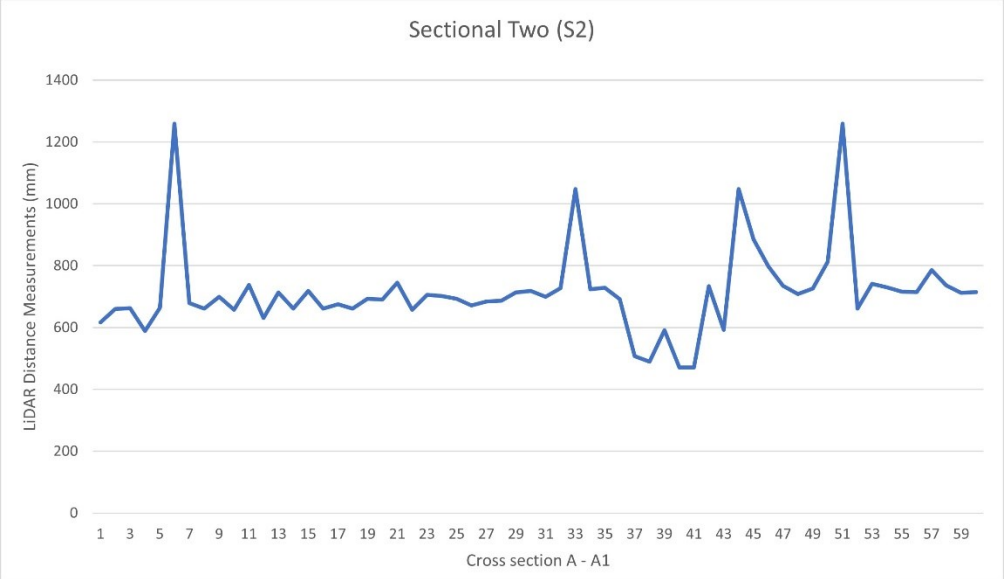

Figure 68:ACCC Rome at 0.5 Sectional Two for LiDAR A

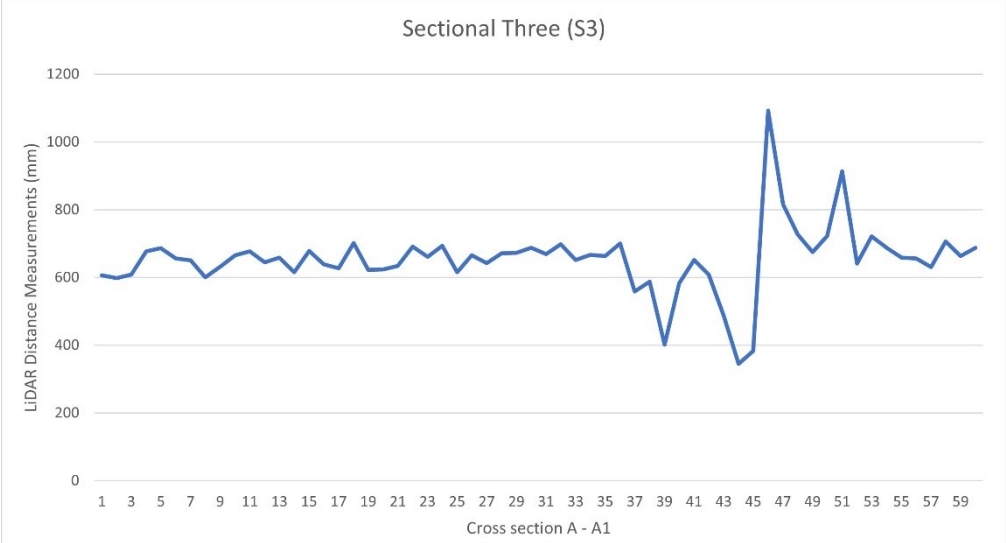

Figure 69:ACCC Rome at 0.5 Sectional Three for LiDAR A

Figure 66 shows the location of the sectionals S1, S2 and S3 for ACCC Rome at 0.5 m for LiDAR A. In Figure 67 for S1, from 1-33 the measurement values are consistently around 700 mm, and then fluctuates down to 400 mm which corresponds to the location of the PTL. After, the location of the PTL at 41 the measurement goes up to 1000 mm. For S2 (Figure 68) the graph shows the measurements are consistent with a few spikes at the

beginning (number 1), near the center (number 33) and closer to the end (number 55). Around 37 – 41, the goes down to 471 giving the nearest value at the center of the PTL sample. S3 (Figure 69), which shows the measurements on the right side of the PTL are consistent around 700 mm until number 39 where it goes down under 400 mm and at number 45 it spikes up over 1000 mm correlating to where the PTL ended, and the background area started.

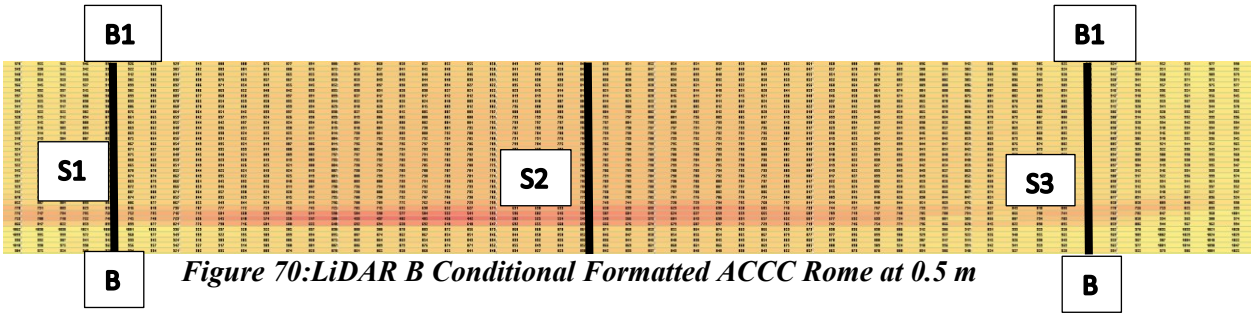

Figure 70:LiDAR B Conditional Formatted ACCC Rome at 0.5 m

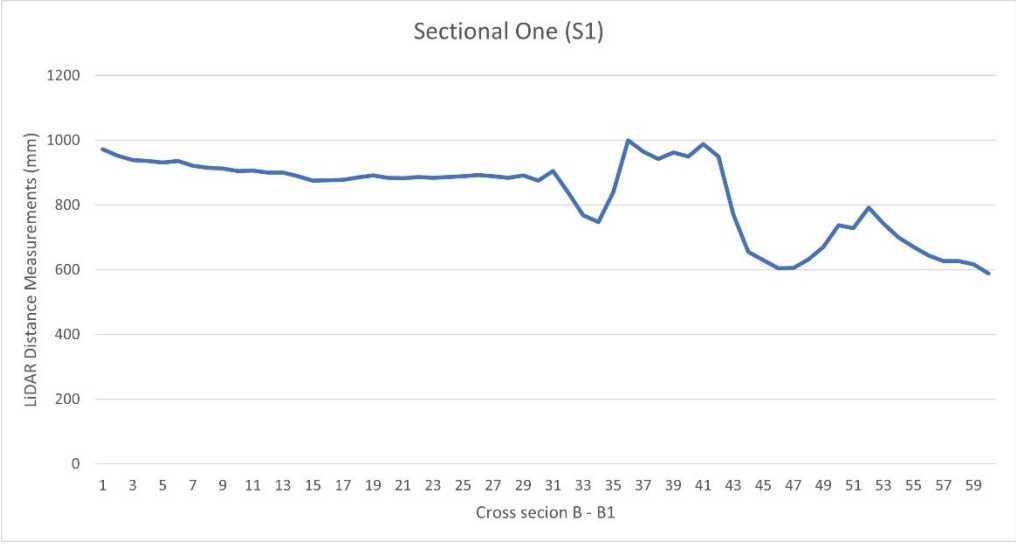

Figure 71:ACCC Rome at 0.5 Sectional One for LiDAR B

Figure 72:ACCC Rome at 0.5 Sectional Two for LiDAR B

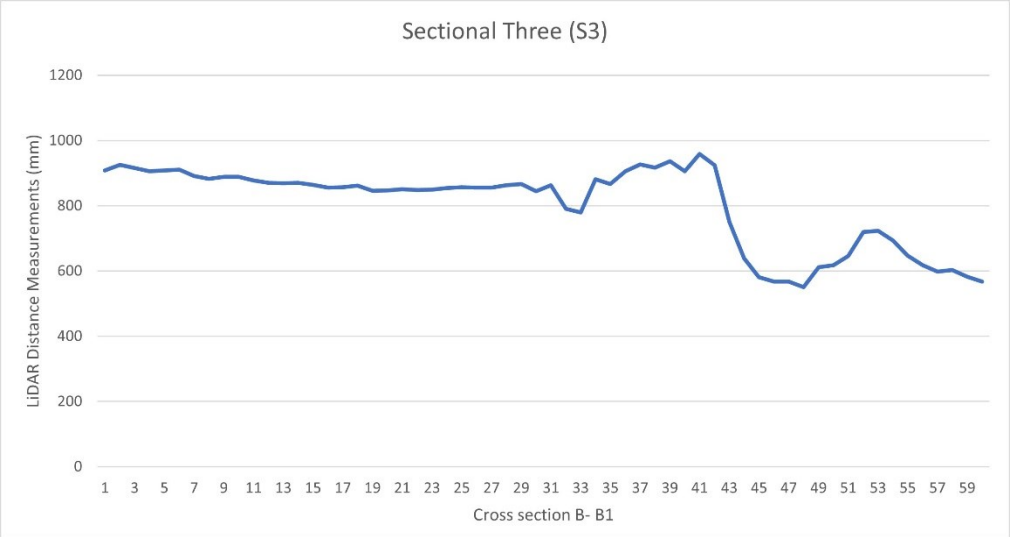

Figure 73:ACCC Rome at 0.5 Sectional Three for LiDAR B

Figure 70 shows the location of the sectionals S1, S2 and S3 for ACCC Rome at 0.5m for LiDAR B. S1(Figure 71), the measurements are consistent at 900 mm then drops until 800 mm at the midpoint (number 33) spikes up to 1000 mm at number 37 then down again to 600 mm at number 45. For S2 (Figure 72), the measurement values are on a constant decline from number 1 to number 29, where is drops to 442 mm at the midpoint.

Then goes up to 850 mm at number 39. Denoting the location of the PTL to be between number 33 and 39. S3 (Figure 73), the measurement values are constant around 900 mm then declines to 580 mm near the location of the PTL.

4.7 Miniature Case Study

This section will look at RMSD per observation of the selected LiDAR systems as they are initially attached to a selected RPAS (3DR Iris+ multirotor RPAS). For safety and regulatory purposes, this test was done in the safety of mechanical and aerospace laboratory and with a safety observer. The propellers were removed as this test focuses on how the RPAS' components will affect LiDAR A and LiDAR B data results. The samples used was sample 1: ACSR Drake de-energized, and the LiDAR systems were placed at the same height and distance away as it was on the bench test.

Figure 74: LiDAR A mounted on 3D Iris+ multirotor RPAS

Figure 75:LiDAR B mounted on 3D Iris+ multirotor RPAS

Table 20:ACSR Drake LiDAR A, B mounted on 3D Iris+ multirotor RPAS results at 0.5 m

	Actual Measurements (mm)	Farthest Measurement (mm)	Nearest Measurement (mm)	Difference (Actual vs Nearest) (mm)
LiDAR A	500	1309	400	100
LiDAR B	500	4081	633	133

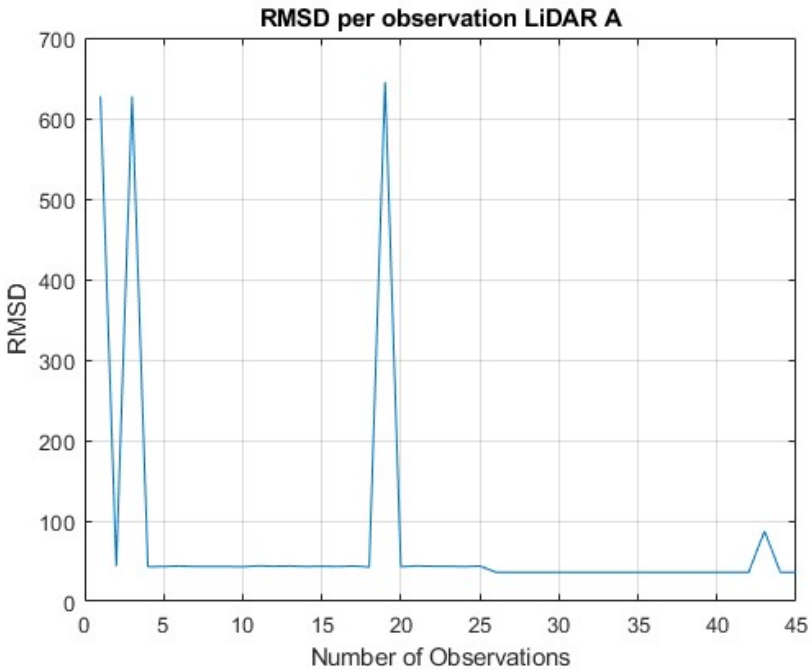

Figure 76: RMSD per Observation of LiDAR A mounted on a RPAS at 0.5 m

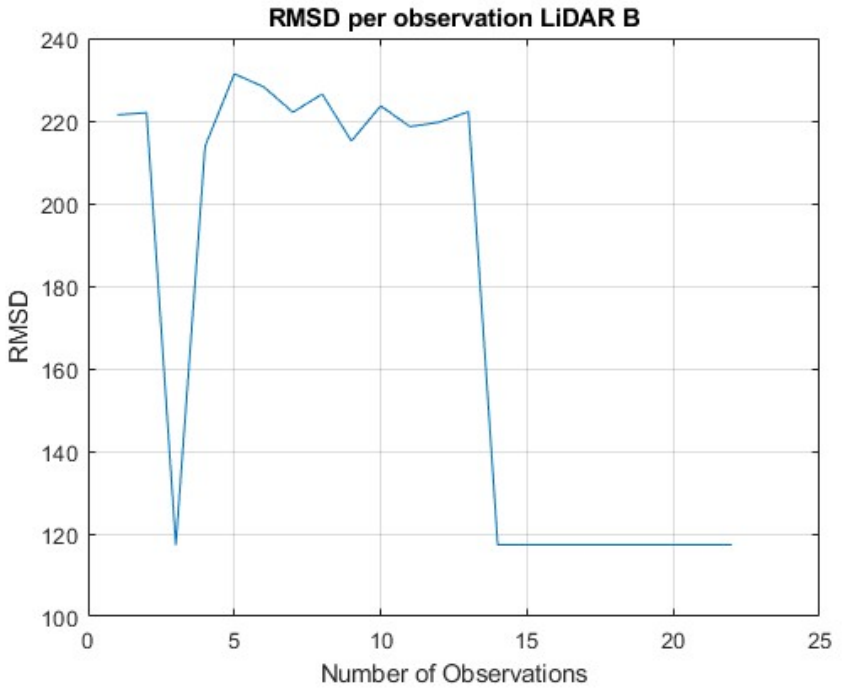

Figure 77:RMSD per Observation of LiDAR B mounted on a RPAS at 0.5 m

4.7.1 Discussion of results

Figures 74 and 75 show how the LiDAR systems with initially mounted on the on-3D Iris+ multirotor RPAS. The RPAS has a gimbal located at the bottom, which was the ideal place for the LiDAR systems to be mounted as this is where it would be mounted in a real-world scenario. Also, the gimbal assists with dampening the vibrations cause by the rotation of the motors and the propellers. The difference between the real-world measurement and the nearest measurement taken by the LiDAR A, B were 100 mm and 133 mm, respectively. The RMSD per Observations graphs on Figures 76 and 77, show comparable results to when the test was performed without the RPAS. To conclude, the miniature case study, the results illustrate that the components of from the RPAS does not have significant enough impact to affect the results of the select LiDAR systems.

Chapter 5: NRC Case Study

5.1: Introduction/ Overview

The LiDAR data used in this section was provided by the National Research Council of Canada. These data were incidentally collected by a field team as they were using an OPAL LiDAR system within proximity of PTLs during other flight tests. It is important to note that the PTLs were not the main subject for the field teams' data collection and only after reviewing the data, did they notice the PTLs. This case study looked at how the OPAL LiDAR system performed with PTL and their structures in its FOV while performing its main mission. The LiDAR system used was a redesigned OPAL™ 3D LiDAR scanner from Neptec Technologies. The mission for which this LiDAR system was used, and data collected show, the primary focus was not to detect/ see the PTL. However, as the PTL were within the FOV for the LiDAR. The data represented in this study will focus entirely on the PTL and their structures. The objective of this case study is to understand how an advanced and expensive LiDAR system will behave around live operating PTLs in a real-world scenario.

Figure 78:OPAL™ PERFORMANCE SERIES –CONICAL 3D LiDAR[39]

5.2 OPAL-CONICAL 3D LiDAR Specifications

Table 22 summarizes the basic specifications of the OPAL-CONICAL 3D LiDAR system. Other features of this commercial system include:

- High resolution (300,000 points per second single return mode)
- Rugged (resistant to shock and vibration)
- Obscurant penetrating (unparalleled performance in dust, smoke, rain, and fog)
- Intelligent (integrated multi-core CPU with PoE and USB ports for GPS/INS and peripherals.)
- User friendly (intuitive 3DRi™ software tools for rapid application development.)
- Consistent (dependable low-reflectivity target detection in real-world scenarios)
- Connectivity (integrated GigE switch and port for GPS/INS

Table 21: OPAL-CONICAL 3D LiDAR Specifications

Measuring range	Up to 1000 m
Weight	11.8 kg
Power consumption	3 – 5 W
Precision	< 2cm
Pulse Repetition Frequency	25kHz, 50kHz, 100kHz, 300kHz
Communication interface	Ethernet (Integrated Gig E switch with PoE), PPS (Time synchronization)
Operating Voltage	18- 36 VDC
Operating temperature	-40 ℃ - 55℃
Data Format Data Stream Format	Time-stamped position (x, y, z) plus intensity IPv4 Multi-cast UDP packets
Field of View	Conical 45°, 60°, 90°, and 120°

5.3 LiDAR Data

The data in this section will not be analyzed using the same method as that of the samples of the PTLs described previously in Chapter 4. The OPAL LiDAR data was collected in the south-eastern area of Ottawa, Ontario Canada, near Mer Bleue Bog and the Geological Survey of Canada Geomagnetic Observatory. The flight path of the helicopter was estimated to be circling the nature preserve as the objective of this flight was to evaluate the LiDAR system for the first time as shown in Figure 80. The Google Earth screenshot of that area is shown in Figure 79.

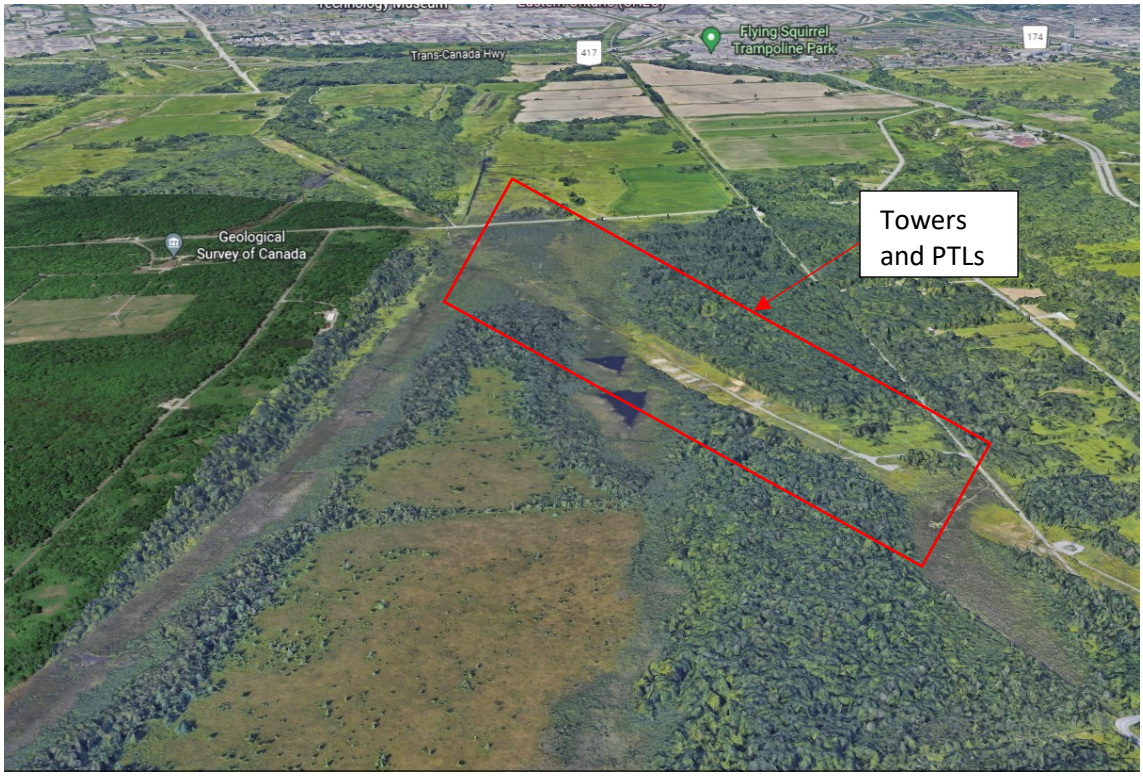

Figure 79:Google Earth screenshot of LiDAR Data Collection Area

*Notes:

Red = the direction of the flight path of the helicopter with the LiDAR system

Blue = highlighting some of the more obvious PTLs

Orange = highlighting a few of the towers

"This is not an ideal dataset, but it is the best one I have found with what we have flown so far. Also note that we are having issues with the LiDAR itself, so there is some jitter in the positional information."- the National Research Council Canada representative.

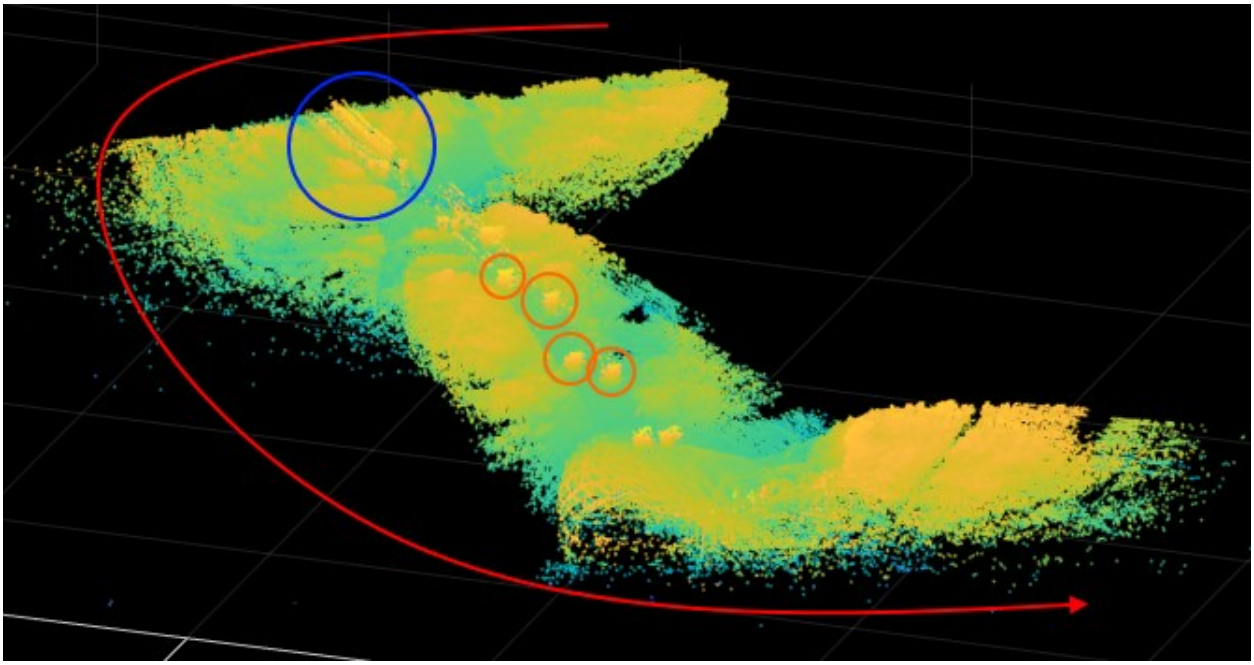

Figure 80:OPAL-Conical 3D LiDAR Data

Figure 79 shows the Google Earth screenshot of the approximate area and the view from the height of which the LiDAR data was taken, and Figure 80 presents it in a point cloud data (PCD) format. The data was taken at a distance ranging from 760 – 790m above ground level (AGL). Not considering interference or any environmental factors, this LiDAR system show immense potential for PTL detection. As previously mentioned, one of the notes upon receiving the data were there was some issues with the LiDAR, and it did not perform at full capacity as it was the first time this LiDAR system was used.

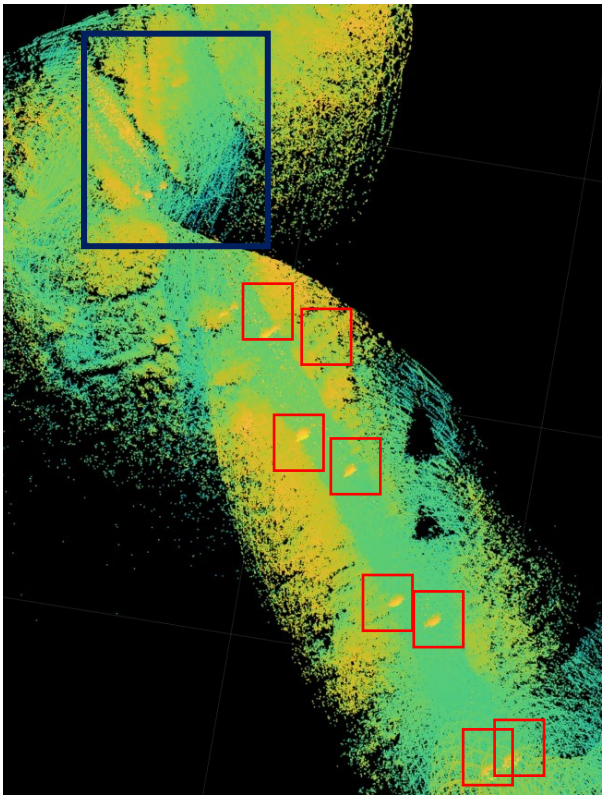

Figure 81: Zoomed in screenshot of OPAL-Conical 3D LiDAR Data

Figure 81 shows a zoomed in version of Figure 80, revealing more of the PTL structures (denoted by the red squares). There are several factors that can influence the data result produced by any LiDAR system, one of them is the change in heat of the PTL (Equation: 2), and how absorption impacts the wavelength of radiation caused by current flowing through PTLs. Radiation also known as electromagnetic waves cause electromagnetic fields. The strength of the electromagnetic field is directly proportional to the amount of current flowing through the PTLs.

The Heat transferred by the process of radiation equation[40] (Equation 2)

$$Q = \sigma (T_{Hot} - T_{Cold}) A \quad \text{(Equation 2)}$$

Q = Heat transferred

σ = Stefan Boltzmann Constant = 5.67×10^{-8} kg s^{-3} K^{-4}

T_{Hot} = Hot temperature

T_{Cold} =Cold Temperature

A = Area of surface

5.4 Contribution to the Research

The approximate cost of the OPAL-Conical 3D LiDAR is $100,000 CAD at the time of writing this document, in comparison to the 150 – 600 CAD for the selected light-weight low-cost LiDAR systems used in this research. This case study was able to understand the capabilities to larger more expensive systems and have some understanding of its performance around PTLs. As previously mentioned, the data shown in Figures 80 and 81, were taken incidentally using the LiDAR system being evaluated. Since the data taken for the case study was not collected under the same conditions as this research or in the same environment using the performance evaluation testing methods, would not provide accurate and comparable results.

5.5 General Conclusion

The OPAL™ performance series 3D LiDAR is a very impressive LiDAR system, as from approximately 760 plus meters it was able to see PTLs and the towers. The data shown was just a testing of the system and the PTLs happen to be in the field of view of

the LiDAR system. There is a level of noise in the PCD, to understand and possibly mitigate noise to the LiDAR system, more data collection will have to be done and data analyzed following what was done in Chapter 4.With an approximate value 100,000 CAD at the time of writing this document, in comparison to the price of the LiDAR systems used in this research of 150 – 300 CAD, there was a clear different in performance, from the specifications to how much information was stored in the PCD.

Chapter 6: Conclusions, Recommendations and Future Research

PTLs are being inspected by a combination of utility line personnel, helicopters with a line person and recently companies have developed PTL inspection robots that attach to the PTL and are able to conduct an inspection in situ. With the introduction of RPAS for PTL inspection, the risk of injury or fatality has been reduced. This approach is also less expensive than traditional methods, in addition to the reduced mission set up time. With the use of RPA for PTL inspection comes the possibility of the introduction of different sensors such as LiDAR systems, and their dual use of inspection and obstacle detection.

6.1 Conclusions

This thesis presents the characterization of small light-weight LiDAR systems with remotely piloted aircraft systems for powerline detection. This thesis only represents one method of light-weight LiDAR characterization as there are many scientific research methods available. Most LiDAR systems are used in PTL inspections are more focused on detection and/or analyzing PTL structures. By changing the focus of these LiDAR systems to just that of PTLs, important questions arise which were, at what accuracy can small LiDAR systems to detection high voltage PTLs and would it be better to invest in a more expensive LiDAR system even if a small RPA is being used. It is important to note that the selection of the LiDAR systems used were determined availability, price, weight, size, and applications for detection. The results of this thesis research as shown, there are some considerations for users to understand when selecting LiDAR systems not just for PTL detection but how detection in general.

Based on the performance from LiDAR A and LiDAR B, they both did not perform as well as claimed by manufacturers. LiDAR A being the HPS-3D160/ 3D solid state LiDAR/ 3D TOF ranging sensor by Hypersen Technologies Co, Ltd and LiDAR B the Cygbot CygLiDAR D1 by Cygbot.

The accuracy as this would is the most important part of a detection system, did not perform as expected Section 4.3 where the real-world measurement versus measurements taken by the LiDAR systems at lowest was 6 mm, 50 mm for LiDAR A, B respectively and the largest difference being 116 mm, 173 mm for LiDAR A, B, respectively. As these LiDAR systems range from 150 to 300 CAD at the time of drafting this research LiDAR A being the more expensive of the two. It can be concluded that LiDAR A performed better based on the performance evaluation test performed. LiDAR A did have more spikes in its RMSD values than that of LiDAR B. These spikes could have represented any factors such as fluctuations in the power supply or limitations in the LiDAR system. Which is why an interference test was performed for the background and it was determined that there was more interference from the background for LiDAR B than LiDAR A. For connectivity LiDAR has more options standard USB like that of LiDAR B. For the specifications and properties at price range of 150 – 600 CAD, this is what should be expected with more expensive and advanced systems currently available on the market. The selected low-cost light-weight LiDAR systems had a harder time detecting objects that were smooth and shiny (ACCC Rome and the aluminum water bottle) in addition to darker objects (almost black) such as the PTL sample ACSR Condor aged.

Most of the objectives for this thesis were met, either partially or fully as follows:

- Determine the accuracy of the chosen LiDAR systems in different operating conditions. This was determined by performing the data comparison and the RMSD
- Be able to detect power transmission lines. This was successful, as shown in Section 4.3.
- Be able to be mounted to most RPAS without significantly decreasing its performance? This was partially successful as due to regulations the RPA was not able to be flown outside during this research.
- The detect and avoid system must be able to withstand electromagnetic interference. This was evaluated in section 4.4.3 with the energized PTL in a high voltage lab and the results determine that the selected LiDAR systems were able to withstand the electromagnetic interference from the PTLs.

After examination of the results from these LiDAR systems, pairing these systems with other sensor(s) such as cameras and ultrasonic rangefinders with data fusion (making it a multi-physics system) would help mitigate some of the limitations of LiDAR while still benefitting from their ability to directly measure distances and generate 3D point clouds.

6.2 Recommendations

To improve the results of this research here are some recommendations:

- For optimal the LiDAR data measurements should be taken in a high voltage laboratory like the one at Kinectrics Inc.
- Different data comparison methods to determine the accuracy of the results.
- A wider range of LiDAR systems in the price range of 150 – 300 CAD to understand if price and specifications influence the accuracy of the LiDAR systems

- Performing more flight test with the LiDAR mounted and having the data collected and run-in real time
- Pairing the selected LiDAR systems with an optical sensor (making this system now a multispectral system)

6.3 Future Research

LiDAR systems are becoming smaller and more efficient with new developments in technology. This thesis presented the characterization of two light-weight LiDAR systems, there are many options available on the market and based on the mission profile should be considered. There is a lot of room for improvement in this experiment as the de-energized PTL data and the energized PTL data were collected in different environments, and the energized data examined showed that there was less interference. This research only focusses on a small section on detection and avoidance for PTL for RPA. Detection and avoidance are better done with a multispectral system as it does not rely on the data from one system.

LiDAR A has a diverse interface allowing for more integration with other systems, with one of the main drawbacks being that it is not fully open- source and the experience with customer support has been slow due to time zone and language barriers. To improve upon what was done in this research, having all data collected in a high voltage lab to mitigate interference from external sources. Diverse systems which can all use the same programming language allowing for better comparisons should be selected for future work.

Bibliography

References [41]–[77] were used for knowledge and learning purposes.

[1] Aerossurance, “Helicopter Wirestrike During Powerline Inspection.” Feb. 2021. [Online]. Available: http://aerossurance.com/helicopters/wirestrike-powerline-inspection/#:%7E:text=On%2021%20June%202018%20OH,safely%20with%20only%20minor%20damage.

[2] “Extreme Jobs - High Voltage Power Line Inspection - YouTube.” https://www.youtube.com/watch?v=9YmFHAFYwmY (accessed Aug. 06, 2022).

[3] “Horrifying moment helicopter burns after crashing as it inspected power lines killing pilot and passenger.” https://www.thesun.co.uk/news/7633064/helicopter-crash-beekmantown-new-york-electrical-lines/ (accessed Mar. 27, 2022).

[4] “NTSB Docket - Docket Management System.” https://data.ntsb.gov/Docket?ProjectID=98576 (accessed Aug. 06, 2022).

[5] “Power Line Distance Motion Picture Fact Sheet - Actsafe Safety Association.” https://www.actsafe.ca/department_type/locations/overhead-power-lines-fact-sheet/ (accessed Aug. 06, 2022).

[6] “Power Transmission | Towers | Hydro-Québec.” http://www.hydroquebec.com/learning/transport/types-pylones.html (accessed Mar. 27, 2022).

[7] “Canada’s Electric Reliability Framework.” https://www.nrcan.gc.ca/energy/electricity-infrastructure/electricity-canada/canada-electric-reliability-framework/18792 (accessed Mar. 21, 2022).

[8] “Multi-Sensor Powerline Inspection | Phase One Geospatial.” https://geospatial.phaseone.com/case-studies/ggs-sieaero-powerline-inspection/ (accessed Mar. 27, 2022).

[9] “Hazards and Safety in High Voltage Power Lines.” https://www.allumiax.com/blog/hazards-and-safety-in-high-voltage-power-lines (accessed Mar. 27, 2022).

[10] “Ti: The Transmission Line Inspection Robot | Fortnightly.” https://www.fortnightly.com/fortnightly/2016/04/ti-transmission-line-inspection-robot (accessed Aug. 24, 2022).

[11] V. N. Nguyen, R. Jenssen, and D. Roverso, “Intelligent Monitoring and Inspection of Power Line Components Powered by UAVs and Deep Learning,” *IEEE Power and Energy Technology Systems Journal*, vol. 6, no. 1, pp. 11–21, 2019, doi: 10.1109/JPETS.2018.2881429.

[12] “The Past, Present, and Future of Powerline Inspection Automation.” https://www.powermag.com/the-past-present-and-future-of-powerline-inspection-automation/ (accessed Mar. 28, 2022).

[13] “Pipeline Power Line Patrol • Seeker Aircraft, Inc.” https://www.seekeraircraft.com/pipeline-power-line-patrol.html (accessed Mar. 28, 2022).

[14] H. D. M and A. R. N, “Method of autonomous power line detection, avoidance, navigation, and inspection using aerial crafts,” no. US 9964658 B2. [Online]. Available: https://lens.org/009-471-728-231-484

[15] V. N. Nguyen, R. Jenssen, and D. Roverso, “Automatic autonomous vision-based power line inspection: A review of current status and the potential role of deep learning,” *International Journal of Electrical Power & Energy Systems*, vol. 99, pp. 107–120, Jul. 2018, doi: 10.1016/J.IJEPES.2017.12.016.

[16] J. H. Mott and B. Kotla, “Design and Validation of a School Bus Passing Detection System Based on Solid-State LiDAR,” in *2020 Systems and Information Engineering Design Symposium (SIEDS)*, Apr. 2020, pp. 1–6. doi: 10.1109/SIEDS49339.2020.9106631.

[17] X. Li and Y. Guo, “Application of LiDAR technology in power line inspection”, doi: 10.1088/1757-899X/382/5/052025.

[18] “lidar | scientific technique | Britannica.” https://www.britannica.com/technology/lidar (accessed Mar. 30, 2022).

[19] P. McManamon, “Field Guide to Lidar,” *Field Guide to Lidar*, Aug. 2015, doi: 10.1117/3.2186106.

[20] H. W. Yoo *et al.*, “MEMS-based lidar for autonomous driving,” *Elektrotechnik und Informationstechnik*, vol. 135, no. 6, pp. 408–415, Oct. 2018, doi: 10.1007/S00502-018-0635-2.

[21] “What is LiDAR technology?” https://www.generationrobots.com/blog/en/what-is-lidar-technology/ (accessed Aug. 06, 2022).

[22] D. Faust, “Examination of Interference between Hypersen HPS-3D160 LiDAR and Intel RealSense D435 Stereo Depth Camera in the RACOON-Laboratory,” 2020.

[23] D. Fernandes *et al.*, “Real-Time 3D Object Detection and SLAM Fusion in a Low-Cost LiDAR Test Vehicle Setup,” *Sensors 2021, Vol. 21, Page 8381*, vol. 21, no. 24, p. 8381, Dec. 2021, doi: 10.3390/S21248381.

[24] Y. Liu, J. Shi, Z. Liu, J. Huang, and T. Zhou, “Two-Layer Routing for High-Voltage Powerline Inspection by Cooperated Ground Vehicle and Drone,” *Energies 2019, Vol. 12, Page 1385*, vol. 12, no. 7, p. 1385, Apr. 2019, doi: 10.3390/EN12071385.

[25] N. Iversen, O. B. Schofield, L. Cousin, N. Ayoub, G. vom Bogel, and E. Ebeid, “Design, Integration and Implementation of an Intelligent and Self-recharging Drone System for Autonomous Power line Inspection,” *IEEE International Conference on Intelligent Robots and Systems*, pp. 4168–4175, 2021, doi: 10.1109/IROS51168.2021.9635924.

[26] Z. A. Siddiqui and U. Park, “A Drone Based Transmission Line Components Inspection System with Deep Learning Technique,” *Energies 2020, Vol. 13, Page 3348*, vol. 13, no. 13, p. 3348, Jun. 2020, doi: 10.3390/EN13133348.

[27] G. Tianyu *et al.*, “Effects of temperature environment on ranging accuracy of Lidar,” 2018, doi: 10.1117/12.2503192.

[28] “Canadian Aviation Regulations.” https://lois-laws.justice.gc.ca/eng/regulations/SOR-96-433/FullText.html#s-900.01 (accessed Mar. 21, 2022).

[29] “eCFR :: 14 CFR Part 107 -- Small Unmanned Aircraft Systems.” https://www.ecfr.gov/current/title-14/chapter-I/subchapter-F/part-107 (accessed Apr. 03, 2022).

[30] “UAS Remote Identification | Federal Aviation Administration.” https://www.faa.gov/uas/getting_started/remote_id (accessed Aug. 16, 2022).

[31] “Canadian Aviation Regulations (SOR/96-433).” https://tc.canada.ca/en/corporate-services/acts-regulations/list-regulations/canadian-aviation-regulations-sor-96-433 (accessed Feb. 24, 2022).

[32] “Names of parts on electric pole.” http://waterheatertimer.org/Names-of-parts-on-electric-pole.html (accessed Aug. 07, 2022).

[33] “ACSR | Southwire Canada.” https://www.southwire.com/ca/en-ca/wire-cable/bare-aluminum-overhead-transmission-distribution/acsr/p/ALBARE6 (accessed Jul. 25, 2022).

[34] “HPS-3D160 / 3D Solid-state LiDAR / 3D TOF Ranging Sensor / HYPERSEN-Hypersen Technologies Co., Ltd.” https://en.hypersen.com/product/detail/10.html (accessed Aug. 24, 2022).

[35] “HPS-3D160 Solid-state Depth camera manual”.

[36] “2D/3D Dual Solid State ToF LiDAR | CYGBOT.” https://www.cygbot.com/2d-3d-dual-solid-state-tof-lidar (accessed Aug. 24, 2022).

[37] “Thermal Energy from Light.” https://serc.carleton.edu/integrate/teaching_materials/energy_sustain/student_materials/thermal_energy_.html (accessed Aug. 14, 2022).

[38] J. Meseguer, I. Pérez-Grande, and A. Sanz-Andrés, “Thermal radiation heat transfer,” *Spacecraft Thermal Control*, pp. 73–86, 2012, doi: 10.1533/9780857096081.73.

[39] “Neptec Technologies Corp. OPAL^{TM} Performance Series CONICAL 3D LiDAR Sensor | Geo-matching.com.” https://geo-matching.com/terrestrial-laser-scanners/opal-performance-series-conical-3d-lidar-sensor (accessed Aug. 15, 2022).

[40] “Heat Transfer Formula: Definition, Concepts and Examples.” https://www.toppr.com/guides/physics-formulas/heat-transfer-formula/ (accessed Aug. 15, 2022).

[41] V. L. D. S. N. Button, “Temperature Transducers,” *Principles of Measurement and Transduction of Biomedical Variables*, pp. 101–154, 2015, doi: 10.1016/B978-0-12-800774-7.00004-0.

[42] “795 Kcmil ACSR (DRAKE) Al 26/4.44+Ga 7/3.45 to ASTM, B230m-99, B231m-99, B232m-01, B498-99 - jytopcable.” https://www.vwcable.com/795-kcmil-acsr-drake-al-26-4-44ga-7-3-45-to-astm-b230m-99-b231m-99-b232m-01-b498-99/ (accessed Aug. 10, 2022).

[43] “Transmission line relocation requests.” https://www.bchydro.com/energy-in-bc/operations/right-of-way-management/transmission-relocations.html (accessed Aug. 06, 2022).

[44] “Highlight patterns and trends with conditional formatting.” https://support.microsoft.com/en-us/office/highlight-patterns-and-trends-with-conditional-formatting-eea152f5-2a7d-4c1a-a2da-c5f893adb621 (accessed Jul. 27, 2022).

[45] “Electric Utility Training by Professional Training Systems, Inc.” http://www.utilitytraining.net/glossary/k.html (accessed Jul. 25, 2022).

[46] “Aluminum Conductor Composite Core (ACCC ®)”.

[47] “What is LiDAR and How Does it Work? | Synopsys.” https://www.synopsys.com/glossary/what-is-lidar.html (accessed Jul. 24, 2022).

[48] “RMSE: Root Mean Square Error - Statistics How To.” https://www.statisticshowto.com/probability-and-statistics/regression-analysis/rmse-root-mean-square-error/ (accessed Jul. 11, 2022).

[49] “What Is MATLAB? - MATLAB & Simulink.” https://www.mathworks.com/discovery/what-is-matlab.html (accessed May 07, 2022).

[50] “www.rs-components.com/raspberrypi Product Name Raspberry Pi 3 Product Description”, Accessed: May 07, 2022. [Online]. Available: www.rs-components.com/raspberrypi

[51] “Names of parts on electric pole.” http://waterheatertimer.org/Names-of-parts-on-electric-pole.html (accessed May 05, 2022).

[52] “- Harris Aerial.” https://www.harrisaerial.com/carrier-h6-hybrid-drone/ (accessed Apr. 03, 2022).

[53] “Investigation Report.” https://www.ntsb.gov/investigations/AccidentReports/Pages/Reports.aspx?mode=Aviation (accessed Mar. 28, 2022).

[54] “The Civil Aviation Daily Occurrence Reporting System (CADORS).” https://tc.canada.ca/en/aviation/publications/aviation-safety-letter/issue-2-2021/civil-aviation-daily-occurrence-reporting-system-cadors (accessed Mar. 28, 2022).

[55] “Fly your drone beyond visual line-of-sight.” https://tc.canada.ca/en/aviation/drone-safety/drone-pilot-licensing/fly-your-drone-beyond-visual-line-sight (accessed Mar. 21, 2022).

[56] “Overhead Power Lines | Hydro Ottawa.” https://hydroottawa.com/en/outages-safety/safety-outside-home/overhead-power-lines (accessed Mar. 21, 2022).

[57] “Utility Line Workers: One of the Top 10 Most Dangerous Professions | T&D World.” https://www.tdworld.com/grid-innovations/transmission/article/20965642/utility-line-workers-one-of-the-top-10-most-dangerous-professions#:%7E:text=Utility%20line%20work%20is%20in,of%20police%20officers%20and%20firemen (accessed Mar. 05, 2022).

[58] “Flying your drone safely and legally.” https://tc.canada.ca/en/aviation/drone-safety/learn-rules-you-fly-your-drone/flying-your-drone-safely-legally (accessed Mar. 05, 2022).

[59] B. Li and C. Chen, “Transmission line detection based on a hierarchical and contextual model for aerial images,” *https://doi.org/10.1117/1.JEI.27.4.043054*, vol. 27, no. 4, p. 043054, Aug. 2018, doi: 10.1117/1.JEI.27.4.043054.

[60] Z. A. Siddiqui *et al.*, “Robust Powerline Equipment Inspection System Based on a Convolutional Neural Network,” *Sensors 2018, Vol. 18, Page 3837*, vol. 18, no. 11, p. 3837, Nov. 2018, doi: 10.3390/S18113837.

[61] A. Taqi and S. Beryozkina, “Overhead Transmission Line Thermographic Inspection Using a Drone,” in *2019 IEEE 10th GCC Conference Exhibition (GCC)*, Apr. 2019, pp. 1–6. doi: 10.1109/GCC45510.2019.1570521870.

[62] W. Zhang, C. Gu, Z. Li, and G. Sheng, “Image Detection Technology on Pin Defect to Overhead Power Lines,” *Proceedings - 2020 5th Asia Conference on Power and Electrical Engineering, ACPEE 2020*, pp. 229–233, Jun. 2020, doi: 10.1109/ACPEE48638.2020.9136237.

[63] T. Mao *et al.*, “Development of Power Transmission Line Defects Diagnosis System for UAV Inspection based on Binocular Depth Imaging Technology,” in *2019 2nd International Conference on Electrical Materials and Power Equipment (ICEMPE)*, Apr. 2019, pp. 478–481. doi: 10.1109/ICEMPE.2019.8727361.

[64] H. Liang, C. Zuo, and W. Wei, “Detection and Evaluation Method of Transmission Line Defects Based on Deep Learning,” *IEEE Access*, vol. 8, pp. 38448–38458, 2020, doi: 10.1109/ACCESS.2020.2974798.

[65] J. Han *et al.*, “A Method of Insulator Faults Detection in Aerial Images for High-Voltage Transmission Lines Inspection,” *Applied Sciences 2019, Vol. 9, Page 2009*, vol. 9, no. 10, p. 2009, May 2019, doi: 10.3390/APP9102009.

[66] M. Lu, A. James, and M. Bagheri, “Unmanned Aerial Vehicle (UAV) charging from powerlines,” *Asia-Pacific Power and Energy Engineering Conference, APPEEC*, vol. 2017-November, pp. 1–6, Mar. 2018, doi: 10.1109/APPEEC.2017.8308912.

[67] L. Fahmani, J. Garfaf, K. Boukhdir, S. Benhadou, and H. Medromi, “Unmanned Aerial Vehicles Inspection for Overhead High Voltage Transmission Lines,” in *2020 1st International Conference on Innovative Research in Applied Science, Engineering and Technology (IRASET)*, Apr. 2020, pp. 1–7. doi: 10.1109/IRASET48871.2020.9092141.

[68] J.-F. Allan, “Robotics for distribution power lines: Overview of the last decade,” in *2012 2nd International Conference on Applied Robotics for the Power Industry (CARPI)*, Sep. 2012, pp. 96–101. doi: 10.1109/CARPI.2012.6473344.

[69] T. Disyadej, J. Promjan, K. Poochinapan, T. Mouktonglang, S. Grzybowski, and P. Muneesawang, “High Voltage Power Line Maintenance amp; Inspection by Using Smart Robotics,” in *2019 IEEE Power Energy Society Innovative Smart Grid Technologies Conference (ISGT)*, 2019, pp. 1–4. doi: 10.1109/ISGT.2019.8791584.

[70] I. M. Aleshin *et al.*, “Review on the Use of Light Unmanned Aerial Vehicles in Geological and Geophysical Research,” *Seismic Instruments 2020 56:5*, vol. 56, no. 5, pp. 509–515, Sep. 2020, doi: 10.3103/S0747923920050035.

[71] S. Bijjahalli, R. Sabatini, and A. Gardi, “Advances in intelligent and autonomous navigation systems for small UAS,” *Progress in Aerospace Sciences*, vol. 115, p. 100617, May 2020, doi: 10.1016/J.PAEROSCI.2020.100617.

[72] H. Zheng, X. Su, Y. Lin, Z. Zhou, and H. Sun, “A Somatosensory-Operation-Based Unmanned Aerial Vehicle for Power Line Inspection in First Person of View,” in *2018 International Conference on Power System Technology (POWERCON)*, 2018, pp. 3846–3854. doi: 10.1109/POWERCON.2018.8601527.

[73] G. Rui, Z. Feng, C. Lei, and Y. Jun, “A mobile robot for inspection of overhead transmission lines,” in *Proceedings of the 2014 3rd International Conference on Applied Robotics for the Power Industry*, 2014, pp. 1–3. doi: 10.1109/CARPI.2014.7030054.

[74] C. A. Liu, R. Dong, H. Wu, G. T. Yang, and W. Lin, “A 3D Laboratory Test-Platform for Overhead Power Line Inspection:,” *https://doi.org/10.5772/62800*, vol. 13, no. 2, May 2017, doi: 10.5772/62800.

[75] M. Buhringer *et al.*, “Inspection of high voltage power Linesa new approach,” *Mobile Robotics: Solutions and Challenges - Proceedings of the 12th International Conference on Climbing and Walking Robots and the Support Technologies for Mobile Machines, CLAWAR 2009*, pp. 455–462, 2010, doi: 10.1142/9789814291279_0056.

[76] NHTSA, “Studies of Long-Term Advanced Systems (Task 2.3).” Feb. 1998. [Online]. Available: https://one.nhtsa.gov/people/injury/research/pub/acas/ch3-4.htm

[77] DFRobot, “HPS-3D160-U Solid-State Area Array LiDAR Wiki - DFRobot.” 2020. [Online]. Available: https://wiki.dfrobot.com/HPS_3D160_U_Area_Array_Laser_Radar_SKU_DFR0728

Appendices

Appendix A- Validation of LiDAR system Object set

Official League Baseball

Dimensions: 4 inches L and 4 inches W

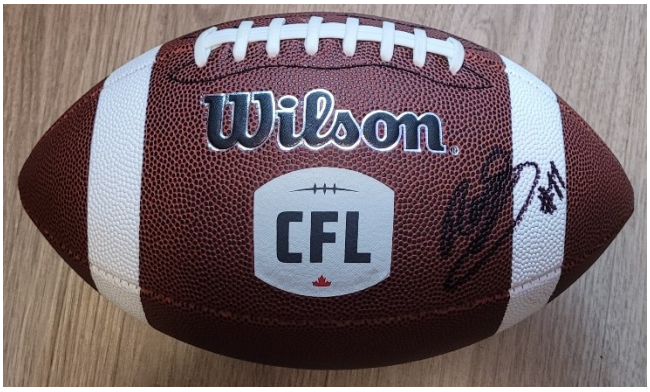

Standard CFL (Canadian Football League) Football

Dimensions: 14 inches L and 10 1/5 inches W

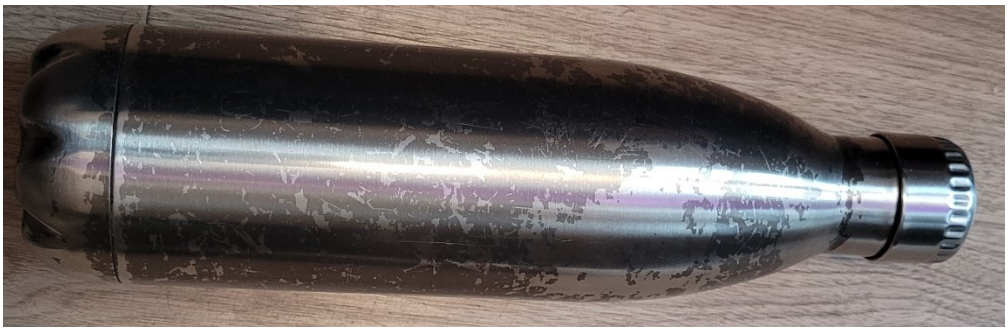

Aluminum Water Bottle

Dimensions: 12 inches L and 4 ½ inches W

Appendix B- Sample MATLAB code used for separating the data.

```
function [Data Organized] =Separate_Data(Data)
index=find(isnan(Data(:,1)));
rd=size(Data,1);
r=size(index,1);
k=2;
Data_Organized{1}=Data(1:index(1)-1,:);
for i=1:r-1
   if index(i+1)-index(i)>1 ||i==r-1
      if i==r-1 && index(r)<rd
         Data_Organized{k}=Data(index(r)+1:rd,:);
      else
         Data_Organized{k}=Data(index(i)+1:index(i+1)-1,:);
         k=k+1;
      end
   end
end
```

Appendix C- Power Transmission Line Specifications Sheets

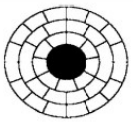

HIGH TEMPERATURE LOW SAG CONDUCTORS

TECHNICAL DATA SHEET

Aluminium Conductor Composite Core

CODE NAME			**ACCC® Rome**
STANDARD			**ASTM B 857 / B 609 or EN 50540**
Mechanical Specifications			
Nominal Aluminum Cross-Sectional Area		mm^2	592,5
Nominal Diameter of Composite Core		mm	9,53
Nominal Cross-Sectional Area of Core		mm^2	71,3
Overall Diameter of Conductor		mm	29,89
Nominal Cross-Sectional Area of the Conductor		mm^2	663,8
Ultimate Tensile Strength of Conductor		kN	187,1
Rate Strength of Core - 313ksi (2158 MPa)		kN	153,8
Core Nominal Mass per Unit Length		kg/km	132
Conductor Nominal Mass per Unit Length		kg/km	1773,8
Aluminum Nominal Mass per Unit Length		kg/km	1641,8
Maximum Continuous Operating Temperature of Conductor		°C	180
Maximum Allowable Emergency Temperature of Conductor		°C	200
Coefficient of Linear Expansion Above Thermal Kneepoint		/°C	1,61E-06
Coefficient of Linear Expansion Below Thermal Kneepoint		/°C	1,90E-05
Final Modulus of Elasticity Above Thermal Kneepoint		Gpa	112,3
Final Modulus of Elasticity Below Thermal Kneepoint		GPa	63,8
Stranding Configuration			
No. of Layers		pcs.	3
No. of Trapezoidal Wires in First Layer		pcs.	9
No. of Trapezoidal Wires in Second Layer		pcs.	12
No. of Trapezoidal Wires in Third Layer		pcs.	16
Electrical Specifications			
Nominal Resistivity of Aluminum at 20°C, DC 63% IACS		Ω/km	0,0474
Temperature Coefficient of Resistance		/°C	0,00403
Frequency		Hz	50
AC Nominal Resistance at 25°C		Ω/km	0,0494
AC Nominal Resistance at 75°C		Ω/km	0,0588
AC Nominal Resistance at 180°C		Ω/km	0,0785
AC Current Rating at Given Temp.	@ 100°C & 50 Hz	Amperes	1225
	@180°C & 50 Hz		1850
GMR (estimated)		m	0,012
Inductive Reactance		Ω/km	0,203
Capacitive Reactance		MΩ-km	0,173

ACCC® is produced with 1350 O-tempered aluminum
ACCC® exhibit lay length (ratios) that conform to ASTM B 857 or EN 50540
Minimum tensile strength of annealed aluminum conform to ASTM B 609 and EN 50540
Conditions: 0,61 m/s (2 ft/s) wind, 0 m (0 ft) elevation, 0,5 emis., 0,5 absorp. 40°C ambient temp., 1033 W/m^2 (96 W/ft^2) sun radiation

EMTA KABLO SANAYI VE TİCARET A.Ş.
İstasyon Mahallesi İbişağa Caddesi No:4 34940 Tuzla, İstanbul/TURKEY
Tel: +90 216 446 66 06 / **Fax:** +90 216 446 43 93
sales@emtaconductor.com

www.emtaaccc.com
www.emtaconductor.com

Manufactured under licence by CTC GLOBAL

EMTA KABLO SANAYİ ve TİCARET A.Ş.
Kadirli Organize Sanayi Bölgesi 1. Cadde
No: 15 Kadirli OSMANİYE
Tel. 0328 739 23 05 (Pbx) Faks: 0328 739 23 06
Kadirli V.D.: 334 050 2150
Ticaret Sicil No: 2333 Mersis No: 0-3340-5021-8000014

Table 1–6

BARE ALUMINUM CONDUCTORS, STEEL REINFORCED (ACSR), CONCENTRIC-LAY STRANDED ASTM B 232 WITH CLASS AA AND A STRANDING, AND VARIOUS TYPES OF STEEL CORE PHYSICAL CHARACTERISTICS

Code Word	ACSR Cross-Section Aluminum			ACSR Cross-Section Total		Overall Diameter		Stranding—Number and Diameter of Strands Aluminum			Steel			Weight Force (Total Conductor)	
									Diameter			Diameter		lbf/1000 ft.	N/km
	Cir. mils	Sq. In.	mm²	Sq. In.	mm²	In.	mm	No.	In.	mm	No.	In.	mm		
(1)	(2)	(3)	(4)	(5)	(6)	(7)	(8)	(9)	(10)	(11)	(12)	(13)	(14)	(15)	(16)
Turkey	#6 AWG	0.0206	13.29	0.0240	15.48	0.198	5.029	6	0.0661	1.679	1	0.0661	1.679	36.1	526.8
Swan	#4 AWG	0.0328	21.16	0.0383	24.71	0.250	6.350	6	0.0834	2.118	1	0.0834	2.118	57.4	837.7
Swanate	#4 AWG	0.0328	21.16	0.0411	26.52	0.257	6.528	7	0.0772	1.961	1	0.1029	2.614	67.0	977.8
Sparrow	#2 AWG	0.0521	33.61	0.0608	39.23	0.316	8.026	6	0.1052	2.672	1	0.1052	2.672	91.3	1332.4
Sparate	#2 AWG	0.0521	33.61	0.0653	42.13	0.325	8.255	7	0.0974	2.474	1	0.1299	3.299	106.7	1557.2
Robin	#1 AWG	0.0657	42.39	0.0767	49.48	0.355	9.017	6	0.1182	3.002	1	0.1182	3.002	115.2	1681.2
Raven	1/0	0.0829	53.48	0.0967	62.39	0.398	10.109	6	0.1327	3.371	1	0.1327	3.371	145.2	2119.0
Quail	2/0	0.1045	67.42	0.1219	78.65	0.447	11.354	6	0.1490	3.785	1	0.1490	3.785	183.1	2672.1
Pigeon	3/0	0.1318	85.03	0.1538	99.23	0.502	12.751	6	0.1672	4.247	1	0.1672	4.247	230.9	3369.7
Penguin	4/0	0.1662	107.23	0.1939	125.10	0.563	14.300	6	0.1878	4.770	1	0.1878	4.770	291.1	4248.3
Waxwing	266800	0.2095	135.16	0.2211	142.64	0.609	15.469	18	0.1217	3.091	1	0.1217	3.091	289.4	4223.5
Partridge	266800	0.2095	135.16	0.2436	157.16	0.642	16.307	26	0.1013	2.573	7	0.0788	2.002	367.3	5360.3
Ostrich	300000	0.2356	152.00	0.2740	176.77	0.680	17.272	26	0.1074	2.728	7	0.0835	2.121	412.7	6022.9
Merlin	336400	0.2642	170.45	0.2789	179.94	0.684	17.374	18	0.1367	3.472	1	0.1367	3.472	365.3	5331.2
Linnet	336400	0.2642	170.45	0.3072	198.19	0.721	18.313	26	0.1138	2.891	7	0.0885	2.248	463.0	6757.0
Oriole	336400	0.2642	170.45	0.3259	210.26	0.741	18.821	30	0.1059	2.690	7	0.1059	2.690	527.1	7692.4
Chickadee	397500	0.3122	201.42	0.3295	212.58	0.743	18.872	18	0.1486	3.774	1	0.1486	3.774	431.6	6298.7
Ibis	397500	0.3122	201.42	0.3630	234.19	0.783	19.888	26	0.1236	3.139	7	0.0961	2.441	546.9	7981.4
Lark	397500	0.3122	201.42	0.3850	248.39	0.806	20.472	30	0.1151	2.924	7	0.1151	2.924	622.8	9089.1
Pelican	477000	0.3746	241.68	0.3954	255.10	0.814	20.676	18	0.1628	4.135	1	0.1628	4.135	518.0	7559.6
Flicker	477000	0.3746	241.68	0.4232	273.03	0.846	21.488	24	0.1410	3.581	7	0.0940	2.388	614.5	8968.0
Hawk	477000	0.3746	241.68	0.4356	281.03	0.858	21.793	26	0.1355	3.442	7	0.1054	2.677	657.	9588.2
Hen	477000	0.3746	241.68	0.4620	298.06	0.883	22.428	30	0.1261	3.203	7	0.1261	3.203	747.	10901.6
Osprey	556500	0.4371	282.00	0.4614	297.68	0.879	22.327	18	0.1758	4.465	1	0.1758	4.465	604	8814.7
Parakeet	556500	0.4371	282.00	0.4938	318.58	0.914	23.216	24	0.1523	3.868	7	0.1015	2.578	717	10463.8
Dove	556500	0.4371	282.00	0.5083	327.93	0.927	23.546	26	0.1463	3.716	7	0.1138	2.891	766	11178.9
Eagle	556500	0.4371	282.00	0.5391	347.81	0.953	24.206	30	0.1362	3.459	7	0.1362	3.459	872	12725.9
Peacock	605000	0.4752	306.58	0.5368	346.32	0.953	24.206	24	0.1588	4.034	7	0.1059	2.690	780	11383.2
Squab	605000	0.4752	306.58	0.5526	356.52	0.966	24.536	26	0.1525	3.874	7	0.1186	3.012	833	12156.7
Teal	605000	0.4752	306.58	0.5835	376.45	0.994	25.248	30	0.1420	3.607	19	0.0852	2.164	940	13718.3
Kingbird	636000	0.4995	322.26	0.5272	340.13	0.940	23.876	18	0.1880	4.775	1	0.1880	4.775	691	10084.4
Rook	636000	0.4995	322.26	0.5643	364.06	0.977	24.816	24	0.1628	4.135	7	0.1085	2.756	819	11952.4
Grosbeak	636000	0.4995	322.26	0.5809	374.77	0.990	25.146	26	0.1564	3.973	7	0.1216	3.089	875	12769.7
Egret	636000	0.4995	322.26	0.6134	395.74	1.019	25.883	30	0.1456	3.698	19	0.0874	2.212	988	14418.8
Flamingo	666000	0.5235	337.74	0.5914	381.55	1.000	25.400	24	0.1667	4.234	7	0.1111	2.822	859	12536.2
Starling	715500	0.5620	362.58	0.6535	421.61	1.051	26.698	26	0.1659	4.214	7	0.1290	3.277	985	14375.0
Redwing	715500	0.5620	362.58	0.6901	445.22	1.081	27.457	30	0.1544	3.922	19	0.0926	2.352	1111	16213.8
Cuckoo	795000	0.6244	402.84	0.7053	455.03	1.092	27.737	24	0.1820	4.623	7	0.1213	3.081	1024	14944.2
Drake	795000	0.6244	402.84	0.7261	468.45	1.108	28.143	26	0.1749	4.442	7	0.1360	3.470	1094	15965.7
Mallard	795000	0.6244	402.84	0.7668	494.71	1.140	28.956	30	0.1628	4.135	19	0.0977	2.482	1235	18023.5
Tern	795000	0.6244	402.84	0.6676	430.71	1.063	27.000	45	0.1329	3.376	7	0.0886	2.250	896	13076.1
Condor	795000	0.6244	402.84	0.7053	455.03	1.093	27.762	54	0.1214	3.084	7	0.1214	3.084	1024	14944.2
Canary	900000	0.7069	456.06	0.7985	515.16	1.162	29.515	54	0.1291	3.279	7	0.1291	3.279	1159	16914.3
Rail	954000	0.7493	483.42	0.8011	516.84	1.165	29.591	45	0.1456	3.698	7	0.0971	2.466	1075	15688.4
Cardinal	954000	0.7493	483.42	0.8464	546.06	1.196	30.378	54	0.1329	3.376	7	0.1329	3.376	1229	17935.9
Ortolan	1033500	0.8117	523.68	0.8678	559.87	1.213	30.810	45	0.1516	3.851	7	0.1011	2.568	1165	17001.9
Curlew	1033500	0.8117	523.68	0.9169	591.55	1.246	31.648	54	0.1384	3.515	7	0.1384	3.515	1331	19424.5
Bluejay	1113000	0.8741	563.93	0.9346	602.97	1.259	31.979	45	0.1573	3.995	7	0.1049	2.664	1255	18315.3
Finch	1113000	0.8741	563.93	0.9849	635.42	1.293	32.842	54	0.1436	3.647	19	0.0862	2.189	1431	20883.9
Bunting	1192500	0.9367	604.32	1.001	645.81	1.302	33.071	45	0.1628	4.135	7	0.1085	2.756	1344	19614.2
Grackle	1192500	0.9366	604.26	1.055	680.64	1.333	33.985	54	0.1486	3.774	19	0.0892	2.266	1533	22372.5
Bittern	1272000	0.9990	644.51	1.068	689.03	1.345	34.163	45	0.1681	4.270	7	0.1121	2.847	1434	20927.7
Pheasant	1272000	0.9990	644.51	1.126	726.45	1.382	35.103	54	0.1535	3.899	19	0.0921	2.339	1635	23861.0
Dipper	1351500	1.062	685.16	1.135	732.26	1.386	35.204	45	0.1733	4.402	7	0.1151	2.924	1522	22211.9
Martin	1351500	1.0625	685.48	1.196	771.61	1.424	36.170	54	0.1582	4.018	19	0.0949	2.410	1737	25349.6
Bobolink	1431000	1.124	725.16	1.202	775.48	1.427	36.246	45	0.1783	4.529	7	0.1189	3.020	1613	23540.0
Plover	1431000	1.124	725.16	1.266	816.77	1.465	37.211	54	0.1628	4.135	19	0.0977	2.482	1840	26852.8
Nuthatch	1510500	1.186	765.16	1.268	818.06	1.466	37.236	45	0.1832	4.653	7	0.1221	3.101	1702	24838.8
Parrot	1510500	1.186	765.16	1.337	862.58	1.506	38.252	54	0.1673	4.249	19	0.1004	2.550	1942	28341.4
Lapwing	1590000	1.249	805.80	1.335	861.29	1.502	38.151	45	0.1878	4.770	7	0.1252	3.180	1792	26152.3
Falcon	1590000	1.249	805..80	1.407	907.74	1.545	39.243	54	0.1716	4.359	19	0.1030	2.616	2044	29829.9
Chukar	1780000	1.398	901.93	1.512	975.48	1.602	40.691	84	0.1456	3.698	19	0.0874	2.220	2074	30267.8
Bluebird	2156000	1.693	1092.26	1.831	1181.29	1.762	44.755	84	0.1602	4.069	19	0.0961	2.441	2511	36645.3
Kiwi	2167000	1.702	1098.06	1.776	1145.80	1.737	44.120	72	0.1735	4.407	7	0.1157	2.399	2303	33609.8

FIRST SAMPLE — PROVIDED (AW)

DARK AGED ALUM. SAMPLE

ACCC ROME is the trapwire short SAMPLE